Alma Mater Studiorum - University of Bologna

DOTTORATO DI RICERCA

Ingegneria Elettrotecnica
Ciclo XXI

Settore scientifico disciplinare di afferenza:
ELETTROTECNICA (ING-IND/31)

TITOLO DELLA TESI

Theoretical and Experimental Study of the Magnetic Separation of Pollutants from Wastewater

Presentata da: Giacomo Mariani

Coordinatore Dottorato	**Relatori**	
Chiar.mo Prof. Ing.	Prof. Ing.	Prof. Ing.
Francesco Negrini	Massimo Fabbri	Pier Luigi Ribani

Esame finale anno 2009

Contents

Forewords and Acknowledgments

Introduction

The use of magnetic fields for separation purposes is an old stuff. Its working principle is remarkably simple: it relies on the fact that materials with different magnetic moments experience different forces in the presence of a magnetic field gradient. It's usually accepted that the magnetic separation was born in 1792, when William Fullarton filled the first patent about its use in iron manufacturing. The earlier application is dated 1852 and was located in New York: its aim was the separation of magnetite from apatite. Following this first application a huge number of industries involved in metal transformations adopted some kind of magnetic separator. Consequently a large amount of patents has been filled on that topic, both in Europe and in the USA.

After Heike Kamerlingh Onnes discovered superconductivity in 1911 an intense work in this field led, in 1962, to the first commercially available superconducting magnets. That meant the availability of large magnetic fields (more than $1T$) over tents of cubic decimeters: the High Gradient Magnetic Separation (HGMS) was born. The HGMS is identical, in its working principles, to the traditional magnetic separation, but it takes advantage of a much greater gradient ($10^4 T/m$ are usually achieved). The gradient is usually enhanced by a special porous bed, located inside the magnetic field source, typically made with ferromagnetic material, such as spheres, rods, plates, wires or wool. Inside the packet bed the material that is going to be separated impacts the ferromagnetic material and is retained. This strong interaction means that also paramagnetic and even diamagnetic particles could be separated from flow streams. HGMS resulted faster and reliable if compared to traditional remotion techniques so that it is a critical technique in industrial plant where ferrous material are managed. More recently magnetic separation have become commonplace in biotechnology where it is used for both protein purification and flow cytometry. Indeed, in biology, the need for magnetic beads that are coated so as to bind particular components arises. Commercial sources for magnetic beads have grown substantially in the past decades and a wide variety of substances may nowadays be selec-

tively removed.

The high working rate and selectivity are peculiar of HGMS as well as the lack of high pressure drop encountered by the stream in comparison to the ones involved in traditional separation. Moreover HGMS filters are usually smaller and safer. For these reasons HGMS has been intensely studied in the last decades leading to a large improvement mostly on the experimental side. Despite all, a wide lack of knowledge still persists. This is mainly due to the intrinsic complexity of the system: on one side there is the whole filter seen as a *big* device and on the other side there are the pollutant particles moving on a scale in which only an unknown and chaotic *small* system is involved.

The first chapter of this thesis describes in some detail the state of the art of the separation with a particular focus on HGMS. In fact the described complex situation led to a large effort in developing theories based on different approaches in order to overcame the problem. Despite that the problem still lacks of knowledge: most of the developed theories were oversimplified and so unreliable. Also the traditional computational approach, based on the finite elements method, results unreliable: only a two dimensional approach is nowadays affordable with ordinary high performance computers.

The second chapter describes the theoretical model developed in order to fill up this lack following a somehow new approach based on the merging of two traditional approach: the trajectories study and the statistical study of the filter. The starting point is a HGMS filter using iron steel wool as active filtering element. The filter is supposed aimed to the removal of iron oxide beads. The iron oxide beads are well known adsorbent of lots of pollutants (in particular heavy metals) and their remotion is worth. This is done analytically studying the trajectories of the pollutant particles inside a small fraction of the filter, called cell. In fact, inside each cell, the developed original code is able to describe analytically both the magnetic and the velocity field thanks to the **MAG3D** routines and to integrate the resulting trajectories thanks to the **ODE** routine. This cell results statistically characterized and the results can be extended to the whole filter with a macroscopic model of the device based on simple hypothesis like the conservation of the number of particles and the uniform flow stream.

The third chapter describes the experimental facility made up at the LIMSA laboratory in order to test the model described in chapter two. This experimental set-up is completely original and required, for its correct working, an accurate study of the problem. The reached experimental configuration was a closed circuit made of removable, interchangeable parts. The

working fluid, made of water and particles of hematite (of two different mean diameters), is moved, thanks to a pump, through one or two filtering elements realized with a commercially available, very fine, iron steel wool. The necessary external magnetic field is provided by a permanent magnet. A particularly important facet in the project and construction of the experimental set-up were the necessary measuring instruments. They achieve the aim to collect, in a real time computerized environment, all the desired data.

The forth chapter reports the results of the performed measurements campaign. First, the collected data are transformed thanks to analytical relations between the various involved quantity (such as electrical resistance and particle concentration). The obtained values are then confronted with the developed model of the whole filter in order to obtain the desired parameters (mainly the filtering efficiency) that are compared with the ones obtained from the cell model.

As described in the conclusion of this work and confirmed by the publications on international journals the obtained results are state that the original developed model is reliable and may by used to supply useful information during the design of future HGMS filters. These results show the feasibility of the HGMS technology when PM are utilized as field sources. This opens the possibility to utilize PM instead of SC magnets evaluating the trade off between capture efficiency and system cost. Indeed using PM shares all the reported benefits of HGMS using SC magnet technology: the reduced electrical usage compared to resistive coil technology, the portability (important for temporary cleanup or remote site) and the minimal inflicted harm on the environment (fewer chemicals than more conventional technologies, nonhazardous non-leachable solid waste production).

An appendix, containing some in-deep analysis of the experimental and theoretical work needed for achieving the main results, concludes the work.

Chapter 1

Filtration and HGMS (High Gradient Magnetic Separation)

A separation process is one in which a mixture of substances is transformed into two or more distinct products. The separated products could differ in chemical properties or some physical properties, such as size, density, electric susceptibility or magnetic susceptibility. Apart from a few exceptions, almost every element or compound is found naturally in an impure state such as a mixture of two or more substances. Moreover most human activities involve, as the main product or as a secondary one, the production of some kind of mixture. Many times the need to separate it into its individual components arises for environmental, economical or industrial reasons. It is a matter of fact that the laws concerning pollution are increasing both in number and in the limited range of tolerable pollutants because public opinion and mass media are deeply interested. For example the Decree of the Italian Ministry for the Environment, Dlgs 300/99, Dlgs 287/2002, 367/2003 about handling and re-use of waste waters and the Decision of the European Union COM (17), 2001, Decree 185/2003. On the other side, in industrial production, the re-employment of contaminated substances as well as the production of better (i.e. more pure) materials are important tasks [BMD06].

1.1 Traditional separation technologies

Nowadays a lot of well working and well established separation technologies are industrially available. All of them have their own limits, due to the physical properties involved in their working principle. Here I give a short review of some of them on the basis of their working principle, without the

claim of being exhaustive.

1.1.1   Filtration and sieving

Filtration is a mechanical or physical operation which is used for the separation of solids from fluids (liquids or gases) by interposing a medium through which only the fluid can pass, as shown in Fig. 1.1. Oversize solids
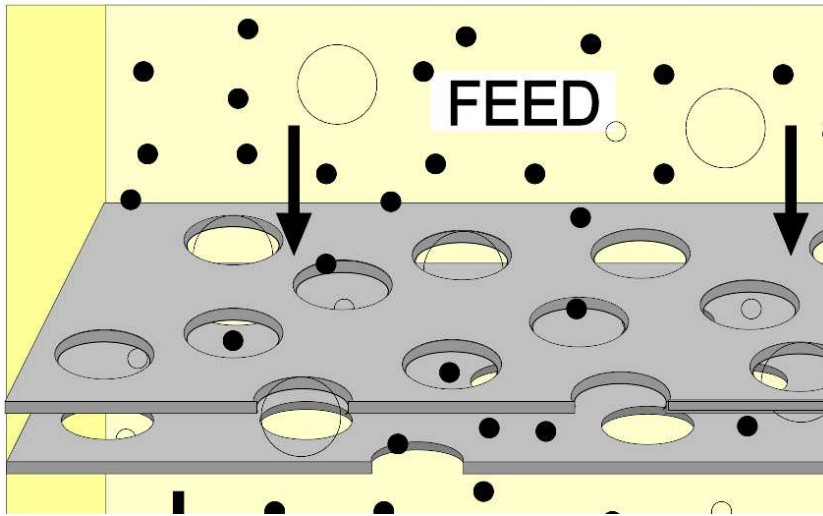

Figure 1.1: Scheme of the working principle of a filter.

in the fluid are retained, but the separation is not complete; solids will be contaminated with some fluid and the filtered liquid will contain fine particles (depending on the pore size and filter thickness) [Che98]. Filtration differs from sieving, where separation occurs at a single perforated layer (a sieve). In sieving, particles that are too big to pass through the holes of the sieve are retained. In filtration, a multilayer lattice retains those particles that are unable to follow the tortuous channels of the filter. Oversize particles may form a cake layer on top of the filter and may also block the filter lattice, preventing the fluid phase from crossing the filter (blinding). Commercially, the term filter is applied to membranes where the separation lattice is so thin that the surface becomes the main zone of particle separation so that these products might be described as sieves. As shown in Fig. 1.2, when the dimension of the particles is under $1\mu m$ the process takes the name of micro-filtration (ultra-filtration when between $0.1\mu m$ and $10nm$) [JM06]. Under the ultra-filtration limit the pressure drop due to the membrane becomes too big and the only filtering technology is osmosis. The main limits of the filters
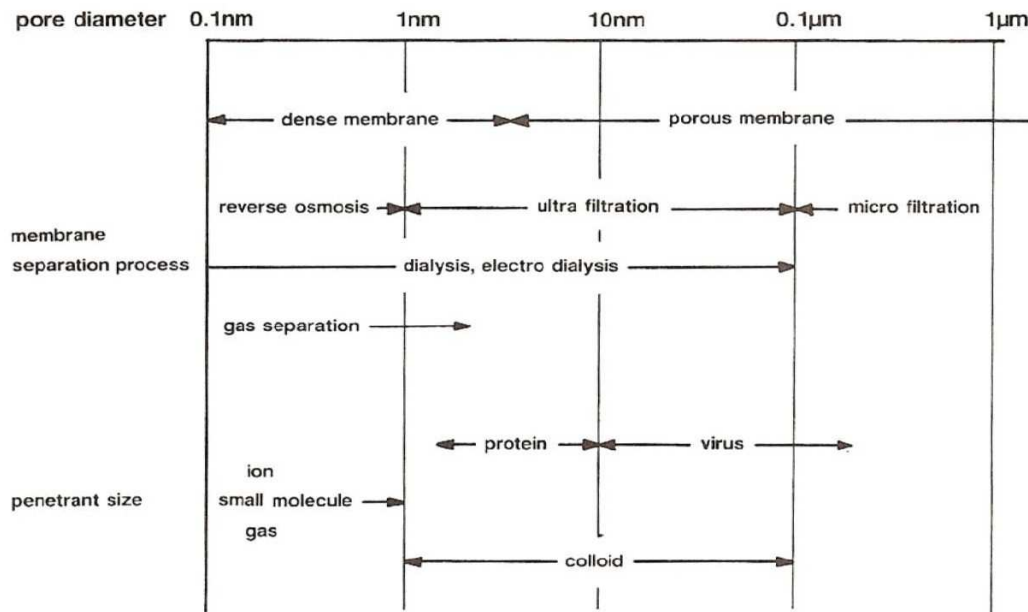
Figure 1.2: Characteristics targets of a membrane as the dimension of the holes
changes (for micro-filtration, ultra-filtration and reverse osmosis).

are their high pressure drop and the short working time [Sto06]. Moreover,
when working in air, the risk of fire arises [Sut08].

1.1.2 Inertial separators

An inertial separator is one which exploits a force related to the mass of
the particles to be separated. It works if the density of the species constitut-
ing the mixture is different [Rho98].

Cyclonic separation exploits both gravitational and inertial forces with-
out the use of filters [MBQ07]. As shown in Fig. 1.3 a high speed ro-
tating (air)flow is established within a cylindrical or conical container
called a cyclone. The air flows in a spiral pattern, beginning at the
top (wide end) of the cyclone and ending at the bottom (narrow end)
before exiting the cyclone in a straight stream through the center of
the cyclone and out of the top. Larger (denser) particles in the rotating
stream have too much inertia to follow the tight curve of the stream
and strike the outside wall, falling then to the bottom of the cyclone
where they can be removed. In a conical system, as the rotating flow
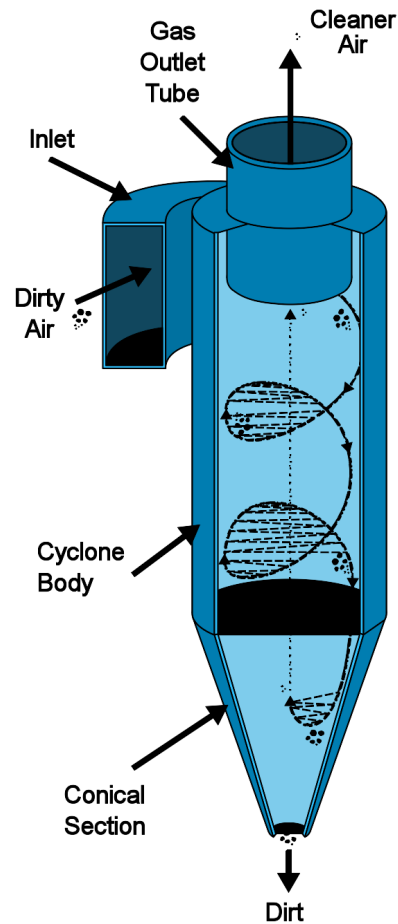
Figure 1.3: Scheme of the working principle of a cyclonic separator.

moves towards the narrow end of the cyclone the rotational radius of the stream is reduced, separating smaller and smaller particles. The cyclone geometry, together with flow rate, defines the cut point of the cyclone. This is the size of particle that will be removed from the stream with a 50% efficiency [SK]. Particles larger than the cut point will be removed with a greater efficiency, and smaller particles with a lower efficiency. The main limit of cyclonic separation is that its use is limited to mixture in which the particles to be separated are hardly distinguishable in density [Sha].

Centrifugation is a process that involves the use of the centrifugal force for the separation of mixtures, used in industry and in laboratory set-

Figure 1.4: Scheme of the precipitation phenomenon.

tings. More dense components of the mixture migrate away from the axis of the centrifuge, while less dense components of the mixture migrate towards the axis [RW01]. Chemists and biologists may increase the effective gravitational force on a test tube so as to more rapidly and completely cause the precipitate ("pellet") to gather on the bottom of the tube [Gra01]. The remaining solution is properly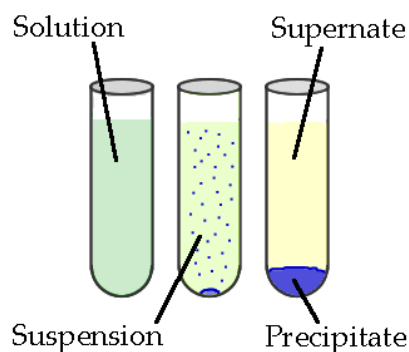 called the "supernate" or "supernatant liquid". The supernatant liquid is then either quickly decanted from the tube without disturbing the precipitate, or withdrawn with a Pasteur pipette. The rate of centrifugation is specified by the acceleration applied to the sample, typically measured in revolutions per minute (RPM) or standard gravity (g). The settling velocity of the particles in centrifugation is according to their size and shape, centrifugal acceleration, the volume fraction of solids present, the density difference between the particle and the liquid, and the viscosity. Centrifugation achieves high quality results, but it requires long time [Leu98].

Precipitation, flocculation and sedimentation: all of them involve as main force the gravitational one [MW]. Precipitation is the formation of a solid in a solution during a chemical reaction, as shown in Fig. 1.4. When the reaction occurs, the solid formed is called precipitate, and the liquid remaining above the solid is called supernate. Powders derived from precipitation have also historically been known as flowers [Adl+67]. Natural methods of precipitation include settling or sedimentation, where a solid forms over a period of time due to ambient forces like gravity or centrifugation [Nat]. According to the IUPAC definition, flocculation is a "process of contact and adhesion whereby the particles of a dispersion form larger-size clusters". Flocculation is synonymous

for agglomeration and coagulation. The action differs from precipitation in that, prior to flocculation, colloids are merely suspended in a liquid and not actually dissolved in a solution. These techniques are slow and require large working volumes [Gar08].

1.1.3   Electric separators

The electric force is the leading one in large number of separators, such as adsorption or electrostatic separator. Adsorption is the accumulation of atoms or molecules on the surface of a material. This process creates a film of the adsorbate (the molecules or atoms being accumulated) on the adsorbent surface [BCZ07]. It is different from absorption, in which a substance diffuses into a liquid or solid to form a solution. The term sorption encompasses both processes, while desorption is the reverse process of "adsorption". In simple terms, adsorption is "the collection of a substance onto the surface of adsorbent solids". It is a removal process where certain particles are bound to an adsorbent particle surface by either chemical or physical attraction. Adsorption is a consequence of surface energy. In a bulk material, all the bonding requirements (whether ionic, covalent, or metallic) of the constituent atoms of the material are filled by other atoms (of the same material). However, atoms on the surface of the adsorbent are not wholly surrounded by other adsorbent atoms and therefore can attract adsorbates. The exact nature of the bonding depends on the details of the species involved, but the adsorption process is generally classified as physisorption (characteristic of weak van der Waals forces) or chemisorption (characteristic of covalent bonding) [McM02]. Electrostatic separation is defined as "the selective sorting of solid species by means of utilizing forces acting on charged or polarized bodies in an electric field". Separation is effected by adjusting the electric and coacting forces, such as gravity or centrifugal force, and the different trajectories at some predetermined time. Separations made in air are called Electrostatic Separation. Separations made using a corona discharge device, are called High Tension Separations. Separations made in liquids are termed separation by dielectrophesis. Electrophoresis is when separations are made if motion is due to a free charge on the species in an electric field [Tar86]. A similar approach is used in the electrostatic separators in which the electric field sources are wires and plates, as shown in Fig. 1.6. The achieved force is huge because the wires are inside the flow, but this kind of separator requires a big working volume.

1.2 HGMS

1.2.1 Working principle

Magnetic Separation is a powerful method utilized from long time in the treatment of strongly magnetic mineral ores and for the removal of ferromagnetic impurities from mixtures [Obe76; Svo87; Ana02; FY05]. The magnetic force acting on a particle with volume V_p can be expressed as

$$\mathbf{F}_m = V_p \mathbf{M}_p \cdot \nabla \mathbf{B}_e = \frac{V_p \chi_{p,eff}}{\mu_0} B_e \nabla B_e \qquad (1.1)$$

where the magnetization of the particles $\mathbf{M}_p$ is proportional to the field $\mathbf{B}_e/\mu_0$ through an effective susceptibility ($\chi_{p,eff}$) that depends on material and on the shape of the particle. The shape dependence is due to the fact that the magnetizing field within the particle is not just due to the applied field, but also includes a de-magnetizing field resulting from the magnetization of the particle itself. For spherical particles the effective susceptibility cannot exceed the value of 3 (see Appendix A.1) [LL87; FY05; Wat73]. Hereafter we will simply call the susceptibility of the powder χ_p subtending the subscript eff.

Both magnetic filters and magnetic separators exploit the magnetic force $\mathbf{F}_m$ acting on a magnetizable particle surrounded by a fluid with different magnetic permeability when a non-uniform magnetic flux density field $\mathbf{B}_e$
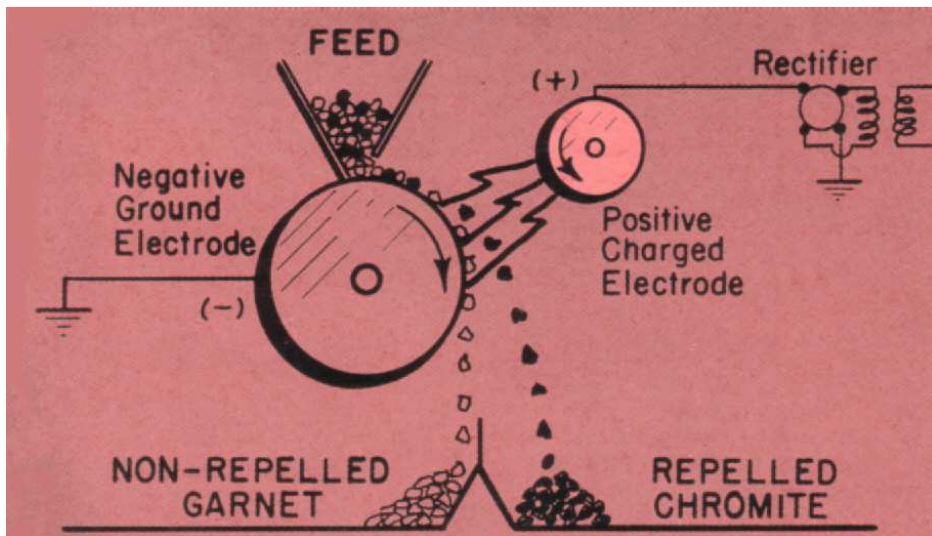
Figure 1.5: Working principle of an electro-static separator.
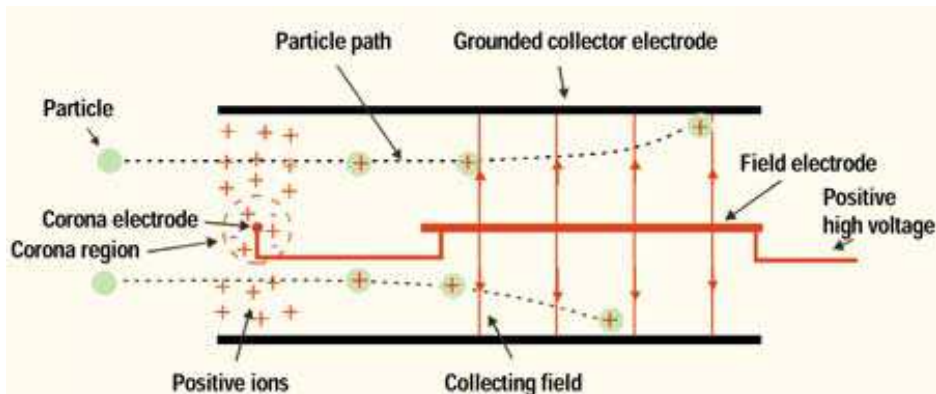
Figure 1.6: Working principle of the electrostatic filters with wires.

is applied. The magnetic force expressed by eq. (1.1) must be able to distinguish between two or more substances acting on them with different (or, in the best case, opposite) strength as shown in Fig. 1.7 and in Fig. 1.8. Magnetic separators (also known as open gradient filters or batch separators) are often used for separation on fixed volumes of solution with the aim of removing some components [ALM03; Nak+03]. The processes are not quick and the gradient of the field is usually lower than $500T/m$. In magnetic filtration that force is used to capture and withhold the particles against the drag force of the surrounding fluid, the gravitational force and the random-
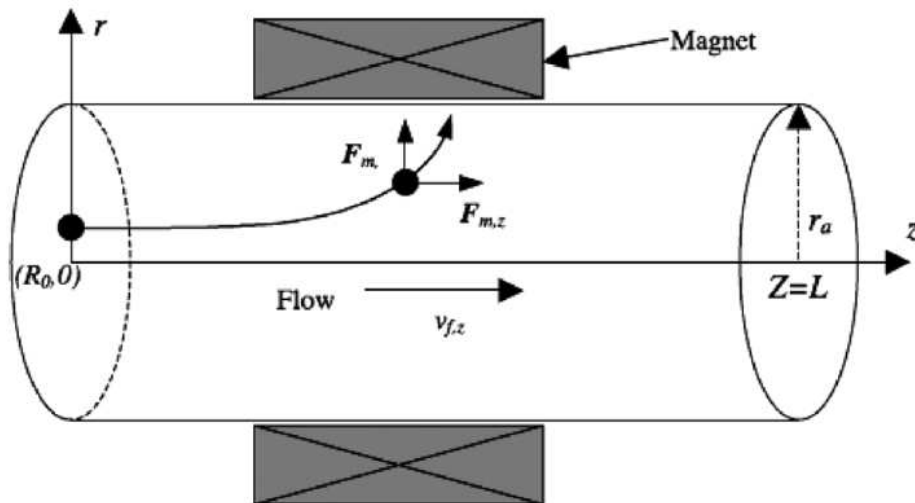
Figure 1.7: Scheme of the magnetic separation working principle.

izing effects of Brownian motion. In this case, the filter is usually provided with some kind of ferromagnetic active element where the particles are collected (such as a grid of wires or some wool). The resulting field gradient is
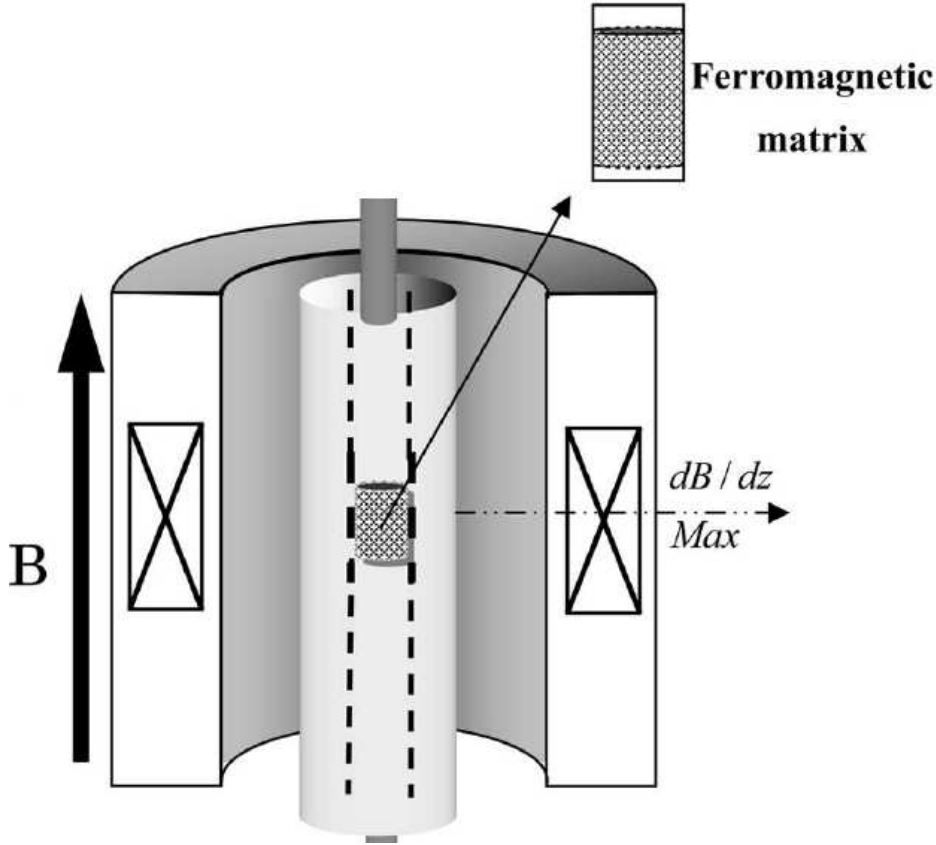
Figure 1.8: Scheme of the magnetic filter working principle.

usually very intense (reaching $10^4 T/m$), large enough to capture also weakly magnetic particles in a quickly moving flow. In this work we will concentrate on filtration, but we will use both the separation and filtration terms as synonyms for coherence with the available literature. The force described by eq. (1.1) results from the product of two terms: the magnetization of the particle and the gradient of the external field. The first arises when the particle is a magnetic dipole (like a lodestone) or when, as in the right form of eq. (1.1), the particle is magnetized by an external magnetic field. That field, which which we call $\mathbf{B}_e$, is usually made of three terms: a relatively uniform field $\mathbf{B}_0$ produced by sources external to the filter, a field produced by the ferromagnetic filtering elements, and the field produced by the magnetic mo-

ments of all the other particles. Usually only $\mathbf{B}_0$ turns out to be important to magnetize the particles, while the field produced by the magnetization of the other particles and of the filtering element can usually be neglected. If the intensity of $\mathbf{B}_0$ is enough it is possible to achieve magnetic saturation of the particles and obtain the maximum possible magnetic force, so that the particles effectively behave like permanent magnets. Moreover, the same field is used to saturate the filtering elements which are usually made of ferromagnetic material. The external magnetic field is usually provided by superconducting (SC) magnets because they are able to provide the desired intensity on large volumes [FS08; Neg+99]. The gradient term of eq. (1.1) is mainly provided by the filtering elements. In fact the external field is usually slowly varying while the filtering element, being constituted by small pieces of ferromagnetic material (wires, fibers and so on) originates a magnetic field which is quickly changing near the surfaces of the elements. The rate of that change, i.e. the value of the field gradient, is inversely proportional to the transversal dimensions of the filtering elements and, when it is able to act on paramagnetic particles as well as on ferromagnetic ones we speak of HGMS (High Gradient Magnetic Separation). The gradient of the field produced by the other particles is usually negligible if they are constituted of paramagnetic or diamagnetic material. When the particles are made of ferromagnetic material a strong particle to particle interaction arises which makes the particles aggregate together. This phenomenon rises the effective particle diameters helping the capture and withholding processes.

The more claimed benefits of HGMS technology compared to traditional ones are:

- low environmental impact;

- small dimension;

- low pressure drop;

- long saturation time;

- high selectivity;

- high working speed.

Anyway the cost of the SC magnet is still an obstacle to the diffusion of HGMS [SML04]. The use of permanent magnet as external sources of the field, as studied in this work, would be less expensive, provided that the reduction of the applied magnetic field is compensated by an increase of the field gradient, realized reducing the size of the ferromagnetic fibers, i.e.

using an extra fine or finer stainless steel wool matrix. Moreover, when using SC magnets or permanent magnets (PM) instead of traditional resistive coil electromagnets other benefits arise: the reduced electrical usage and the portability with cryogen-free magnet (important for temporary cleanup or remote site) [Coe02].

1.2.2 State of the art

Due to the development of SC magnet technology, enabling the production of a high magnetic field on large volumes at a relatively low cost, High Gradient Magnetic Separation (HGMS) has been intensively studied in different fields including weakly magnetic ores treatment, coal treatment, pollution control and also for the filtration of paramagnetic powders from liquid waste on an industrial scale [Bru+05; Yav+06a; ERP97]. Despite a lot of research has been carried on, in both the theoretical field and the experimental one, the HGMS is still a complex and not well understood subject. The most used models borrow a lot from the deep-bed filtration (DBF) ones in which the filtering elements working principles are not well understood, but a parametric approach is followed [EIA09]. Anyway a more extensive comprehension of the process is very desirable because it can allow a more accurate design of the filter reducing the problems connected to the plugging of the filter and its saturation. The plugging of the filter is a critical phase in industrial application because it often involves stopping the filtering activity at all or to switch, via a bypass, to a second one [Sah+99]. The saturation of the filter can have dramatic consequences: it can lead to an increase of the pressure drop (which can damage the filter itself) and to a reduction of the efficiency of the filter. The efficiency loss is due to the layer of particles growing on the filtering elements which, increasing their radius, reduces the gradient of the magnetic field and, in particular when filtering paramagnet or diamagnetic particles, leads to a reduction of the effective filtering elements magnetization.

Mathematical models

As previously stated a general theory of the functioning of magnetic filters doesn't exist nowadays. One of the reasons for this failure is that the forces acting on sub-micro-metric particles, such as Brownian force, Van Der Waals forces, London dispersion forces and frictional forces, depends on the shape and on the size of the particles and on the surrounding conditions which are very difficult to know and describe on the scale of the particles [Kir04; KS77]. Moreover it's not straightforward to determine if it is possible to extend the

physical results obtained on a macroscopic scale to the particle scale. A second limit that makes the study of the magnetic filters hard to develop is the extension of the results obtained from the study of the mentioned forces acting on the particles to the whole filter. The first attempt to develop a theory for the DBF, dated 1970, consists on the Herzig conservation equation governing the process [HLG70]. The key parameter resulted the efficiency of deposition of particles, which requires, for its estimation, a model for the particle capture. During the last three decades mainly four approaches have been followed in order to develop such a model:

- empirical;

- stochastic;

- network;

- trajectory analysis.

While empirical models are the easiest to develop they are limited to particular designs and physical conditions [HU80]. Among the three remaining models the analysis of the trajectory turned out to be the more studied because of the logical relations with the problem: in the calculation of Lagrangian trajectories is, in fact, possible to include both short-range forces and long-range forces contribution. In DBF theory the long-range forces (the gravity force and, in particular, the drag one which is determined by the geometry of the system as a whole) are responsible for the motion of the particle through the filter, the short-range forces are responsible for their capture and retention. The main difference between the classical DBF and magnetic one relies on the acting forces: when the magnetic one is considered is possible to neglect all the other forces except for the drag one. In other words we have no distinction between long and short range forces, but the two considered forces act on both scales.

Here I try to give a short review of the most important branches in the field. The first important attempt to apply this approach to HGMS was made by Watson in 1973 [Wat73]. Watson numerically solved the problem of the trajectory of a paramagnetic particle flowing orthogonally to a ferromagnetic circular wire of radius a, magnetically saturated with magnetization equal to M_s, infinitely long when an external uniform magnetic field H_0 was present, as shown in Fig. 1.9. He founded out a new parameter: the critical distance R_c for the capture of the particle as a function of the rate of its initial velocity V_0 and of the *magnetic velocity* V_m, a function of the magnetic parameters. This function is widely used by many authors because, when related to the
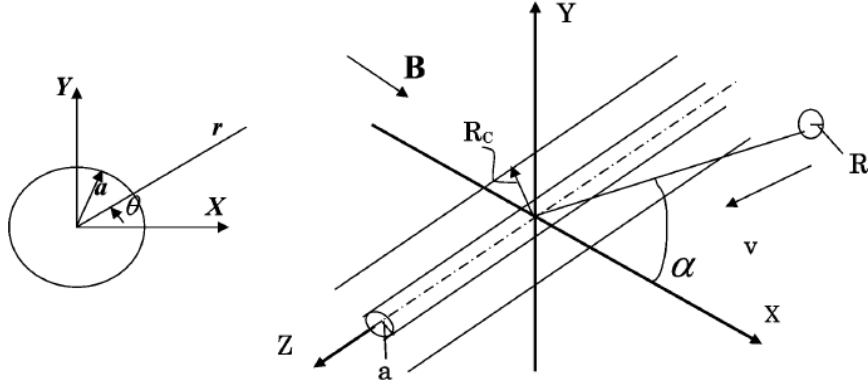
Figure 1.9: Paramagnetic particle carried by a fluid approaches a cylindrical ferromagnetic wire perpendicular to the wire axis described by Watson in 1975.

fluid velocity, it keeps into account their relative influence to the motion of the particles. The same Watson developed its own theory founding an explicit expression for the magnetic velocity [Wat75]:

$$V_m = \frac{2}{9} \frac{\chi M_s H_0 R^2}{\eta a} \qquad (1.2)$$

in which χ is the magnetic susceptibility of the particle and η the viscosity of the slurry. The passage from the single wire to the whole filter characterized by an average filling factor F was made considering the cumulative cross section of a slice of the filter, like the one shown in Fig. 1.10, and integrating over the length L of the filter obtaining:

$$\frac{N_{out}}{N_{in}} = \exp\left(-\frac{4FR_cL}{3\pi a}\right) \qquad (1.3)$$

where N_{out} and N_{in} are the number of particles in the influent and in the effluent, respectively. These results are only valid when the considered flow is a laminar one (with Reynolds number $R_e = \rho V_0 a/n > 1$). A similar approach was followed and extended to the study of the sediment by Breschi et al. at the Applied Superconductivity Laboratory of the University of Bologna (LIMSA) in the late nineties [Bre97; CBN98; Neg+99; Fab+03a; Fab+03b]. An improvement to the Watson's model was made in recent years by Akbar et al. considering, instead of the length of the filter, a normalized length L_a defined as [Esk+07]:

$$L_a = \frac{V_m}{V_0} \frac{L}{a} \qquad (1.4)$$
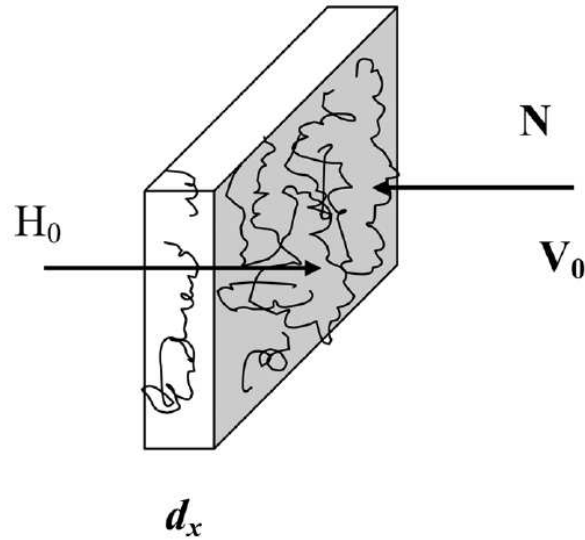
Figure 1.10: Section of filter of thickness dx with the fluid containing N particles per unit volume incident on the filter with an entrance velocity V considered by Watson in 1973.

On another side Clarkson and Kelland, in 1975, improved the Watson's model adding to it the contribution due to the gravitational and the inertial forces, as visible in Fig. 1.11 [CKK76]. Considering a Reynolds number between 0.1

Figure 1.11: Criteria for capture defined by Clarkson and Kelland.

and 40 they were able to add a corrective term K_f to eq. (1.3) in order to

Figure 1.12: Schematic of ribbon-like fiber, infinite in z-direction, with approaching particle, showing two possible modes of build-up of particle layers; case (a) and case (b) (after Luborsky 1975).

take into account the random fiber to fiber interaction obtaining:

$$R = 1 - \frac{N_{out}}{N_{in}} = 1 - \exp\left(-\frac{2K_f F R_c L}{\pi AB}\right) \tag{1.5}$$

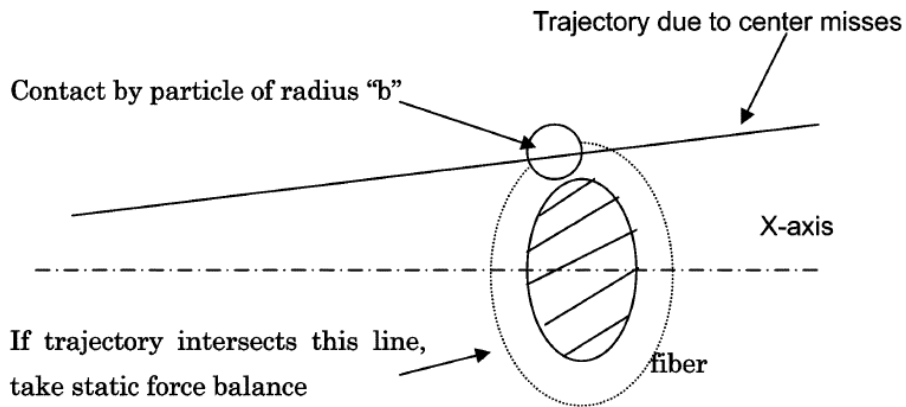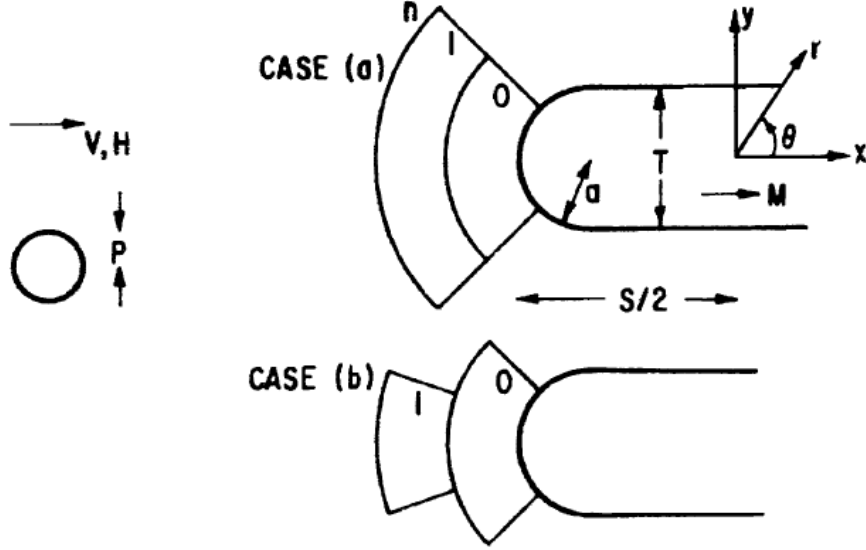where AB is the cross section area of the elliptical fibers [Gol04]. Thanks to that equation the authors could state that increasing the radius of the fibers the capture efficiency of the filter decreases while, increasing the radius of the particles, the efficiency grows. In the same years, Luborsky et al. extended Watson's model considering, instead of cylindrical infinity long wires, ribbon-like and rod-like infinity long wires, as shown in Fig. 1.12, substituting the reduced cross section ε to the critical distance R_c [LD75]. The expression for the capture efficiency that they obtained:

$$R = 1 - \exp\left(-\frac{fFL\varepsilon}{3S}\right) \tag{1.6}$$

in which S is a geometrical parameter. R is supposed to be made of two terms. The first one, responsible for the mechanical recovery fraction, was considered as:

$$R_{mec} = 1 - \exp\left(-\frac{fFL\zeta}{3S}\right)$$

in which they introduced the reduced mechanical cross section parameter ζ
to take into account the *traps* due to the irregular disposition of the fibers.
The other term, responsible for the magnetic capture, can so be expressed
as:

$$R_{mag} = 1 - \exp\left[-\frac{fFL(\varepsilon + \zeta)}{3S}\right]$$

These results, and the analogue ones obtained by Uchima in the 1976 [Uch+76],
suggested that not only magnetic particles, but also non magnetic ones, could
be captured be randomly packed filter. To be aware of that effect Uchima
suggested to arrange the wires parallel to the main flow obtaining a simple
equation for the capture efficiency:

$$R = S_c^* F \tag{1.7}$$

in which the capture cross section S_c^* is expressed as:

$$S_c^* = \frac{4}{\pi}\left[\frac{L}{A}\frac{V_m}{V_0}\right]^{1/2}$$

Uchima realized a prototype of filter with wires arranged that way achieving
a good experimental agreement [HU80]. Aware of the limits comported by
the study of friction-less flow, in 1978, Birss and colleagues considered an
idealized wires disposition in order to develop a model in which Newtonian
fluid flow was considered [Bir+78b; Bir+78a]. In their model, thanks to a
rotational symmetry, they were able to model the system using a *muffin-tin*
velocity potential with fully radial symmetry obtaining as shown in Fig. 1.13:

$$R = 1 - \frac{v_{r_0}}{v_0}\exp(-KFr_{i_a}^2) \tag{1.8}$$

in which v_0 is the ideal velocity of the flow, v_{r_0} is the velocity in r_{r_0} (r_{r_0}
is the distance from the wire at which $dv/dr = 0$ and r_{i_a} is a geometry-
dependent distance. The improvements due to this new approach resulted
limited compared to a modified Uchima's model [BPS80]. In recent years
Herdem modified the model developed by Birss and Gerber introducing two
new parameters: the volume fraction of the wires in the system γ and the
measure of the non-circularity of the capture cross section a_f [HKA00]. Con-
sidering N as the number of magnetic particles per unit volume entering the
filter they defined, for a unitary area, the number of particles entering per
unit time as $N_{in} = N\langle V\rangle$ where $\langle V\rangle$ is the average velocity of the fluid in
the filter. In a similar way they defined $N_{out} = N_{ne}\langle V_e\rangle$ where N_{ne} is the

number of non-captured particles per unit of volume and $\langle V_e \rangle$ the average escape velocity. They expressed the probability that a particle would not be captured as:

$$\bar{\omega} = (1 - a_f \pi a^2 r_{ca}^2)^n$$

where $r_{ca} = r_c/a$ is the capture radius; introducing the normalized capture cross section S_a^* they can rewrite it as:

$$\bar{\omega} = N(1 - a_f \pi a^2 S_a^*)^n \tag{1.9}$$

and assuming that $S_a^* \approx \frac{4}{\pi} L_a^{0.5}$ the equation of the filter capture efficiency can be written as:

$$R = 1 - \exp\left(-\frac{4\gamma a_f}{\pi} L_a^{0.5}\right) \tag{1.10}$$

In 1988 Sandulyak experimentally improved that model writing a semi-empirical relation in the following form [San88]:

$$R = \lambda \left[1 - \exp\left(-\alpha L\right)\right] \tag{1.11}$$

in which he introduced the ratio between the number of the magnetizable particles and the total number of the particles λ and the empirical constant α, in general dependent on geometrical and magnetic properties of the system. A further, recent, improvement to the Sandulyak's model has been developed by Abbasov et al. considering only the magnetic force F_m and the drag force F_D both in a simplified form [AKH99; AA02]. About the former they
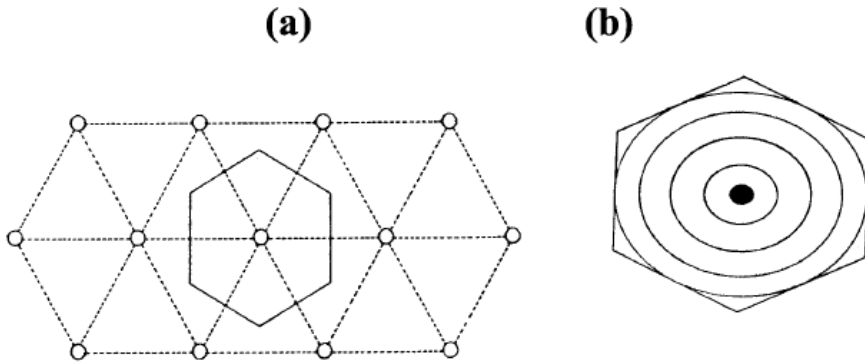

Figure 1.13: (a) Array of wires with Wigner-Seitz cell. (b) Muffin-tin velocity well around a wire (after Birss 1978).

described it acting on a particle near a wire as:

$$F_m \approx \frac{\pi \delta^3}{2} \frac{\mu_0 \chi \mu^{1.38} H^2}{d(R/a)} \tag{1.12}$$

where χ is the *effective* susceptibility defined as $\chi = \chi_p - \chi_f$ (in which χ_p is the susceptibility of the particle and χ_f is the one of the fluid), H is the external magnetic fluid and δ is the effective particle size. The drag force acting on a spherical particle in a fluid of density ρ_f and with drag coefficient C_D was stated to be:

$$F_D \approx C_D \pi \rho_f U^2 \delta^2 / 8 \tag{1.13}$$

where U is the local velocity of the fluid. From these two equations, after some maths necessary to express the relation between R/a and U, they described the efficiency of the filter as:

$$R = \lambda \left\{ 1 - \exp \left[-2.1 \times 10^{-3} (V_m/V_f)(L/d)\alpha L \right] \right\} \tag{1.14}$$

The authors emphasized that eq. 1.14 was valid only for a very low Reynolds number ($R_e << 1$). In order to overcome this limitation they took in consideration also the lift component of the drag force obtaining the following:

$$R = \lambda \left\{ 1 - \exp \left[-2.12 L \left(\frac{\chi H^{0.75} \delta}{\rho_f V_f^2 d^{2.7}} \right) \right] \right\} \tag{1.15}$$

where the strong dependency of the filtering process on fluid velocity and particle diameter are visible.

On another side there was some effort to develop a model for the filtering process based on the analysis of some dimensionless parameter. Herdem et al. defined the *magnetic pressure parameter* as [HKA00]:

$$P_M = \frac{K \mu_0 \mu^{1.38} H^2 (1 - \varphi)\delta L}{d} \tag{1.16}$$

in which K is the effective magnetic susceptibility and d the filter diameter. P_m has the dimension of a pressure and depends only on magnetic values. They used eq. (1.16) in writing the logarithmic capture efficiency of the filter as:

$$\beta = 1.4 \times 10^{-2} \left(\frac{P_M}{\Delta P} \right)^2 \left(\frac{1 - \varepsilon}{\varepsilon} \right)^{0.6} L_D \tag{1.17}$$

where L_D is the length of the filter normalized with respect to d. A similar approach was followed by Gerber in the case of randomly spaced spherical magnetic elements [GL89]:

$$R = \lambda \left\{ 1 - \exp \left[-5.36 \times 10^{-2} L_d \left(\frac{P_m}{\Delta P} \right)^{0.6} \right] \right\} \tag{1.18}$$

A different side of the problem, often neglected in the literature because of its over complications, is the one of the time evolution of the system. As said it turns out to be very important, in particular in industrial applications, to determine the breakthrough characteristics of the filters. Most of the studies based on the DBF resulted in a underestimation of the working time because the mass-balance model predicts the breakthrough characteristics starting decreasing as soon as the filtration starts [CKT82]. The experimental analysis
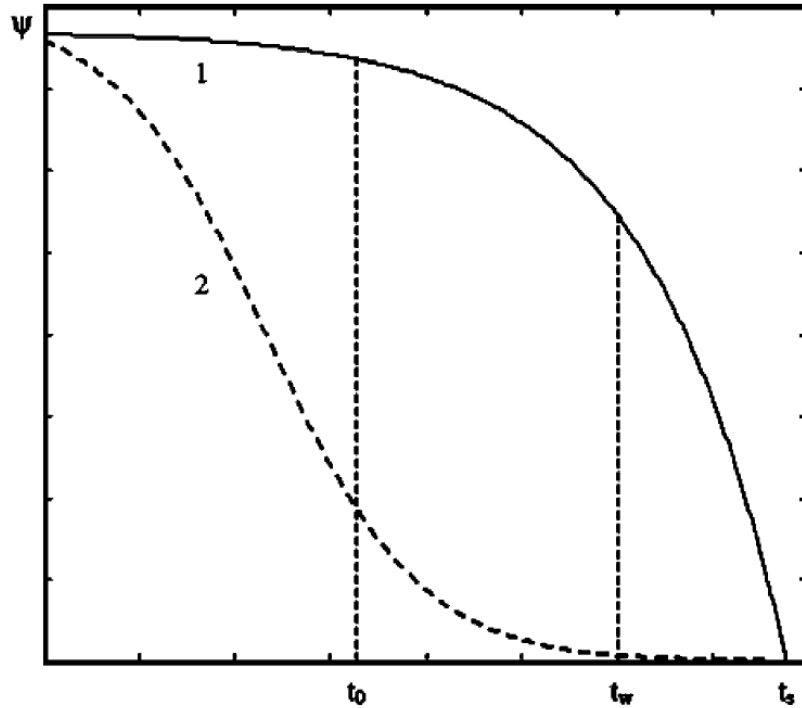
Figure 1.14: The filtering efficiency Ψ as function of the time. The dashed curve is obtained from DBF model while the solid one is obtained from the exponential law described in eq. (1.19) (after Abbasov 2003).

shows that the filter efficiency remains almost constant in a first period, t_0, drops down slowly in a second period, $t_W - t_0$, and stops working at a near time, t_S, as visible in Fig. 1.14. To describe that dynamic behaviour Koksal et al. proposed the following equation [KAH03]:

$$R = \lambda \left\{ 1 - \exp\left[\alpha(t - t_W) - \beta x \right] \right\} \tag{1.19}$$

where α and β are the capturing and detachment coefficients off the particles, respectively. The two parameters, considered as stochastic characters, must

be determined on the bases of the knowledge of the forces and phenomenons
(such as pores and fibers saturation and detachment and recapture along the
whole filter) acting on the particles. They used the expression given in eq.
(1.16) for β and defined α as:

$$\alpha = 7.12 \times 10^{-2} \frac{\eta v_f}{Dd} \left(\frac{P_m}{\Delta P} \right)^{-0.4} \tag{1.20}$$

where D is the filtration velocity of the cleaner liquid. Considering $t_W \approx 1/\alpha$
they derived:

$$t_S = \frac{1 + \beta x}{\alpha}$$

achieving a good agreement with the experimental behaviour of their filter.

Another way is becoming followed nowadays: the computational ap-
proach. This latter method has been recently experienced in Japan by Okada
et al. [OM05]. They applied a Computational Fluid Dynamics (CFD) model
to simulate HGMS process with magnetic force, drag force and diffusion.
The base equation of the problem is in the form:

$$\frac{\partial}{\partial t}(\rho\varphi) + \vec{\nabla} \cdot (\rho\vec{u}\varphi) = \vec{\nabla} \cdot (\Gamma\vec{\nabla}\varphi) + S \tag{1.21}$$

where ρ is the fluid density, φ is the transported scalar variable (in that case
the particle mass fraction), $\vec{u}$ the fluid velocity field, Γ the scalar diffusion
constant and S the scalar source term. From left to right, the four terms in
eq. (1.21) are commonly referred as the transient, convection, diffusion and
source one. In order to solve the equation only the magnetic and drag forces
are considered. The particles are considered spherical and non-interacting
and the fluid flow is a two-dimensional laminar one. The resulting system
is solved with a commercial, finite elements code able to describe the time
evolution of the system as the shape of the deposits changes. Anyway the
problem is still too oversimplified and the results are of quite small interest.

HGMS applications

The problem of separation is almost omnipresent in manufacturing and in
industrial production: from ore treatment to food, from steel purification to
pharmaceutics and so on [NS03]. Sedimentation and centrifugation are often
used when speed is not an issue while magnetic separation can provide a faster
method, especially if the removing substance has some magnetic properties
[Hub+01; Fle91; Moe+04]. However, even in the absence of intrinsically mag-
netic components the use of specifically designed magnetic beads, targeted

(a) **(b)**

Figure 1.15: (a) Natural kaolinite. (b) Kaolinite after HGMS cleaning.

to the product of interest, can make a magnetic separation feasible for virtually any system [Yav+09; Zha07]. Such processes offer very different kinds of trade-offs in speed and selectivity as opposed to the more conventional approaches. Limiting the review of the available applications of the magnetic separation to separation of material from liquids we can evidence one of the most important features when compared with solid state filters (membranes): in magnetic filter the pressure drop is virtually absent while for the membranes, particularly when talking of ultra-filtration (diameter of the particles of the order of the micron) or nano-filtration (sub-micron diameters), the induced flow resistance is very significant and a big amount of energy must be provided in order to maintain the flow through the filter. Moreover solid state filters have to be changed or cleaned more often [KAH03]. A short list of the main actual applications of HGMS follows [Yav+06a; Yav+09]:

Kaolin de-colorization China clay (also known as kaolin) is a clay mixture primarily consisting of kaolinite mineral. The name cames from a Chinese region (Ching-te chen) where a particularly appreciated porcelain was produced using that mixture. Today kaolin is primarily used in paper manufacturing with two functions: as a filler between the pulp fibers and as surface coating for a white glossy finish. The color of the kaolin is influenced by the contained impurities, which are often iron-based as visible in Fig. 1.15a. Because of the resistance of the kaolin to chemical cleaning, HGMS has been used in kaolin industry since the seventies leading to high quality kaolin as visible in Fig. 1.15b and is nowadays responsible for more than 70% of the world production of white porcelain and paper [Ode76]. A typical plant would have an HGMS with a filter diameter of $2m$ and a capacity up to $20t/h$ [HW82;

HBW82].

Paper Similar to the kaolin purification is the paper treatment to achieve a
more white paper [NT06; Kak+04];

Steel factories On average, generating $1t$ of steel requires $151t$ of water for
cooling and cleaning purposes; the resulting wastewater is filled with
many magnetic particulates and other iron-containing impurities and
must be cleaned [Ha+; Tas; Kar03]. The choice of HGMS as filtering
technology has emerged a natural one saving a great amount of time
and space removing up to 80% of contaminants [Obe+75; HNW76].

Power plants and pollution In power plants (both conventional and nu-
clear) HGMS is used to remove ferromagnetic or paramagnetic partic-
ulates which extends the lifetime of cooling systems. Magnetic separa-
tions can also be used to treat pollution. Fly ash from coal power plants
is 18% iron oxide. Magnetic filtration has been applied to capture 15%
of waste fly ash, thus providing a means for recycling. Estimates show
that this can replace some of the magnetite used in industry [HBW82].

Ores separation The treatment of ores with magnetic separation is carried
out primarily on iron-containing ores. Conventional chemical and set-
tling methods are not suited for this purpose given the similar density
and reactivity of transition metal minerals. The magnetic nature of
iron species, however, is unique and thus a natural target for magnetic
separations. Among the iron ores taconite is most often subjected to
magnetic treatments. From a taconite ore (33% iron) Kellard was able
to recover iron at 95% on a 5 cm/s flow rate [Kel73]. Today, Metso Min-
erals, Inc. (formerly Sala International AB) offers magnetic separators
that can separate iron from ores with nearly 100% efficiency (depend-
ing on the particulate sizes, magnetic field and flow rate). Magnetic
separation of pyrite (FeS_2) from coal for desulfurization is also a com-
mon process [MK78]. The weakly magnetic nature of pyrite, however,
requires that the raw ore be pre-treated thermally to convert the pyrite
(FeS_2, $M_s = 0.3emu/g$) to more strongly magnetic pyrrhotite (Fe_7S_8,
$M_s = 22emu/g$). Up to 91% removal of sulfur from coal can be achieved
by microwave heating followed by a magnetic separation [UAA03].

Food industry Strict food quality standards require the food products to
be contaminant free, where mainly rare earth elements (REEs) consti-
tute the majority. The food industry, therefore, has found magnetic
separations to be an ideal method to remove REEs from food ingre-
dients. Similar to the ore beneficiation or desulfurization, the target

substances are weakly magnetic and require the high gradients of a magnetic field to be removed in a continuous food production line. Bunting Magnetics Co. offers magnetic metal separators and metal detectors for the quality of food and extended service life of the processing equipment, especially for cheese processing, chocolate plants, pet food processing, flour mills, spice plants, vegetable processing. Removal of both ferrous and nonferrous tramp metals is achieved by their line of food safety products for the food processing industry.

Water treatment With new lowered maximum permissible concentration for arsenic in drinking water ($10\mu g/l$) in the USA in 2006 (Arsenic Rule, 2006), techniques for better arsenic remediation without much desorption have gained more importance [SF03]. Currently, coprecipitation, adsorption in fixed-bed filters, membrane filtration, anion exchange, electrocoagulation, and reverse osmosis are methods of interest. However, cost efficiency and waste quantity requires further development that would aid in resolving the problem [Hos+05]. Arsenic adsorption and desorption are heavily influenced by adsorbent particle size [May+07; Yea+05]. Nanoscale magnetite (Fe_3O_4, $12nm$) can remove 200 times better than its commercial counterparts, which allows a significant cut in waste, instead of $1.4kg$ of bulk iron oxide to remove arsenic ($500\mu g/l$) from $50l$ of solution, $15g$ of nano magnetite can be used [Yav+06a; Yav+06b]. Apart from surface area increment, an obvious gain while going down to nanoscale, available open sites with the proper chemistry (free Fe on the surface) can be accounted for this unexpected result. Size dependent magnetic properties bring controllability and along with mobility, a critical nanoscale advantage, provides unique applicability, if put in a system, in especially household uses where electricity is not readily available [Mit+03]. In the seventies De Latour and Kolm treated water samples from the Charles River (Fe_3O_4 seeding, 5 ppm Al^{3+}) with a high flow velocity HGMS ($V_0 = 136mm/s$, $H_0 = 1T$) and reduced coliform bacteria from $2.2 \times 10^5/l$ to $350/l$, turbidity by 75%, color by 95%, and suspended solids by 78% [Lat73; LK75; GB83]. Later, Bitton and Mitchell removed 95% of the viruses from water by magnetic filtration following a $10min$ of contact period with magnetite (added to be $250ppm$). The following years, Boliden Kemi AB reduced phosphorus of water supplies at least 87% [GB83]. Also known as Sirofloc process, micron-sized magnetite is also used to remove color, turbidity, iron, and aluminum from water sources as an alternative to metal-ion coagulation [GMS88]. Recently, Denizli and coworkers magnetically modified yeast cells for facile capture of mercury

with fast biosorption rates (within $60min$) and efficiency ($76.2mg/g$ for Hg^{2+}) [Yav+06a; Yav+06b].

Biotechnology The ability to control remotely inspired many biotechnologists and medical scientists to investigate magnetic solutions for several biochemical processes, such as protein and cell separations and purifications, magnetic drug targeting and delivery, and enzyme-based biocatalysis [Wu+04]. Unlike industrial applications, in-lab or batch applications require tailor-made magnetic materials but remain fine with steady, not continuous, bench-top or batch, process solutions. In order to achieve bio-compatibility biochemists tend to use naturally existing minerals, such as magnetic iron oxides (magnetite, Fe_3O_4 and maghemite, $\gamma - Fe_2O_3$), due to their biologically safe nature i.e. in the ferrofluids [Tar+03; ACA05].

Chapter 2

Mathematical Model

The lack of knowledge related to the high gradient magnetic separation phenomenon limits its applicability and reliability, so that, as stated, it requires a more deep study on both the theoretical and the experimental points of view. The theoretical analysis of the process involve the study of a many body system (a huge number of particles interacting with the ferromagnetic matrix has to be considered) on different scales (both particle scale and filter scale) at the same time. Moreover, at the microscopic scale, the considered laws of physics are often quite uncertain, being tested only at the macroscopic scale. The *finite elements method*, in a fully three dimensional approach, is not affordable with an ordinary computer: considering the whole filter as a one cubic meter object and the elements of the ferromagnetic matrix having linear dimension on the micro-metric scale would lead to a mesh of, at least, 10^{10} elements. As a consequence, approaches like the one of Okada [OM05] are limited to a bi-dimensional one. On the other side the study of the problem starting from the single wire approximation with an analytical solution is oversimplified and leads to not completely reliable results [WB86; Obe76].

The approach exposed in this chapter is used to develop a model which is original and versatile, but applies to the experimental setup described in Chapter 3 in particular. Its aim is to overcome both the exposed limits through a mixture of a statistical approach and an analytical one. The problem looks upon the removal of a hypothetical pollutant, for example arsenic, through its bounding into an iron oxide. The liked adsorption processes, which strongly depends upon the adsorbent dimensions, are well known and established ones [Oli+02]. Some typical reactions for heavy metals are shown in more details in Appendix B.1. As a consequence of this hypothesis the resulting problem concerns the removal of a given iron oxide from a working fluid without caring about any specific pollutant. This possibility relies on the assumption that the bounding does not change the magnetic properties

of the iron oxide. This is a good assumption: being the bounding a super-
ficial phenomenon while the magnetic properties are related to the volume
of the particles a relative influence is unlike. Starting from the study of an
"average" element of the filter with analytically known induction field and
velocity field it turns out to be possible to study the particle trajectories.
From the analysis of the trajectories in such a complex geometry is possible
to characterize the considered element. The element is then related to the
whole filter thanks to a model for the conservation of the number of the
particles.

2.1   The Cell

2.1.1   Cell geometry

As stated a magnetic filter is a macroscopic device with dimensions of
the order of the tenth of a centimeter. The considered filter is an HGMS one
in which the filtering element is constituted by iron steel wool with irregular
shape and random disposition of the fibers (as visible in Fig. 2.1a). Since
the spacing among the fibers of the wool are several orders of magnitude
lower than the filter length and of unknown geometry, the magnetic field and
the fluid-dynamic regime has been determined in an elementary "mean" cell,
using an integral model with spatially periodic conditions. The geometry
of the fibres has been modelled with triangular prisms and tetrahedrons in
order to reproduce as much as possible the real geometry of the wool. The
cell is characterized by the *packaging factor* Γ which is defined as the ratio
between the steel fibres volume and the cell volume:

$$\Gamma = \frac{V_{wool}}{V_{cell}} \tag{2.1}$$

The distribution of the non-intersecting polyhedrons is chosen in order to
obtain a given packaging factor Γ. The dimensions of the cell have to be
chosen in order to keep the computational burden for the computers accept-
able. On the other side the cell must be meaningful on the average. This
means that it's not appropriate to consider a cell which contains only a fiber
(nor an empty one). Considering fibers with transversal dimensions of the
order of $20\mu m$ a cell of $1mm \times 1mm \times 1mm$ has been chosen [Mar+09a].
Moreover, the cell is enlarged with a frame of variable thickness in order to
achieve a more correct boundary condition of the magnetic induction field
and of the fluid velocity field. The thickness is chosen inversely proportional
to the packaging factor in order to contain a minimum, but non zero, number
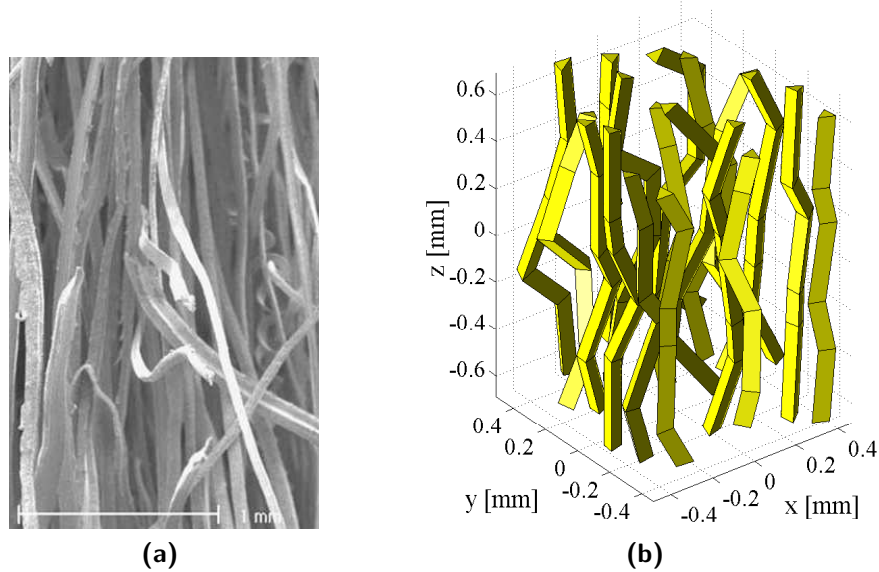
Figure 2.1: (a) SEM view of steel wool and (b) a possible random geometry of an elementary "mean" 3D cell

of fibers in it. An analysis has been carried out in order to check the validity of this approach: a large number of tests have been performed studying the change in the trajectories when considering the cell surrounded by one or two layers of cell. The obtained trajectories turn out to be undistinguishable (such as the magnetic field and for the velocity one), so that the cell approximation resulted validated [Mar+09b]. The cell can be adapted to a 2D flow considering long fibres made of parallel prisms, without bending and breaking, in the central plane of the cell. Fig. 2.1a shows a SEM (Scanning Electron Microscope) view of a steel wool sample. Fig. 2.1b shows a randomly generated geometry for a cubic cell of 1 *mm* side. All the fibers are interacting, i.e. they all contribute on equal basis, both to the velocity and flux density field within the cell. Anyway, the fibers are supposed rigid: no mechanical model of the drag and magnetic forces acting on them and corresponding displacements has been made. This means that the cell geometry is assumed to be unaffected by the external applied field.

2.1.2 Flux density field

As seen in Section 1.2.1 each particle is magnetized by a field which is made of three terms: a relatively uniform field $\mathbf{B}_0$ produced by sources ex-

ternal to the filter, a field produced by the ferromagnetic filter element (steel wool fibers) and the interaction field produced by the magnetic moments of the particles. Neglecting the latter and assuming that the stainless steel wool fibers are magnetized to saturation $\mathbf{M}$, the flux density field can be directly evaluated analytically from the known sources by superposition, i.e. adding the fields produced by all the magnetized prisms and tetrahedrons of the periodicized cell. Following Fabbri [Fab08; Suh00; Fab09] the magnetic flux density $\mathbf{B}$ produced at the point $\mathbf{r}$ can be expressed analytically. By definition, the magnetic vector potential produced by an uniformly magnetized polyhedron is given by:

$$\mathbf{A}(\mathbf{r}) = \frac{\mu_0}{4\pi} \int_V \frac{\mathbf{M} \times (\mathbf{r} - \mathbf{r}')}{|\mathbf{r} - \mathbf{r}'|^3} d^3 r' \tag{2.2}$$

Being M uniform it can be rewritten as:

$$\mathbf{A}(\mathbf{r}) = \frac{\mu_0 \mathbf{M}}{4\pi} \times \int_V \frac{(\mathbf{r} - \mathbf{r}')}{|\mathbf{r} - \mathbf{r}'|^3} d^3 r' = \frac{\mu_0 \mathbf{M}}{4\pi} \times \int_V \nabla' \frac{1}{|\mathbf{r} - \mathbf{r}'|} d^3 r' \tag{2.3}$$

where a well known vector identity was used. Applying the Gauss' theorem:

$$\mathbf{A}(\mathbf{r}) = \frac{\mu_0 \mathbf{M}}{4\pi} \times \oint_{\partial V} \frac{\mathbf{n}}{|\mathbf{r} - \mathbf{r}'|} d^2 r' = \frac{\mu_0}{4\pi} \sum_{S_f \in \partial V} \mathbf{M} \times \mathbf{n}_f \int_{S_f} \frac{1}{|\mathbf{r} - \mathbf{r}'|} d^2 r' \tag{2.4}$$

where $\mathbf{n}_f$ is the outgoing unit vector normal to the surface S_f. Defining the harmonic function W_f as

$$W_f(\mathbf{r}) = \int_{S_f} \frac{d^2 r'}{|\mathbf{r} - \mathbf{r}'|} \tag{2.5}$$

it can be proven that W_f and its gradient depend on the given polygonal face S_f, but they are independent of their orientation $\mathbf{n}_f$ [Fab08; Fab08]. It follows that it is possible to write eq. (2.4) as:

$$\mathbf{A}(\mathbf{r}) = \frac{\mu_0}{4\pi} \sum_{S_f \in \partial V} \mathbf{M} \times \mathbf{n}_f W_f(\mathbf{r}) \tag{2.6}$$

The calculation of $\mathbf{B} = \nabla \times \mathbf{A}$, assuming W_f differentiable, is straightforward. The total induction field in every point turns out to be:

$$\mathbf{B}_e(\mathbf{r}) = \mathbf{B}_0 - \sum_{\forall polyhedron} \frac{\mu_0}{4\pi} \sum_{S_f \in \partial V} (\mathbf{M} \times \mathbf{n}_f) \times \nabla W_f(\mathbf{r}) \tag{2.7}$$

The implementation of the former equation is achieved in a fast way, thanks to the analytical knowledge of the function W_f and its gradient. Fig. 2.2 shows a detail of the map of the flux density field (arrows) and its squared modulus (color shading) inside a detail of a cell section.
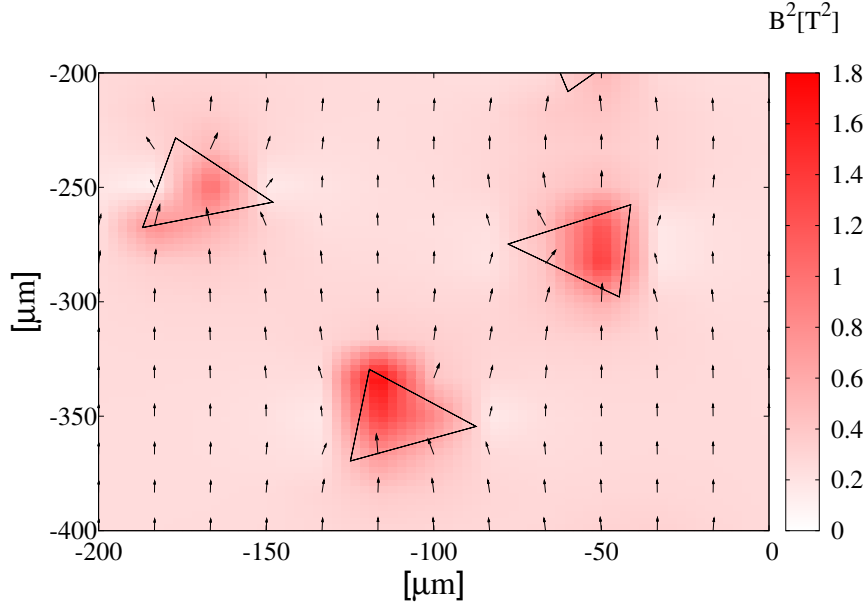
Figure 2.2: Detail of the map of the flux density field (arrows) and its squared modulus (color shading) inside a cell section, obtained for $B_0 = 0.5$ T, $\mu_0 M = 1$ T, $\Gamma = 3.5 \times 10^{-3}$ and with an average radial dimension of the wool fibers of $r_c = 15 \mu m$.

2.1.3 Fluid Velocity and Pressure fields

A modification of the Method of Fundamental Solutions (MFS) [You+06] for incompressible steady-state 3D Stokes problems has been developed, that applies to 2D problems also. The Helmholtz decomposition theorem is used to decompose the Stokes flow into the sum of a known potential flow and a viscous flow, so that the fundamental solutions are the solutions of the bi-harmonic equation for the stream function vector. As stated in [You+06; MSG99] the decomposition of the Stokes flow into the sum of a potential flow and a viscous flow leads to a purely boundary-type mesh-less method, particularly suitable for exterior problems and for solving inverse or degenerate problems in which missing or degenerate boundary data or the solutions at a few points within the domain are required. Moreover, comparing with other formulations such as the velocity–vorticity and vorticity–potential there is a reduction of the number of variables that can decrease the computational time and the required storage. Once the unknown coefficients of the fundamental solution are determined from the imposed no-slip velocity boundary

conditions, the distributions of velocity and pressure over the entire computational domain can be directly evaluated. Finally the method used is easy to implement, as far as the numerical algorithm is concerned, since it's based essentially on the same kernels of the magneto-static problem [Suh00].

The incompressible steady-state Stokes problem is governed by the conservations of mass and momentum (neglecting the inertial term, that is with low Reynolds number R_e):

$$\nabla \cdot \mathbf{u} = 0 \tag{2.8}$$

$$-\nabla p + \eta \nabla^2 \mathbf{u} = 0 \tag{2.9}$$

subjected to the no-slip boundary conditions on the surface of the fibers in the cell and to

$$\mathbf{u}|_{\partial cell} = \mathbf{u}_0 \tag{2.10}$$

on the cell boundary, where $\mathbf{u}$ is the velocity vector field, p is the pressure, η is the dynamic viscosity, $\mathbf{u}_0$ is a known boundary velocity related to the mass flow rate in the filter. The assumption of low Reynolds number is permissible considering for the mean flow rate Q, the diameter of the particles d_p, the area A_{hole} of the holes crossed by the fluid the values in Table 2.1 and Table 2.2 (that are the experimental conditions described in Chapter 3) obtaining:

$$Re = \frac{\rho_{H_2O} Q d_p}{\pi \eta_{H_2O} A_{hole}} \approx 10$$

Taking the curl of (2.9) with constant η, and using (2.8), we obtain the steady-state vorticity transport equation for Stokes flows as follows:

$$\nabla^2 \nabla \times \mathbf{u} = 0 \tag{2.11}$$

Equation (2.8) and the boundary condition (2.10) are identically satisfied with the Helmholtz decomposition:

$$\mathbf{u} = \mathbf{u}_0 + \nabla \times \boldsymbol{\Psi} \tag{2.12}$$

provided that the solenoidal part zeroes at the cell boundary. Moreover, in order to obtain uniqueness, the stream function vector $\boldsymbol{\Psi}$ can be constrained to be solenoidal. Thus, from (2.11) and (2.12) we obtain the bi-harmonic equation for the stream function vector: $\nabla^2 \nabla^2 \boldsymbol{\Psi} = 0$. Finally, since the problem is linear, the stream function vector can be expressed as the superposition of the contributions of the polyhedrons in the cells. In order to determine the Green functions for a given polyhedron inside the cell, we start

considering the isotropic case, i.e. the flow past a sphere. In this case the Green functions are well known [LL06]:

$$\boldsymbol{\Psi}\left(\mathbf{r}\right) = \nabla \times \left(\mathbf{s}_1 r + \mathbf{s}_2/r\right) = \frac{\mathbf{r} \times \mathbf{s}_1}{r} - \frac{\mathbf{r} \times \mathbf{s}_2}{r^3} \qquad (2.13)$$

$$\mathbf{u}\left(\mathbf{r}\right) = \mathbf{u}_0 - \frac{\mathbf{s}_1 + \left(\mathbf{s}_1 \cdot \mathbf{r}\right)\mathbf{r}/r^2}{r} - \frac{\mathbf{s}_2 - 3\left(\mathbf{s}_2 \cdot \mathbf{r}\right)\mathbf{r}/r^2}{r^3} \qquad (2.14)$$

$$p\left(\mathbf{r}\right) = p_0 - 2\eta\left(\mathbf{r} \cdot \mathbf{s}_1\right)/r^3 \qquad (2.15)$$

where $\mathbf{s}_1$ and $\mathbf{s}_2$ are arbitrary vectors and p_0 is the rest pressure. Due to the linearity of the problem we can extend these results to arbitrarily shaped bodies through a linear superposition integral of volume sources, defining the stream function vector as follows:

$$\boldsymbol{\Psi}\left(\mathbf{r}\right) = \nabla \times \int_V \left(\mathbf{S}_1\left(\mathbf{r}'\right)\left|\mathbf{r} - \mathbf{r}'\right| + \mathbf{S}_2\left(\mathbf{r}'\right)/\left|\mathbf{r} - \mathbf{r}'\right|\right) d_3 r' \qquad (2.16)$$

where $\mathbf{S}_1$ and $\mathbf{S}_2$ are arbitrary sources placed in the polyhedrons, i.e. outside the fluid volume. Assuming that the volume sources in (2.16) are uniform inside each polyhedron of the cell, we can obtain simple analytical relations based on (2.5) and on the following bi-harmonic function:

$$U_f\left(\mathbf{r}\right) = \int_{S_f} \left|\mathbf{r}' - \mathbf{r}\right| \, d_2 r' \qquad (2.17)$$

that is singularity-free and related to function W_f by the equation $\nabla^2 U_f = 2W_f$. The stream function vector, the velocity field and the pressure take the following simple form, where the sum ranges over each polygonal face S_f belonging to the boundary ∂V of the polyhedrons that model the fibers in the cell:

$$\boldsymbol{\Psi}\left(\mathbf{r}\right) = \sum_{S_f \in \partial V} \left[\left(\mathbf{S}_1 \times \mathbf{n}_f\right)U_f\left(\mathbf{r}\right) + \left(\mathbf{S}_2 \times \mathbf{n}_f\right)W_f\left(\mathbf{r}\right)\right] \qquad (2.18)$$

$$\mathbf{u}\left(\mathbf{r}\right) = \mathbf{u}_0 - \sum_{S_f \in \partial V} \left[\left(\mathbf{S}_1 \times \mathbf{n}_f\right) \times \nabla U_f\left(\mathbf{r}\right) + \left(\mathbf{S}_2 \times \mathbf{n}_f\right) \times \nabla W_f\left(\mathbf{r}\right)\right] \qquad (2.19)$$

$$p\left(\mathbf{r}\right) = p_0 - 2\eta \sum_{S_f \in \partial V} \left(\mathbf{S}_1 \cdot \mathbf{n}_f\right)W_f\left(\mathbf{r}\right) \qquad (2.20)$$

The functions W_f and U_f are analytical so that it is easy to differentiate them in order to get the velocity field and, since our main interest is the velocity field, only the velocity boundary conditions are required. The fulfillment of
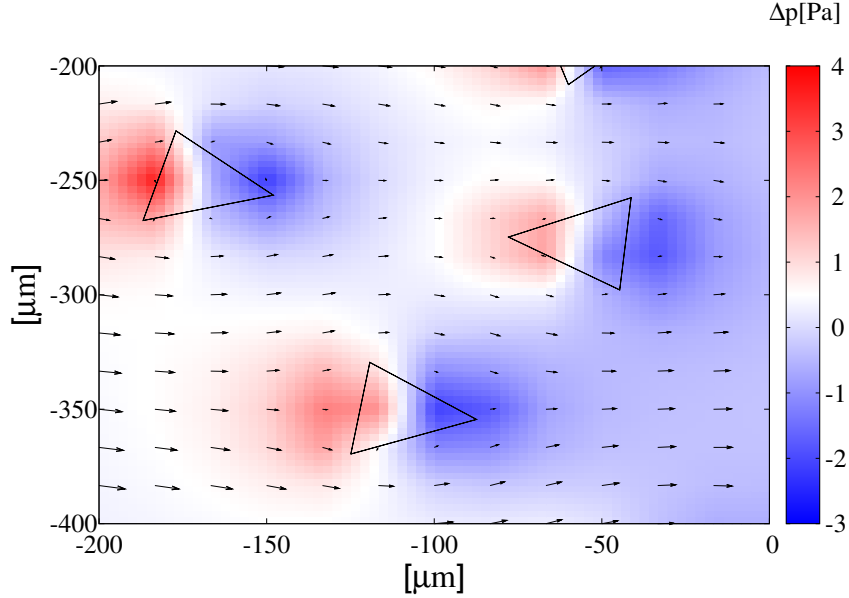
Figure 2.3: Detail of the map of the velocity field (arrows) and of the pressure drop
(color shading) inside a cell section for $u_0 = 14mm/s$, $\eta = 0.09Pa \cdot s$,
$\Gamma = 3.5 \times 10^{-3}$ and with an average radial dimension of the wool fibers
of $r_c = 15\mu m$.

the boundary condition (2.10) and of the no-slip conditions would lead to
an integral equation for the unknown sources that is avoided imposing that
the velocity on the surfaces of the fibers is zero in the mean sense. Thus,
for an arbitrary cell geometry, we impose the conditions of null velocity
on a fixed number of points on the faces (outer fold) of the polyhedrons
that lead to an over-determined system for the components of the uniform
volume sources in each polyhedron, which is solved with a least squares
approach. Note that the fluid dynamic and the magneto-static problems
share the same cell geometry. Both are based on the fundamental solutions
of their governing equations, and their solution methodologies do not depend
on the discretization of interior computational regions [Suh00]. Unlike the
magneto-static problem where the sources are known, the basic concept of
the fluid-dynamic problem is to find the solution of the partial differential
equations (2.8) and (2.9) by superposition of their fundamental solutions
with sources of proper intensity. Since the method locates the sources outside
the computational domain, no special treatments for the singularities of the
Green functions are required. However the way we impose the boundary

conditions "on average" leads to an error near the edges of the fibers that is visible in Fig. 2.3, where, near the top corner of the top left section of tetrahedron, the velocity doesn't approach zero the right way. Anyway we can neglect this effect acting on the stopping criterion in the particle trajectory calculation. This approach is essentially 3D, but can be easily adapted to a 2D problem also, as shown in Fig. 2.3.

2.1.4 Particles trajectories and capture parameter

Each particle is supposed spherical, suspended in the fluid flowing through the wool and only subject to the magnetic force and to the fluid drag force, expressed by the Stokes' relation [LL06]. Since wastewater with a low concentration of the particles and at room temperature is considered, the gravitational force, the randomizing effects of Brownian motion and the interaction field among particles have been neglected [MHB05]. The non-interaction of the particles is justified by the assumption of a low particle concentration. About gravity force and Brownian motion we can consider particles of diameter $d = 10^{-6}m$, a mean velocity field $u_0 = 0.1 m/s$, the dynamic viscosity $\eta = 10^{-3} Pa/m$, an induction field $B_e = 0.5 T$ and gradient $\nabla B_e = 10^4 T/m$, an effective magnetic susceptibility $\chi = 1$, a working fluid temperature of $300 K$ and the density of the particles $\rho = 5 \times 10^3 kg/m^3$. Defining the Boltzmann energy associated to the Brownian motion as:

$$E_B = k_B T$$

and using, for the drag force, the Stokes' approximation:

$$\mathbf{F}_d = 3\pi\eta d\mathbf{u} \tag{2.21}$$

we can calculate the following ratios to demonstrate the stated negligibility:

$$\frac{E_B}{E_K} = \frac{k_B T}{1/2\rho V u^2} \approx 10^{-4}$$

$$\frac{F_g}{F_d} = \frac{\rho d^2 g}{18\eta u} \approx 10^{-11}$$

$$\frac{F_g}{F_m} = \frac{\rho g \mu_0}{\chi B_e \nabla B_e} \approx 10^{-5}$$

where E_K is the kinetic energy of a particle, V its volume, F_g the gravity force acting on a particle and F_m the magnetic one. Thus, the trajectory of one particle is independent from all the others and can be obtained numerically integrating its dynamic motion equation:

$$V_p\rho_p\frac{d^2\mathbf{x}}{dt^2} = 3\pi\eta d_p\left(\mathbf{u}\left(\mathbf{x}\right) - \frac{d\mathbf{x}}{dt}\right) + \frac{V_p\chi_p}{2\mu_0}\nabla B_e^2\left(\mathbf{x}\right) \tag{2.22}$$

where $\mathbf{x}$ is the time-dependent position of the particle, ρ_p is the density of the particle matter and d_p the particle diameter. Note that the last term of (2.22), obtained from (1.1), shows that the magnetic force is proportional to the gradient of the squared modulus of the flux density. It follows from the vectorial identity:

$$\nabla(|\mathbf{B}|^2/2) - \mathbf{B} \cdot (\nabla \mathbf{B}) = \mathbf{B} \times (\nabla \times \mathbf{B})$$

thanks to $\nabla \times \mathbf{B} = \mu_0 \mathbf{J} = 0$. Using a dimensional analysis we can write eq. (2.22) in term of $\mathbf{x}^* = \frac{\mathbf{x}}{r_c}$ and $t^* = \frac{|u_0|t}{r_c}$ (in which r_c is the average radial dimension of the wool fibers):

$$\begin{cases} \mathbf{x} = r_c\mathbf{x}^* \\ t = \dfrac{r_c}{|\mathbf{u}_0|}t^* \end{cases} \Rightarrow \begin{cases} \dfrac{dx}{dt} = |\mathbf{u}_0| \cdot \dfrac{d\mathbf{x}^*}{dt^*} \\ \nabla = \dfrac{1}{r_c}\nabla^* \end{cases}$$

obtaining:

$$\frac{\rho_p d_p^2 u_0}{18\eta r_c}\frac{d^2\mathbf{x}^*}{dt^{*2}} + \frac{d\mathbf{x}^*}{dt^*} = \frac{\mathbf{u}}{u_0} +$$

$$\frac{d_p^2\chi_p B_0 M}{36r_c u_0 \eta}\left| \frac{\mu_0 M}{B_0}\nabla^*\left(\sum_{polihedrons}\phi\right)^2 + 2\nabla^*\hat{\mathbf{B}} \cdot \sum_{polihedrons}\phi\right| \quad (2.23)$$

in which

$$\phi = \sum_{S_f \in \partial V}\left(\hat{\mathbf{M}} \times \mathbf{n}_f\right) \times \nabla W_f(\mathbf{x})$$

and the ^ symbol stays for unitary vector. From eq. (2.23) we define the following parameter:

$$\Omega = \frac{d_p^2\chi_p M B_0}{36\eta u_0 r_c} \quad (2.24)$$

which takes into account the relative influence of the drag and the magnetic force acting on a particle. A second parameter, $\Omega_m = \frac{\mu_0 M}{B_0}$, is ignored since it is constant for given outer field and wool matter. Moreover, consistently with the hypothesis of a low Reynolds number used in the calculation of the fluid velocity field $\mathbf{u}$, the comparison of the inertial force magnitude $V_p\rho_p u_0^2/r_c$ to the drag and the magnetic force shows that the left hand side of (2.22) is negligible in the following limits:

$$\frac{V_p\rho_p u_0^2}{r_c} \ll 3\pi\eta d_p u_0 \quad \Rightarrow \quad u_0 \ll \frac{18\eta r_c}{\rho_p d_p^2} \quad (2.25)$$

$$\frac{V_p\rho_p u_0^2}{r_c} \ll \frac{V_p\chi_p M B_0}{2r_c} \quad \Rightarrow \quad u_0 \ll \sqrt{\frac{\chi_p B_0 M}{2\rho_p}} \quad (2.26)$$
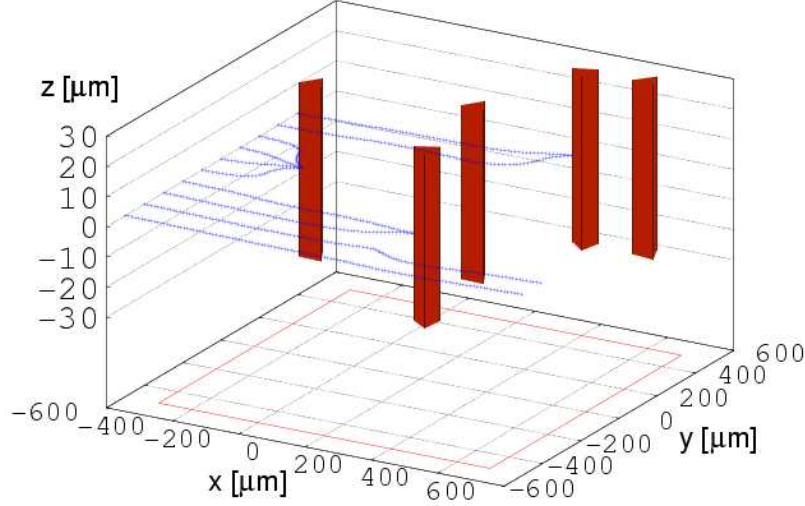
Figure 2.4: Some trajectories obtained from the integration of eq. (2.27) in a two dimensional cell. On the *floor* of the cell its real dimensions are visible.

Thus the trajectories, obtained integrating the quasi-static equation

$$\frac{d\mathbf{x}}{dt} = \mathbf{u}(\mathbf{x}) + \frac{d_p^2 \chi_p}{36\eta\mu_0} \nabla B_e{}^2(\mathbf{x}), \qquad (2.27)$$

depend only on the capture parameter Ω, on the starting point and on the cell geometry, i.e. on the packaging factor [YYT00]. Equation (2.22) and (2.27) have been integrated numerically in a cell with the 5th order Runge-Kutta Method [AP98]; it is assumed that the Van Der Waals force are localized on the fibers boundary so that, when a particle is near a wire (i.e. its distance from the wire is less than its diameter), we can consider the particle stopped [Kir00]. An example of trajectories integration is shown in Fig. 2.4. Defining the capture (or retention) efficiency σ_{cell} of a cell as the ratio between the numbers of captured and entering particles [Tso+06], we characterized it from a statistical point of view. The capture efficiency, for a fixed Ω, is obtained generating 5-10 different random cell geometry (for every packaging factor Γ) and studying 20-50 randomly starting trajectories of the particles. The numbers of the geometries and of the trajectories were chosen in order to reach a low statistical error but containing the computational time too. Every trajectory could give two opposite results: captured or passed through (usually through the face of the cell opposite to the entering one). Figure 2.5 shows the obtained capture efficiency: as visible it increases with Ω, i.e. it
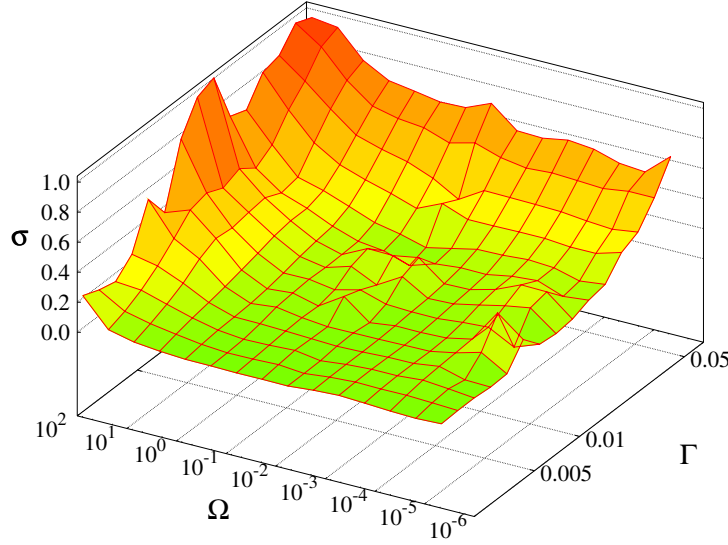
Figure 2.5: Capture efficiency σ of a cell as a function of the capture parameter Ω and of the packaging factor Γ from the integration of the quasi-static equation.

increases with B and M and decreases when u_0 or r_c grow. It is also possible to see that σ increases with Γ, that is as the distance between the fibers decreases. In Fig. 2.6 the points represent the obtained average value of the capture efficiency of a cell (σ_{cell}) for the two considered models (dynamic, eq. (2.22), and quasi-static, eq. (2.27)) when a specific packaging factor is considered to improve reliability and readability. The bars are obtained as the variance of the same set of geometry-trajectories results. The integration of the quasi-static equation (2.27) is at least two times faster than the integration of the dynamic one (2.22). In Fig. 2.6 the marker symbol corresponds to the stronger lower limit on Ω for the validity of the quasi-static model, as obtained from (2.25) and (2.26). It has been calculated using the values shown in Table 2.1 which refers to the experimental set-up described in Chap. 4. As shown in Fig. 2.6 the results predicted by the two models are quite similar for all the range of Ω investigated, also below the theoretical limiting value. It's worth to note that both the quasi-static and the dynamic models would give a non-zero capture efficiency also without magnetic field applied. In fact, the stream lines tend asymptotically to zero, but the particles, having a finite radius, may *touch* the fibers for every unperturbed velocity, provided the right starting point is choosen: indeed, if the maximum fiber to fiber distance would be less than the particles minimum radius every particle would
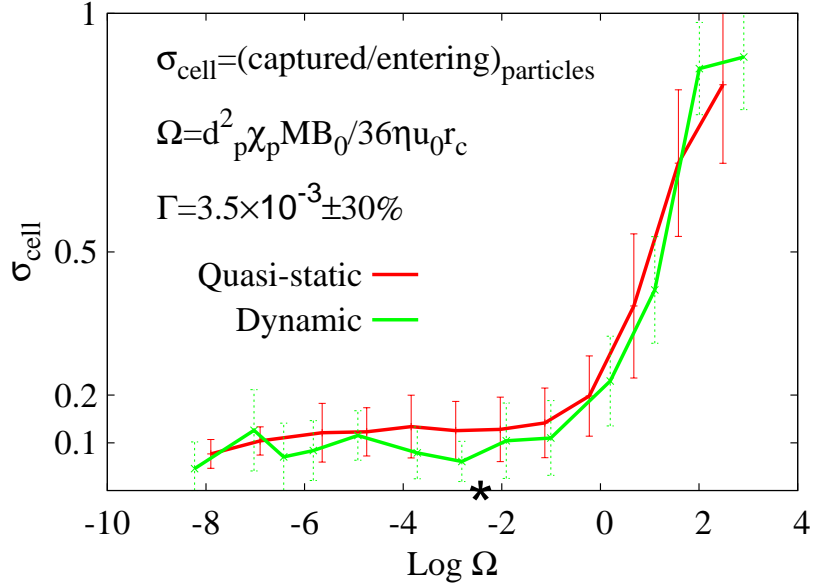
Figure 2.6: Capture efficiency σ of a cell as a function of the capture parameter Ω for a given wool packaging factor Γ from the integration of the dynamic equation (green) and the quasi-static one (red). The bars show the variance. The marker corresponds to the lower limiting value of Ω for the validity of the quasi-statyc results.

Table 2.1: Reference values for powder (hematite), wool (AISI 434) and working fluid (water).

d_p	χ_p [Oka+02]	$\mu_0 M$ [BCD03]	B_0 [Fab+08]	r_c [Gmt]	η
$0.8 \pm 20\%[\mu m]$	2×10^{-3}	$1[T]$	$0.5[T]$	$15[\mu m]$	1 [mPa·s]

be captured, like in a sieve.

We can simply deduce the capture efficiency of the whole filter σ_{filter} from σ_{cell}, in the well verified hypothesis that the particles exit the cell through the face opposite to the entering one. In fact, by definition, knowing the average number of cells N_{cell} the flow pass through and supposing Ω and Γ being constant in all the cells, the filter capture efficiency can be determined directly as follows:

$$1 - \sigma_{filter} = (1 - \sigma_{cell})^{N_{cell}} \tag{2.28}$$
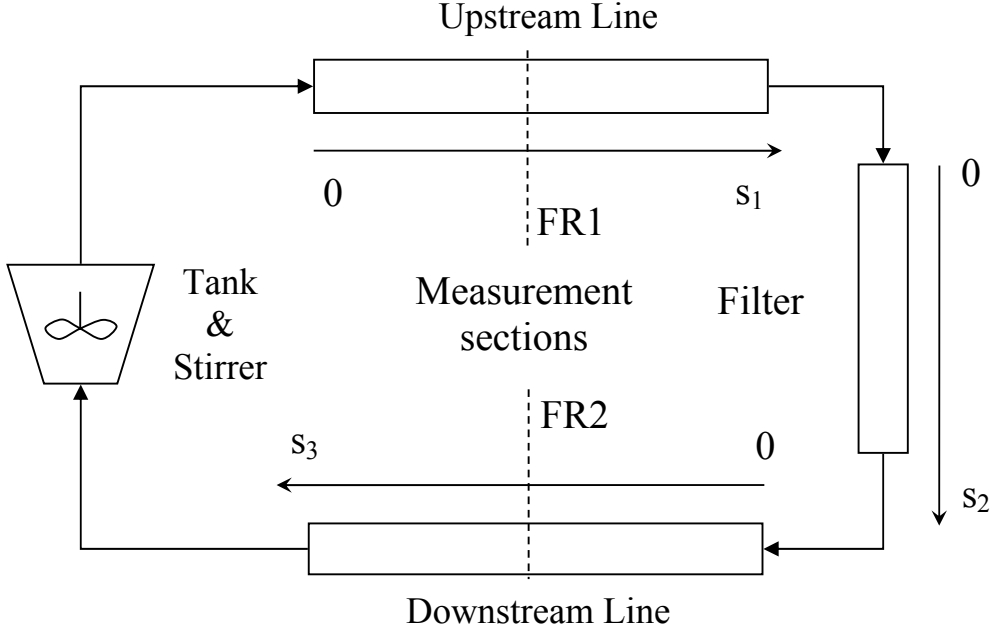
Figure 2.7: Scheme of the experimental set-up.

2.2   System mass balance

The passage from the cell model to the whole filter one is developed in this section. Stating from elementary considerations about the conservation of mass it's possible to describe the number of particles in a (closed) circuit in which some kind of deposition occurs. The expression, which, provided the initial condition, results a function of time, is comparable with the experimental measurements of the concentration, as will be shown in Chapter 3. In the considered experimental set-up, whose scheme is shown in Fig.2.7, the fluid flows inside a closed-cycle circulating system thanks to a pump. The flow starts from a $1l$ tank, visible in Fig. 2.8, filled with a mixture of water and particles with an initially known concentration and returns to the same reservoir after passing through two lines and, optionally, the magnetic separation unit in the middle of them. The concentration $c_{i,k}$ in the experimental set-up has been modelled through a set of local mass balance equations like the following:

$$V_0 \frac{\partial}{\partial t} b_k(t) = -Q \left[C_{3,k}(L_3, t) - b_k(t) \right]$$
$$b_k(0) = \hat{b}_k$$

$$(2.29)$$

Figure 2.8: Picture of the tank used in the circuit.

Table 2.2: Geometrical parameters of the experimental circuit.

A_0	$\cdots$	$V_0 \left[m^3\right]$	1.00×10^{-3}
$A_1 \left[m^2\right]$	0.30×10^{-3}	$V_1 \left[m^3\right]$	1.00×10^{-3}
$A_2 \left[m^2\right]$	0.80×10^{-3}	$V_2 \left[m^3\right]$	0.25×10^{-3}
$A_3 \left[m^2\right]$	0.30×10^{-3}	$V_3 \left[m^3\right]$	0.50×10^{-3}

for the tank and:

$$
\begin{aligned}
&A_i \tfrac{\partial}{\partial t} c_{i,k}(s_i, t) = -Q \tfrac{\partial}{\partial s_i} c_{i,k}(s_i, t) - \lambda_{i,k} A_i c_{i,k}(s_i, t) \\
&c_{i,k}(s_i, 0) = \hat{c}_{i,k}(s_i) \\
&c_{i,k}(0, t) = b_k(t) && , i = 1 \\
&c_{i,k}(0, t) = c_{i-1,k}(L_i, t) && , i = 2, 3
\end{aligned}
\tag{2.30}
$$

for the lines and the filter. Q is the volume flow-rate, the index i refers to the sections in which the circuit is divided (tank 0, upstream line 1, filter 2, downstream line 3): A_i represents the area of each section, V_i its volume, s_i the distance in the relative one-dimensional reference system of each pipe whose length is given by $L_i = V_i/A_i$. The mass balance equation for the concentration b_k in the tank (A_0) lacks of the spatial gradient that has been omitted due to the presence of a stirrer which provides homogeneity. The stirrer, visible in Fig. 2.9, was realized in LIMSA laboratory to fit the specific situation requirements. Table 2.2 shows the geometrical parameters of the experimental system. Since both eq. (2.22) and eq. (2.27) depends on the particles diameter, each powder is divided into *populations* sharing similar properties, according to the experimental size distribution (see Ap-

Figure 2.9: Picture of the stirrer realized at LIMSA.

pendix C.1). The index k stands for the powders populations, being $c_{i,k}$ the powder concentration in the section i for the population k. The experimental concentration x_i is the sum of the single concentration:

$$x_i(t) = \sum_{k=I,II,III} c_{i,k}(s_i, t) \tag{2.31}$$

Every population is decaying with a rate $\lambda_{i,k}$ which takes into account both spatial (essentially in the filter) and temporal (essentially in lines, due to sedimentation and walls adsorption) decay rate of the particles. In the filter the decay rate for each population is related to the filter capture efficiency for the same population, by definition, by

$$1 - \sigma_{filter,k} = e^{-\lambda_{2,k} V_2/Q} \tag{2.32}$$

which, considering that, as described later and visible in Appendix C.1, only population 2 is important in order to verify the model the relation can be simply written as:

$$1 - \sigma_{filter} = e^{-\lambda_{2,II} V_2/Q} \tag{2.33}$$

The analytical integration of eq. (2.29)-(2.30) leads to a set of equations like the following:

$$x_i(t) = \sum_k e^{-\lambda_k \left(\frac{V_{k-1}}{Q} - \frac{A_k}{Q} s_k \right)} b_k \left(t - \frac{V_{k-1}}{Q} - \frac{A_k}{Q} s_k \right) \cdot$$
$$\cdot U \left(t - \frac{V_{k-1}}{Q} - \frac{A_k}{Q} s_k \right)$$

where $U(t)$ is the Heaviside step function. This equation shows that, for each population, the resulting concentration is the product of two different behaviours: there is a front periodical wave resulting from the concentration in the tank and a decay due to the deposition. It's worth to note that the model has been developed in the hypothesis of high velocity, i.e. neglecting the parabolic velocity profile in the pipe present in laminar flow. In different words I commited an error considering only a mean velocity for each cross section of the pipe. Anyway the committed error is negligible: both of the discussed characters of the concentration (periodic wave and decay) will be visible in the experimental measurements. The equations have been numerically integrated imposing, for each population, the continuity of the concentration through the contiguous sections. The main unknowns are the flow rate of the circuit, Q, the decaying constants, $\lambda_{i,k}$, and the mass fractions for each population in the initial sample, m_k, which have to be determined fitting the experimental results. To check the experimental condition two phases are considered:

A calibration one in which the filter is not inserted, the two lines are filled with clean water and the tank is filled with a known particle concentration. Unlike what one would expect the decaying rate is nonzero because the population with the lower mean diameter is adsorbed by the walls of the circuit. In this phase the oscillating part of the solution is evident and so it is useful for the calculation of the flow rate and for the calibration of the concentration meters (described in section 3.3).

A filtering one in which, after phase one, the filter, filled with clean water, is inserted between line 1 and line 3. Here the decaying rate of the filter is measured, from which the capture efficiency will follow as shown in eq. (2.33).

The fitting will be performed over each measuring experience and the obtained parameter averaged.

Chapter 3

Experimental Set-Up

In order to verify our model I designed and built a laboratory device. The first prototype, visible in Fig. 3.1, was constituted by an open circuit. Starting from a tank the working fluid was moved to a second one passing
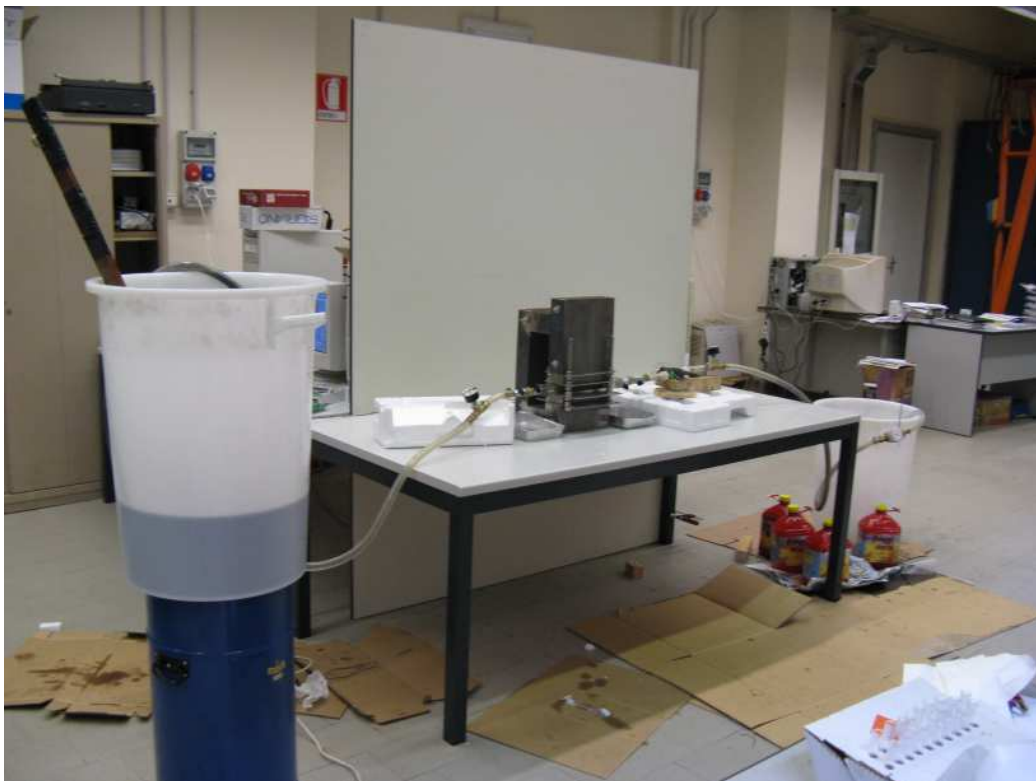

Figure 3.1: Photo of the first experimental set-up.

through the filter. The first of the two tanks, each of $100l$ of capacity, were initially filled with at least $20l$ of water in order to achieve a working time of around $5min$. During each experience the desired quantity of powder was kept in suspension through human mixing. Anyway the working time resulted short and the results of difficult interpretation. In fact the continuous filtration of a constant quantity of powder resulted in the saturation of the filter (or at least of some of the cells interested in the separation process) requiring a different model of the phenomenon. To overcome these problems the model visible in Fig. 3.2 has been designed and realized. The scheme of the prototype is visible in Fig. 2.7. As visible, the hydraulic circuit is a closed one: starting from the tank, which is provided with a stirrer, the working fluid is moved through the filter by the electric pump *BE-M 20, NOVAX 20* capable to erogate a maximum power of $340W$, made in Italy by ROVER, posed after the tank. A stirrer working inside the tank is not mandatory, but necessary in order to achieve a uniform initial concentration of the working fluid in the tank and to avoid gravitational deposition of the particles. The measuring instruments are collocated, after the tank, in the following order:

- a barometer;

- a valve (to control the volume flow rate);

- a second barometer;

- a concentration meter (**FR1**);

- a second concentration meter (**FR2**);

- a volume flow integrator.

The filter is placed between the first and the second concentration meters. All of them are connected via a transparent gum pipe of inner diameter $18mm$. Every instrument, including the filter, was easy to remove from the circuit letting it in a working condition.
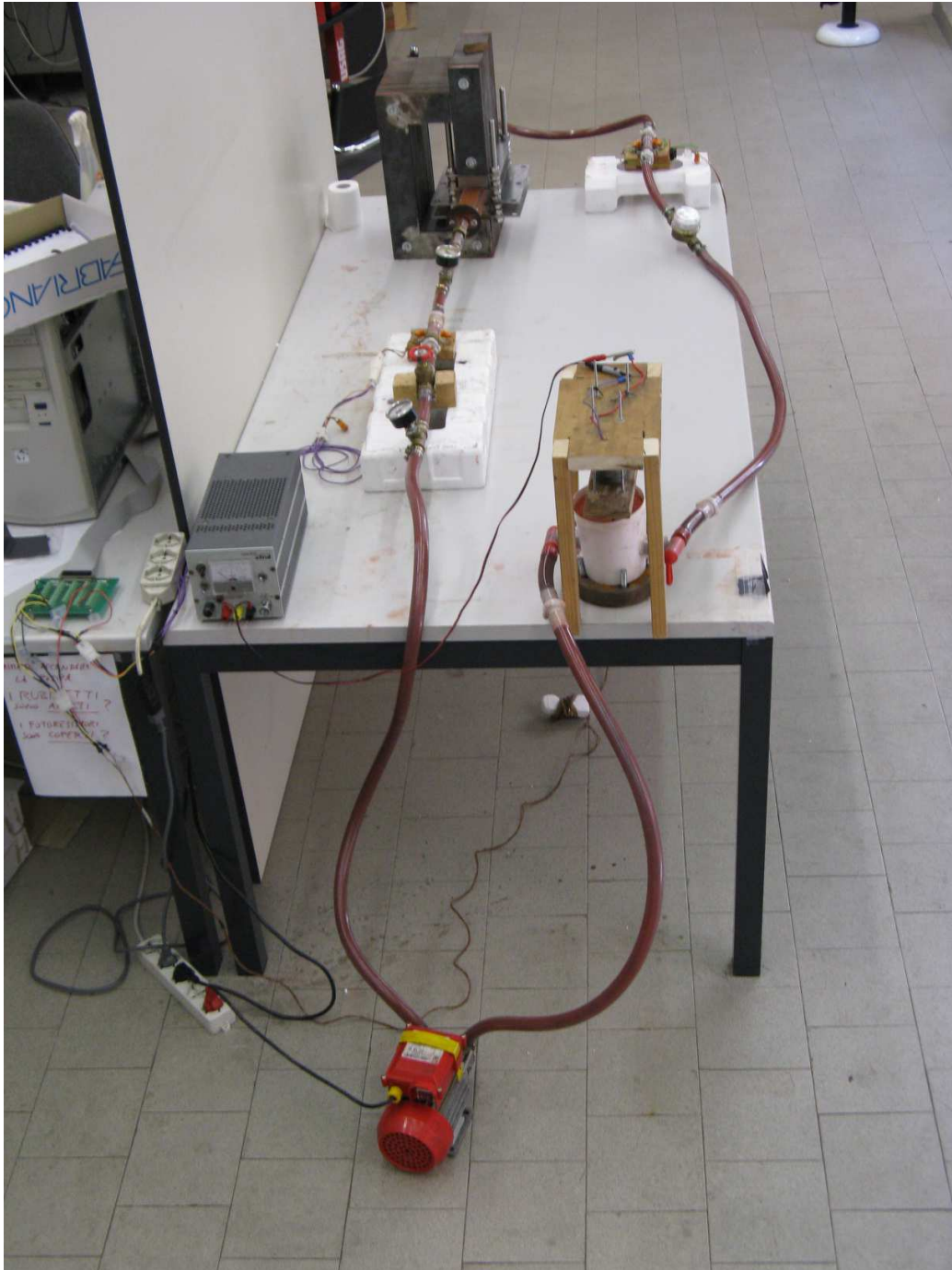
Figure 3.2: Photo of the experimental set-up.

3.1   The filter

The filter was made of stainless steel AISI434 wool with fibers of effective diameter lower than 30 μm, obtained from GMT Inc. [Gmt] in the form of rolls of diameter of about $30cm$, as visible in Fig. 3.4. The fibers of the wool, as visible in Fig. 2.1a, are similar to long prisms with triangular cross section [Mas+06]. The wool magnetization, as visible in Fig. 3.3 is of about $8 \times 10^5 A/m$ at saturation. The packaging of the wool required some attentions. In

Figure 3.3: Hysteresis cycle of AISI434 steel [BCD03].

fact the first attempts, in which the wool was simply inserted in the tube, led to the formation of channels through which the flow is facilitated, as visible in Fig. 3.5. After some attempts I developed a more performing filtering

Figure 3.4: Picture of a roll of iron steel wool.

Figure 3.5: Picture of a filter packaged in the wrong way: a channel through with the flow is facilitated is visible.

element, where the wool envelops a drilled test-tube to force the water to flow radially through the wool as shown in Fig. 3.6a-3.6b [Fab+08]. The holes in the test-tube, each with a diameter of about $1.5mm$, are disposed into nine rows of three. As shown in Fig. 3.6c it is placed in a transparent tube, with a rectangular inner cross section of $24 \times 40\,mm^2$ and an outer one of $34 \times 60\,mm^2$. The tube itself is placed in the air gap of the magnet, as visible in Fig. 3.6c. It is possible to place a light behind the tube to improve the filtering element visibility. The transparent tube can be filled with one or two filtering elements. The hand made filtering elements are disposed as ordinary litter after one usage.

The flux density field source consists of a pair of PM made of six Sm-Co *XGS26* ingots $70mm \times 70mm \times 30mm$ provided by SAIMAG s.r.l., having nominal remanence of $1.05T$ oriented perpendicularly to the wide face, separated by a gap of $40mm$ and coupled with a movable magnetic circuit made of laminated M330-50A steel (Fig. 3.7a). The measured map of the transverse component of the flux density field produced on the central plane of

(a)   (b)

(c)

(d)
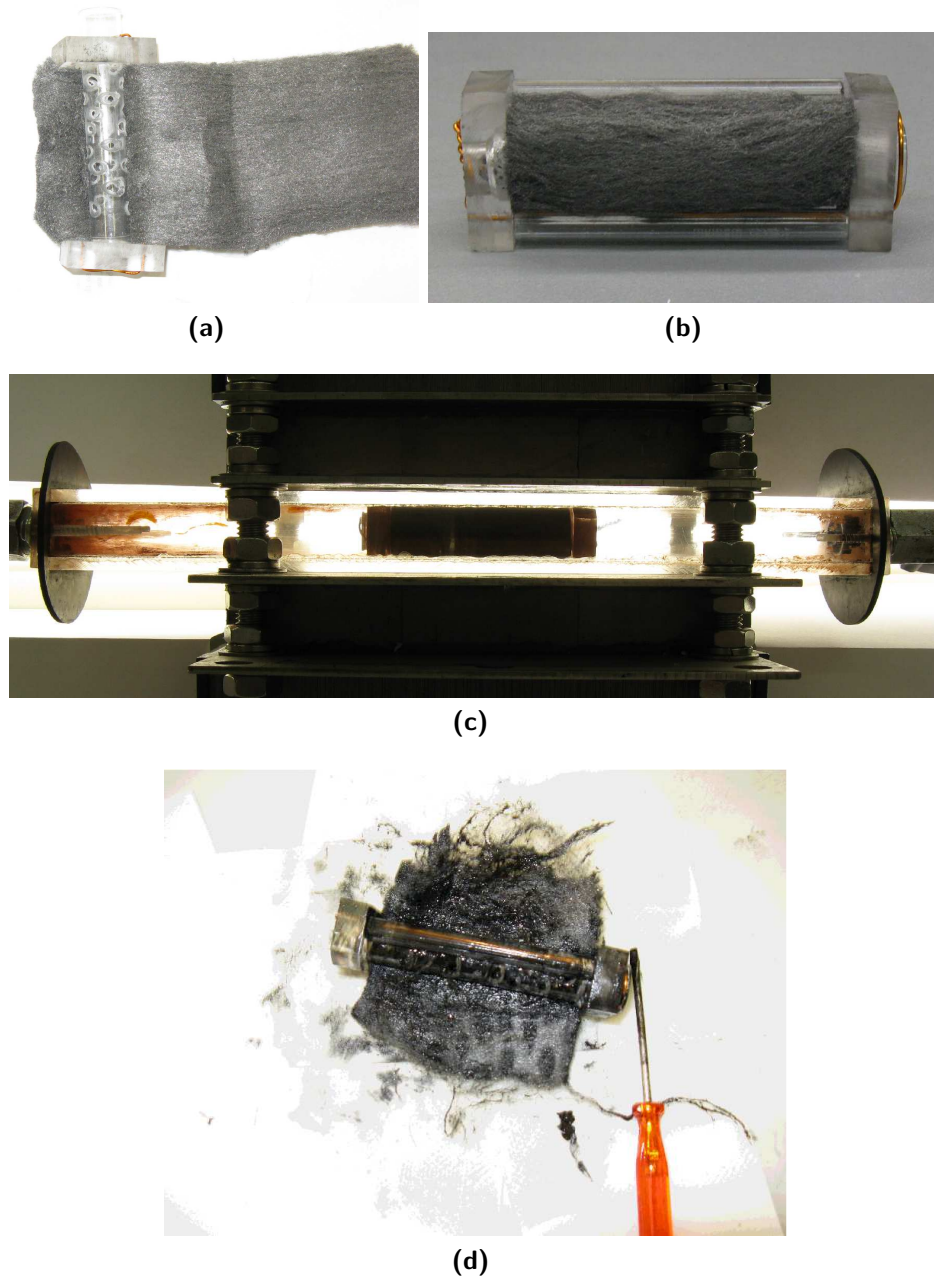
Figure 3.6: Images of the filtering element: opened (a) closed (b) and in the magnet airgap (c) before an experiment and (d) opened after an experiment.
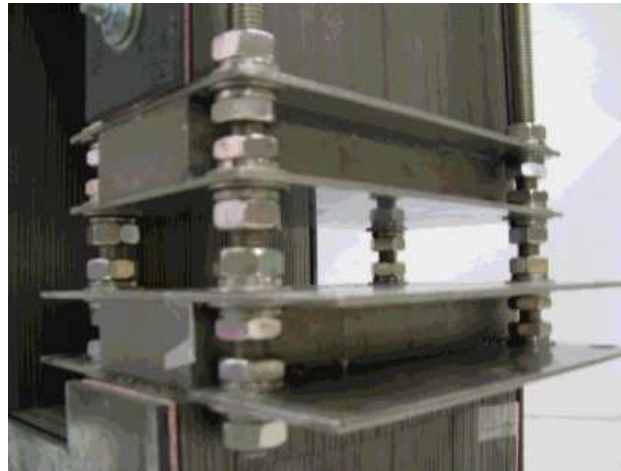
(a)
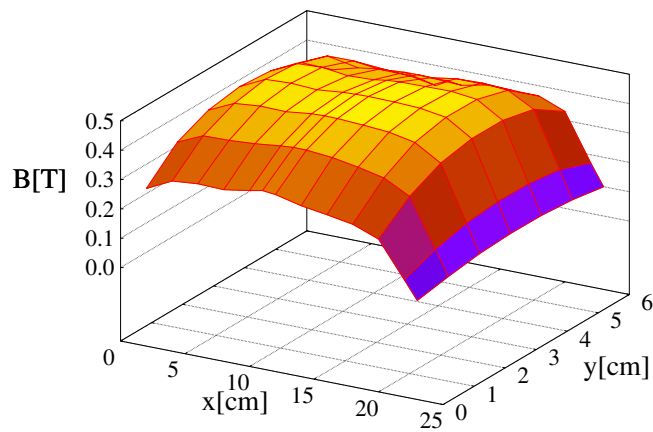
(b)

Figure 3.7: Image of the PM (a) and map of the transversal magnetic flux density field (b).

the experimental system is shown in Fig. 3.7b. The measure was performed with the LAKESHORE Gauss probe *HMNT-4E04-VR*. A maximum value of $500mT$ is detected. This value is decreased by 20% in the inlet and outlet regions of the filter. The other components are negligible in the filter region. The stray field at $50cm$ from the magnets is well below $5mT$.

3.2   The powders

In order to simulate the adsorbent we initially bought some magnetite' powder from Kremer Pigmente GmbH and, following the producers' conventional name, labeled it #48800. The powder[1] is normally used in the manufacturing of painting and is very cheap (between 5 € and 10 € per kg). The size distribution of that powder, shown in Fig. 3.8a, was measured using FRITSCH *Laser-Particle-Sizer "Analysette 22"*. The measure was made in the laboratory of the Chemical, Mining and Environmental Engineering Department of the University of Bologna (DICMA). The first observation of the working fluid, made in test tubes filled with water, shows that the magnetite dynamic viscosity in water resulted in a very fast deposition of the particles. In fact the time constant for sedimentation was of the order of seconds. To avoid particle deposition we decided to use cooking-oil as working fluid, which resulted in a very low deposition velocity. The effective magnetic susceptibility of that ferrimagnetic powder, measured with a dynamo-meter in the LIMSA laboratory, is about 1.4. However the particles turn out to strongly aggregate when magnetized and to be very sensitive to the external magnetic field gradient. In order to test our model we decided to reduce the magnetic susceptibility of the working powder and we bought two different size-distribution samples of the same specie of hematite. Their magnetic susceptibility is known to be $\approx 2 \times 10^{-3}$ [Oka+02]. The two different hematite powders were obtained from Kremer Pigmente GmbH and labeled #48100 and #48651. Figure 3.8b shows the frequency of the particle size distribution of both powders measured using the same FRITSCH *Laser-Particle-Sizer "Analysette 22"* used for #48800 at DICMA. Neglecting the peaks on the left due to the instrument limits, it can be seen that the distribution is approximatively log-normal for all the three powders (as shown in Appendix C.1). Three populations with uniform properties have been considered for each powder: a central one labelled *I* and other two, labelled *II* and *III*, that take into account the lower and higher diameters, respectively. The deposition rate of powder of hematite resulted lower than the one of the magnetite letting us decide to use water as working fluid with a time constant for sedimentation of the order of the minutes.
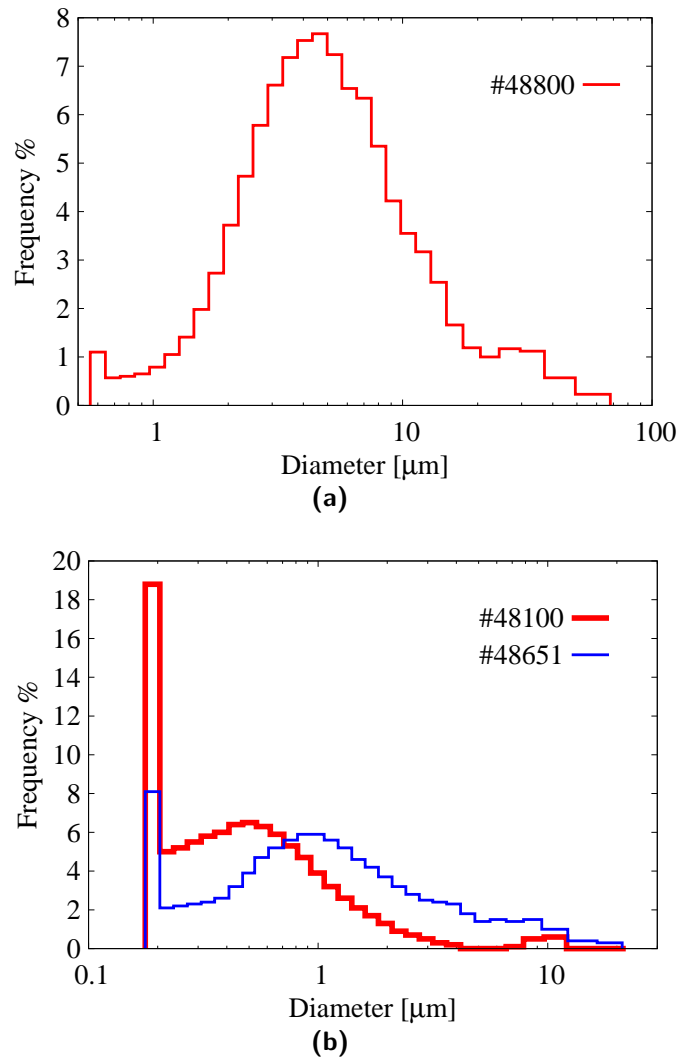
Figure 3.8: Experimental size distributions for the magnetite powder (a) and for the two hematite ones (b).

3.3 The measuring set-up

3.3.1 Concentration

The particle concentration inside the working fluid was measured by means of two *homemade* concentration-meters. They are homemade because commercially available ones are too limited. In fact they usually work with

---

[1]As well as the ones discussed later

only a particular working fluid (such as water or oil only, with no possibility of change). Moreover they usually work on samples while, to operate continuously, a on-line instrument was necessary. Each concentration-meter is made with a couple of Silonex *NORPS-12* light-dependent resistor (Fig. 3.9 and Fig. C.9 in Appendix C.4) and Kingbright *L-7678C2VGC-H "superflux"* led lamp (Fig. 3.9 and Fig. C.8 in Appendix C.4)) placed one in front of the other and with the gum pipe between them as visible in Fig.

3.10. The light dependent resistor, whose circuital symbol is ⌇ where the arrows stand also for the positive terminal, is characterized by a maximum response as function of the frequency of the incident light around $6KHz$, has shown in Fig. C.10a (in Appendix C.4). The chosen led emits light, following the distribution shown in Fig. C.10b (in Appendix C.4), as a maximum emission around $6KHz$ too so it is compatible with the light dependent resistor. We suppose the concentration of the powder related to turbidity of the working fluid by a linear function. The turbidity itself determines the ratio of the light which, emitted from the led lamp, is adsorbed by the powder, i.e. the ratio of the light which hit the photo-resistor. The intensity of the light and the measured resistance are related by a $\log - \log$, relation as stated by the manufacture [Nor], so that the resulting relation between concentration and measured resistance is, in the working range of the photo-resistor, in the form (see Appendix C.2): $C = a + b * \log R$.

A third turbidity-meter FR0, described in Appendix C.3 has been made in order to measure the concentration of samples collected into test tubes. In order to acquire the resistance on the photo-resistor we
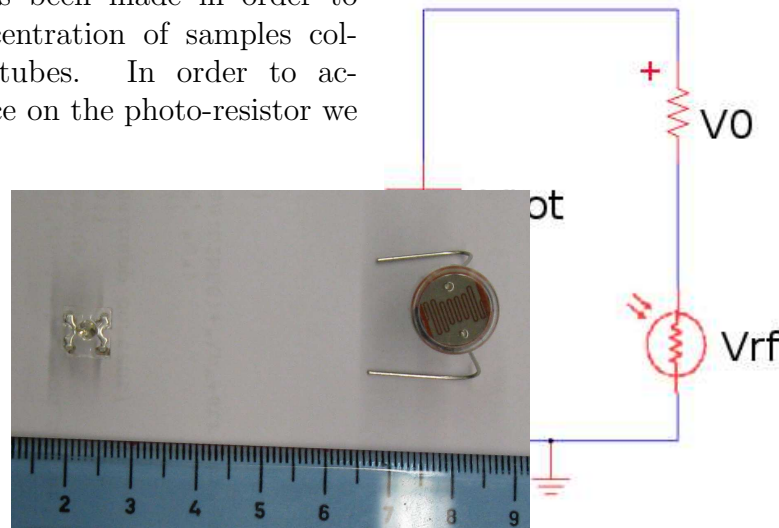

Figure 3.11: Image of the measuring circuit.

Figure 3.9: Picture of the led (left) and of the light dependent resistor (right) used in making the concentration meters.
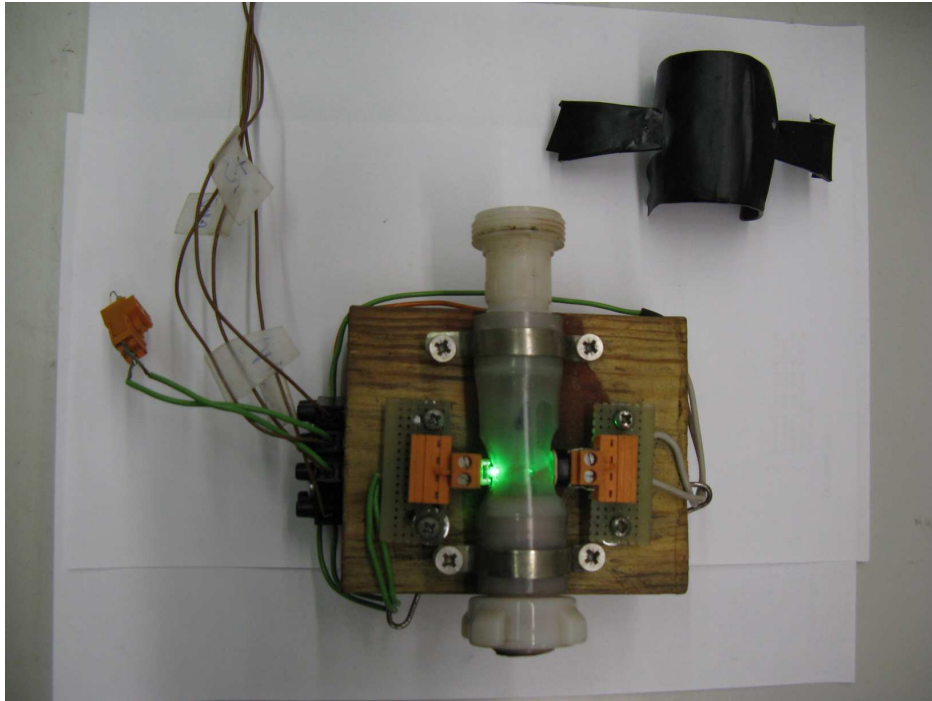
Figure 3.10: Picture of a concentration-meter. The led lamp (powered) is on the left side of the pipe while the photo-resistor is on the right side. In the upper right corner a hat used to avoid the environmental light modifying the measured value is visible. On the left it is visible R_0.

used a Personal Computer equipped with *GNU/Linux Real Time Application Interface* [BMN06] coupled to National Instrument *PCI-MIO-16E-1* I/O terminal with a sampling rate of $10Hz$. The schematic corresponding to the two circuits shown in Fig. 3.12 are realized with SCILAB/SCICOS [BB05]. Figure 3.12a shows the schematic relative to the led supply while Fig. 3.12b shows the one relative to the resistance acquisition. Figure 3.13 shows the graphical user interface (GUI) used to control the acquisition process. That GUI was provided with the RTAI source code and compiled for the specific hardware during the initial set-up of the software-side acquisition system. In Fig. 3.13 the mainly used components of the GUI are shown:

(a)

(b)
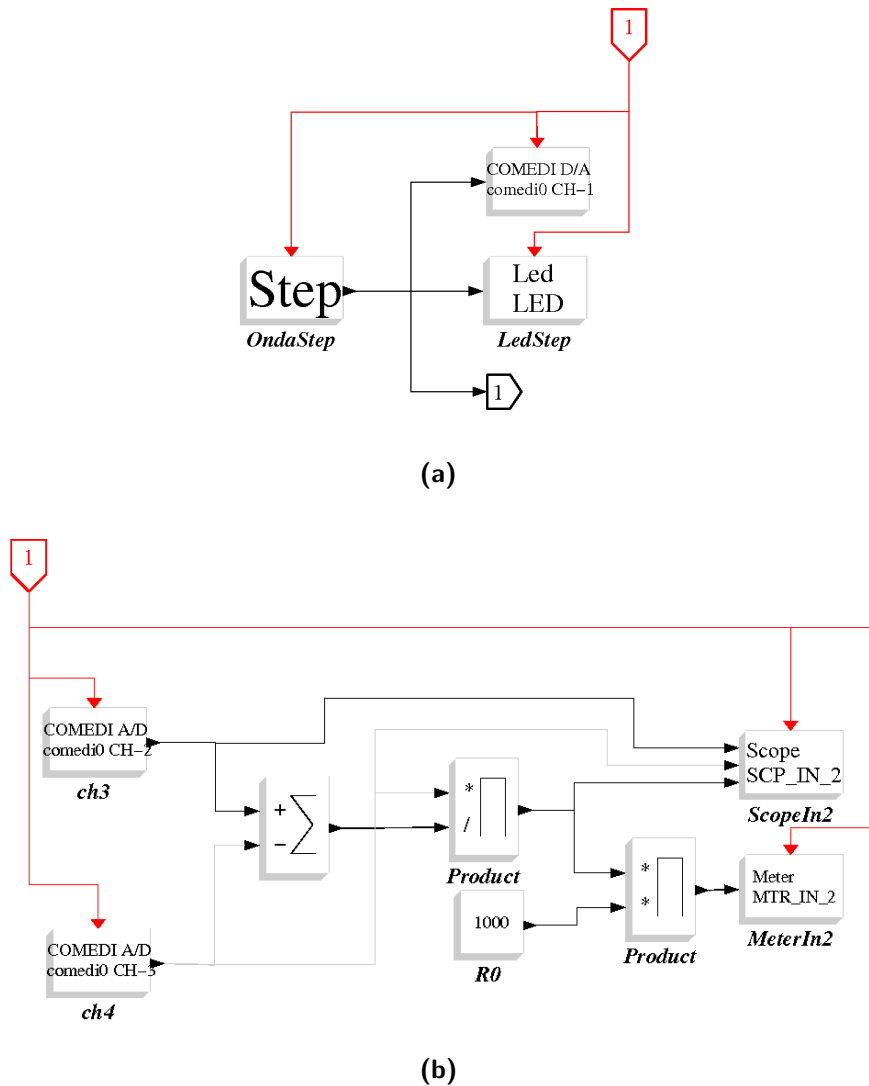
Figure 3.12: Schematic of the acquisition system, made with *SCILAB/SCICOS*.
(a) Led survey and (b) resistivity acquisition.

scopes that, like real ones, are able to show the measured quantity for every
used channel (with different colours) and save them on files;

meters that show the desired quantity in a dynamic way, for example, on
the right low corner, a clock measuring the (real-)time of the running
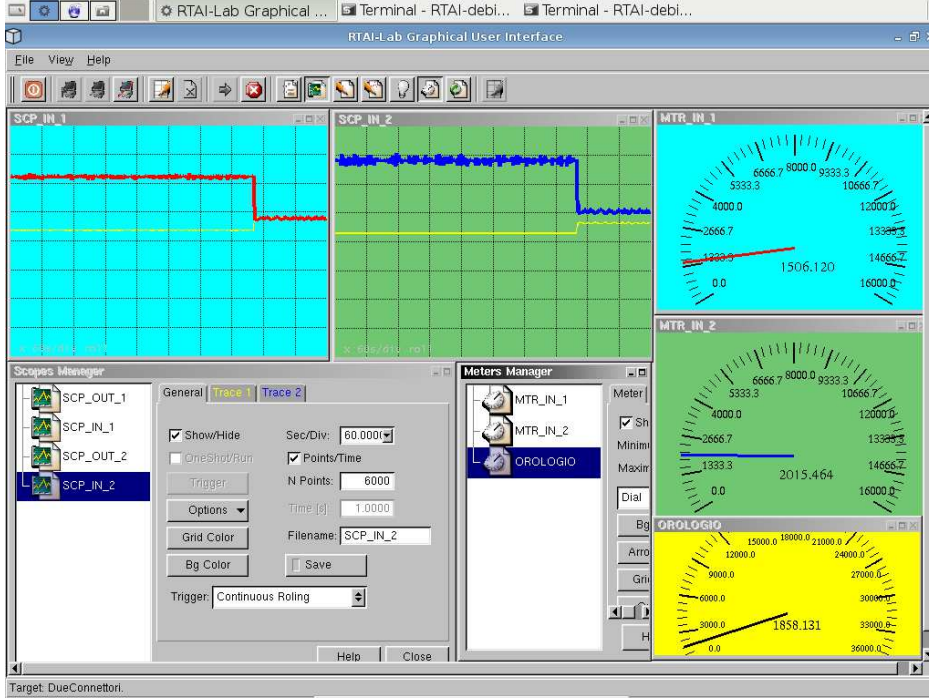process is shown;

panels used to set varius parameters.

Figure 3.13: Screen-shot of the xrtailab graphical user interface used to control the acquisition process.

Given a fix voltage $V_{tot} = 5V$ over a serie constituted by a known resistance R_0 and the one of the photo-resistor R_{FR} as visible in Fig. 3.11, the acquisition system gave the last one as:

$$R_{FR} = R_0 \left(\frac{V_{tot}}{V_0} - 1 \right) \tag{3.1}$$

where V_0 is the voltage over R_0. It is possible to determine the concentration of the powder in the working fluid for a given working condition with two known values of the C-R_{FR} couple. The first couple of points is provided by a calibration phase (as described in Section 2.2). That phase, which is performed during every experiment, consists of a $600sec$ measurement with a known initial concentration and without a filtering element. Moreover the initial concentration, even if the powder is weighted with an accurate *GALILEO-SARTORIUS* balance (with an absolute error of $10^{-2}g$), is subjected to inaccuracy, mainly because of the uncertainty about the working fluid volume. The calibration phases are, for example, visible as the left curves in Fig. 4.2-4.3. The right curves in the same figures are obtained after turning off the pump, inserting the filter and turning on the pump again.
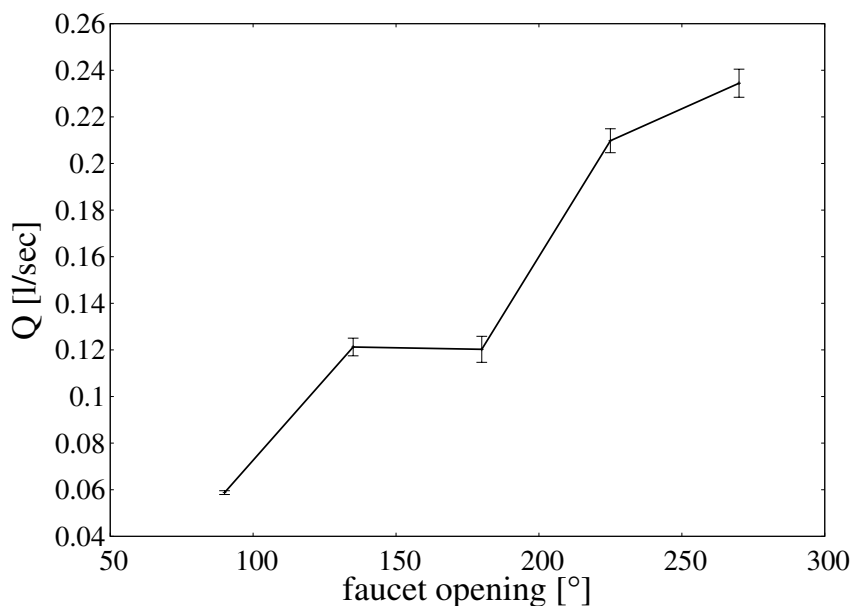
Figure 3.14: Image of the measured correlation between the valve opening and
the volume flow rate.

The second couple of $C - R$ points is choosen at the end of the filtration
phase. In fact, a $0 - 0$ couple is usually usually reached. Moreover, for the
fitting, a more precise value for that couple is obtained measuring the con-
centretation of a corrisponding sample with the off-line concentration-meter
(see Appendix C.3).

3.3.2   Volume flow rate and temperature

The measure of the volume flow rate was initially performed with three,
independent, methods:

- direct measure with the volume flow rate integrator;

- pressure drop estimation;

- mass-balance-model-parameters fitting.

The results were compared to choose the best approach, which turned out to
be the last one. In fact the error of the volume flow rate integrator resulted
very high for slow flows. The two barometers *111.12*, made by WIKA, are
designed to work between $0bar$ and $2.5bar$ with an error of $0.1bar$ [Bar].
They are inserted with the valve between them, to give us the knowledge of
the volume flow rate which is proportional to the pressure drop [LL06], but

with a big error too, due to a sort of hysteresis in the opening-closing loop. The measure of the pressure drop due to the wool constituting the filtering element resulted unaffordable because of the low packaging factor.

Anyway a correlation between the valve opening and the volume flow rate was deduced and gave us the possibility of choosing the desired range of volume flow rate as visible in Fig. 3.14. More reliable values were then obtained from the fitting of the parameters involved in the particle balance model (Section 2.2). The resulted value turned out to be dependable in all working conditions.

We regularly checked the temperature of the working fluid with a thermocouple connected to a MITEK *MK1330* multi-meter. The temperature turned out to change, probably because of the pump heating, from a room temperature of about $25°C$ to about $35°C$ whithout any appreciable influence on the separation process.

Chapter 4

Measurements and results

As stated in Chapter 2 and in Chapter 3 the used RTAI acquisition system is able to collect measured values of voltage and, from them, calculate the corresponding resistances. The resistance is then transformed into the more interesting concentration. This is done through the $C = a + b \log R$ relation between concentration and resistance (see Appendix C.2, eq. C.3). That relation needs to be fitted for every experimental condition in order to determine the two parameters a and b. In fact during each experience the pipes between the leds and the light-dependent resistors get dirty and, even if the following cleaning is accurate, the subsequent starting conditions are significantly different. Moreover, while cleaning is performed, some twisting or torsion is occasionally transmitted to the two active elements changing their alignment and, consequently, to the range of the intensity of the incident light [Mar+10].

4.1 Measurements

4.1.1 Rough results

Magnetite #48800

The first experimental campaign has been carried out using the #48800 magnetite to simulate the adsorbent. The high deposition velocity led to the use of cooking oil as working fluid, thanks to its higher viscosity compared to water (Fig. 4.1a). Anyway the high magnetic susceptibility of the magnetite powder caused two undesired phenomenons:

1. auto-aggregation of the particles so that the un-interacting particles hypothesis resulted wrong;

2. as a consequence of 1 the gradient of the magnetic field due to the composite nature of its source (three ingots for each face) resulted enough to retain particles, as visible in Fig. 4.1b.

This problem, well visible in Fig. 4.1, implies the inapplicability of our model so that the experiments carried out with the magnetite powder resulted useless with respect to what exposed in Chapter 2 and in Chapter 3. Anyway the model, being a general purpose one, is able to predict the behaviour of the magnetite powder at lower granulometry, i.e. with an higher adsorbent

(a) Picture of the filtering process with filtering element

(b) Picture of the filtering process without filtering element

Figure 4.1: The pictures show a filtration moment, with and without filtering element, for the magnetite powder #48800. The comparison illustrates the inapplicability of the developed model to the considered experimental conditions.

specific surface. In that situation the capture would be good enough for most applications with a very high adsorbing efficiency.

Hematite #48100 **and** #48651

To test the developed model in a congruent way the two hematite #48100 and #48651 had been chosen. Their magnetic susceptibility is in the range of paramagnetism so that no undesired phenomenon, such as capture in slowly varying magnetic fields or particle-particle interaction, arise. Moreover the hematite density and viscosity (relatively to water) resulted such that deposition velocity was quite low and water usable and consequently chosen as working fluid. After some initial test the working parameters for the circuit described in Table 2.1 were chosen as:

C_0 , the initial concentration, was chosen equal to $0.2g/l$ in order to avoid deposition and clogging on the filtering element. The resulting mass was $m_p = V_{tot} * C_0 = 0.55g$, where $V_{tot} = V_0 + V_1 + V_2 + V_3 = 2.75l$ (see Section 2.2).

u_0 , the unperturbed velocity in the filtering element region, is determined from the flow rate, on the basis of the effective area of the drilled holes in the pipe. Considering a flow rate Q of about $0.15l/s$, i.e. the valve opening equal to about $180°$, the resulting velocity is $u_0 = Q/A_{tot} \approx 0.2m/s$, where $A_{tot} = 27\pi(d_h/2)^2 \approx 50mm^2$. It's worth noting that with this opening the pressure drop on the filter, as stated, is under the experimental sensibility of the manometers. On the other side the pressure drop through the valve resulted of about $1bar$.

In Fig. 4.2 and in Fig. 4.3 some examples of these results are shown. The *rough* data in each imagine are acquired during a filtration experience with the following sequence of steps:

1. the circuit, in which the filter in not inserted, is filled with clean water (thanks to the pump);

2. the pump is stopped;

3. the powder, weighed as described in the end of Section 3.3.1, is dropped in the tank;

4. the stirrer is plugged;

5. a 10 minutes data acquisition is started [1];

---

[1]These data are visible in the left of each figure. For example, in Fig. 4.2 (up), they are the ones between about $670ms$ and $1270ms$.
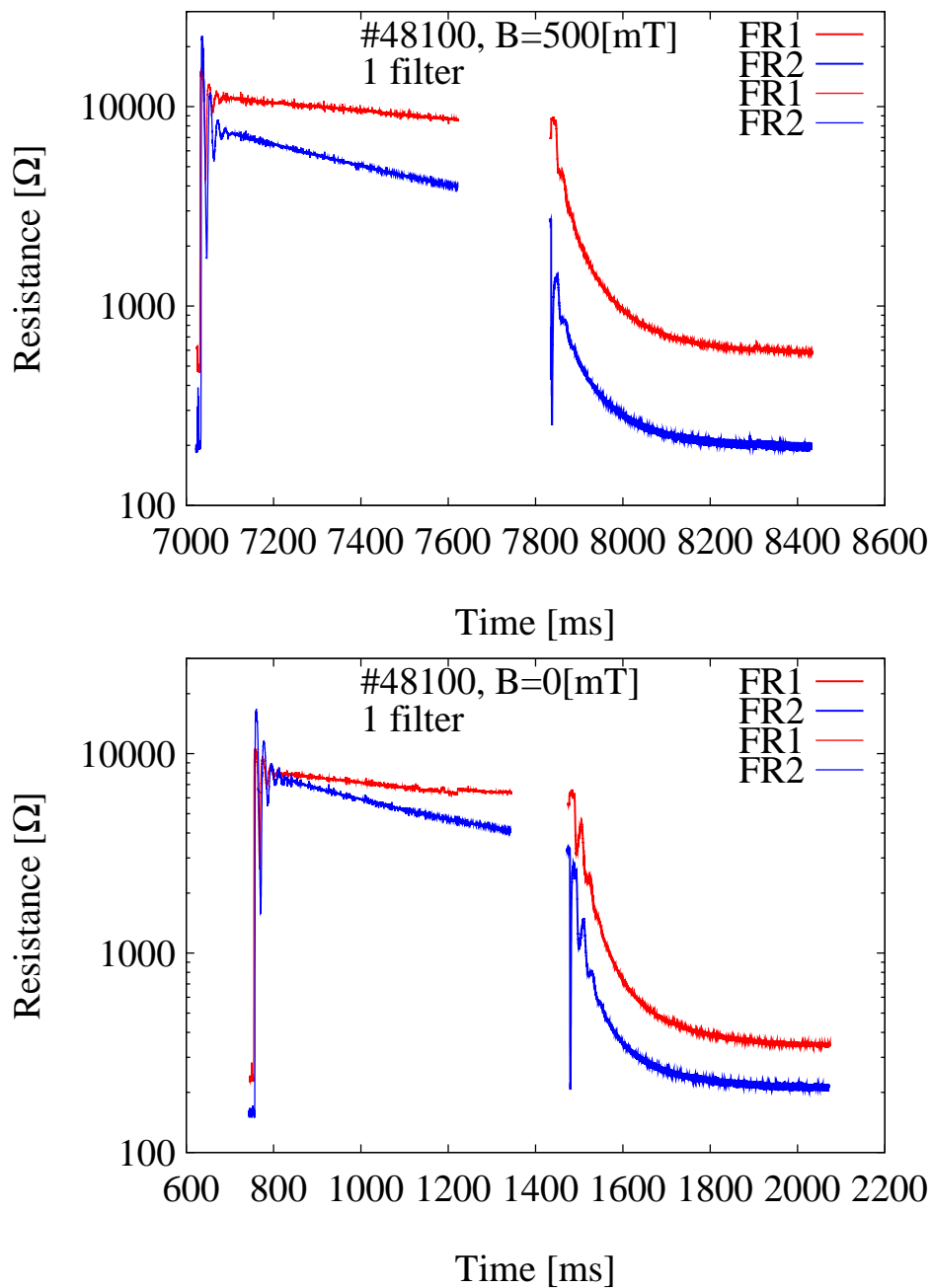
Figure 4.2: Resistance obtained (up) with and (down) without the external magnetic field applied on the FR1 (red) and FR2 (blue) for #48100, in both cases with one filtering element.
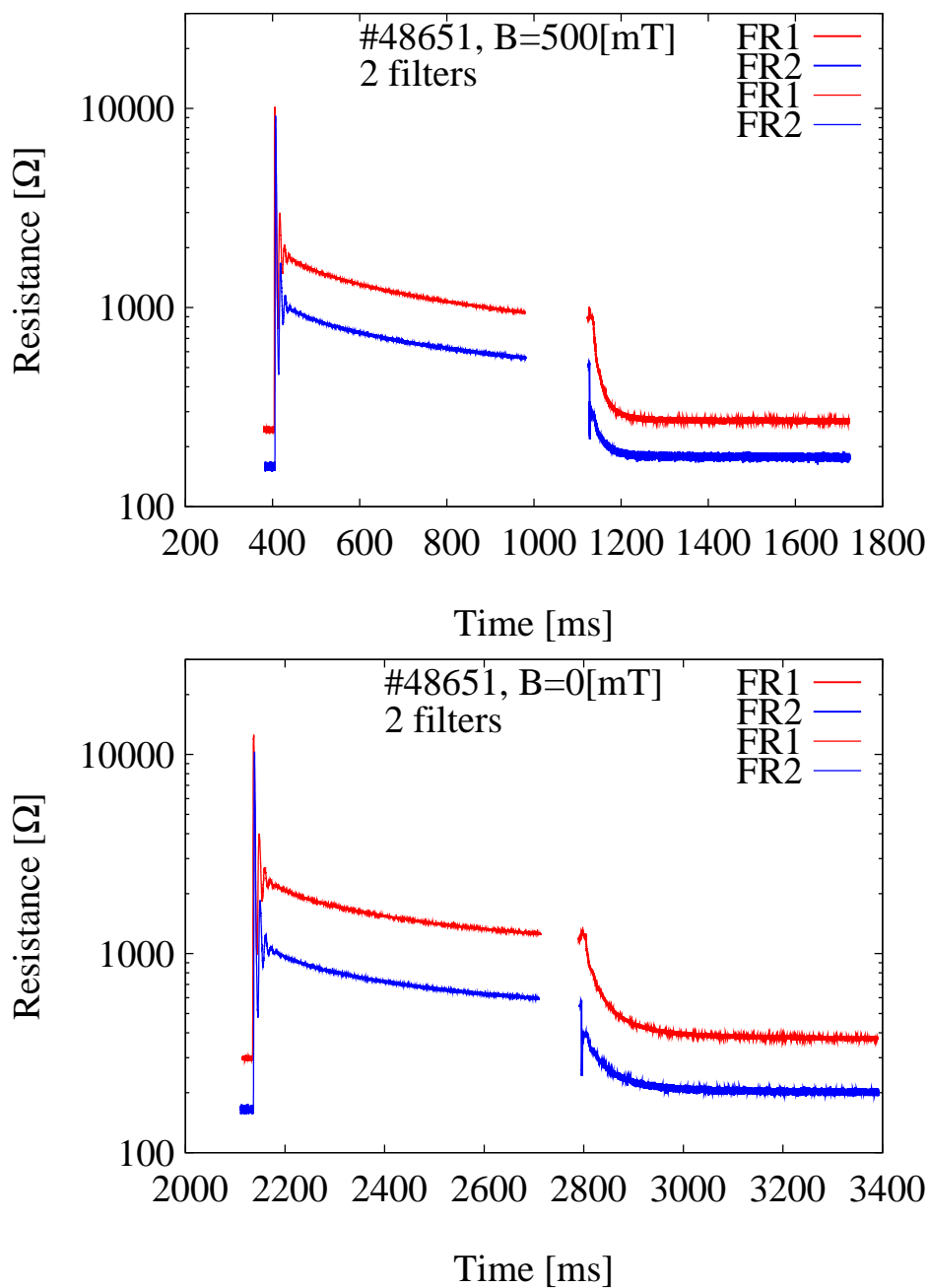
Figure 4.3: Resistance obtained (up) with and (down) without the external magnetic field applied on the FR1 (red) and FR2 (blue) for #48651, in both cases with two filtering elements.

6. the pump is turned on;

7. after 10 minutes the pump is turned off and the filter, filled of clean water, is inserted [2];

8. a second 10 minutes data acquisition is started [3];

9. after 10 minutes the pump is turned off and the whole circuit cleaned.

It can be seen in these images that in both phases the resistances measured with the two concentration meters (FR1 and FR2) are quite different. Instead, in particular during the calibration phase (in which the filter is not inserted and FR1 and FR2 are very close) and at the end of the filtering experience (in which the water is almost clean), the values should be nearly equal. The main features of this lack of bias are two: the starting value and the slope of the two curves. These aspects are compatible with the resistance-concentration function developed in Appendix C.2 which lies in a linear relation between the two for each turbidity meter.

4.1.2 Processed results and mass balance model

The application of eq. (C.3) is done, for each experimental session, using gnuplot[4]. The two couples $c - R$ used for the calculation of a and b are the following:

1. The resistance corresponding to the average initial concentration C_0 is determined at the start of the calibration phase[5].

2. The resistance corresponding to the quasi-null concentration is determined from the last collected point[6].

---

[2]The filter can be constituted by one or two filtering elements (as stated in Section 3.1). As described later in the main text Fig. 4.2 shows the results obtained with one filtering element and #48100 while Fig. 4.3 shows a two filtering elements experience and #48651.

[3]These data are visible in the right of each figure. For example, in Fig. 4.2 (up), they are the ones between about $1480ms$ and $2080ms$.

[4]*gnuplot* is a plotting program with tons of maths utilities whose source code is copyrighted but freely distributed [Gnua].

[5]For example for FR1 (the upriver concentration meter) in Fig. 4.2 (up) a resistance value of about 1022Ω, corresponding to about $7050sec$, has been chosen. This value is averaged in the initial periodic behaviour of the resistance due to the mixing of the highly concentrated powder in the tank ($\hat{b} = m_p/V_0 = 0.55g/l$) and the clean water filling the remaining part of the circuit.

[6]Indeed, at the end of each measuring session, the water, checked with FR0, resulted almost clean.
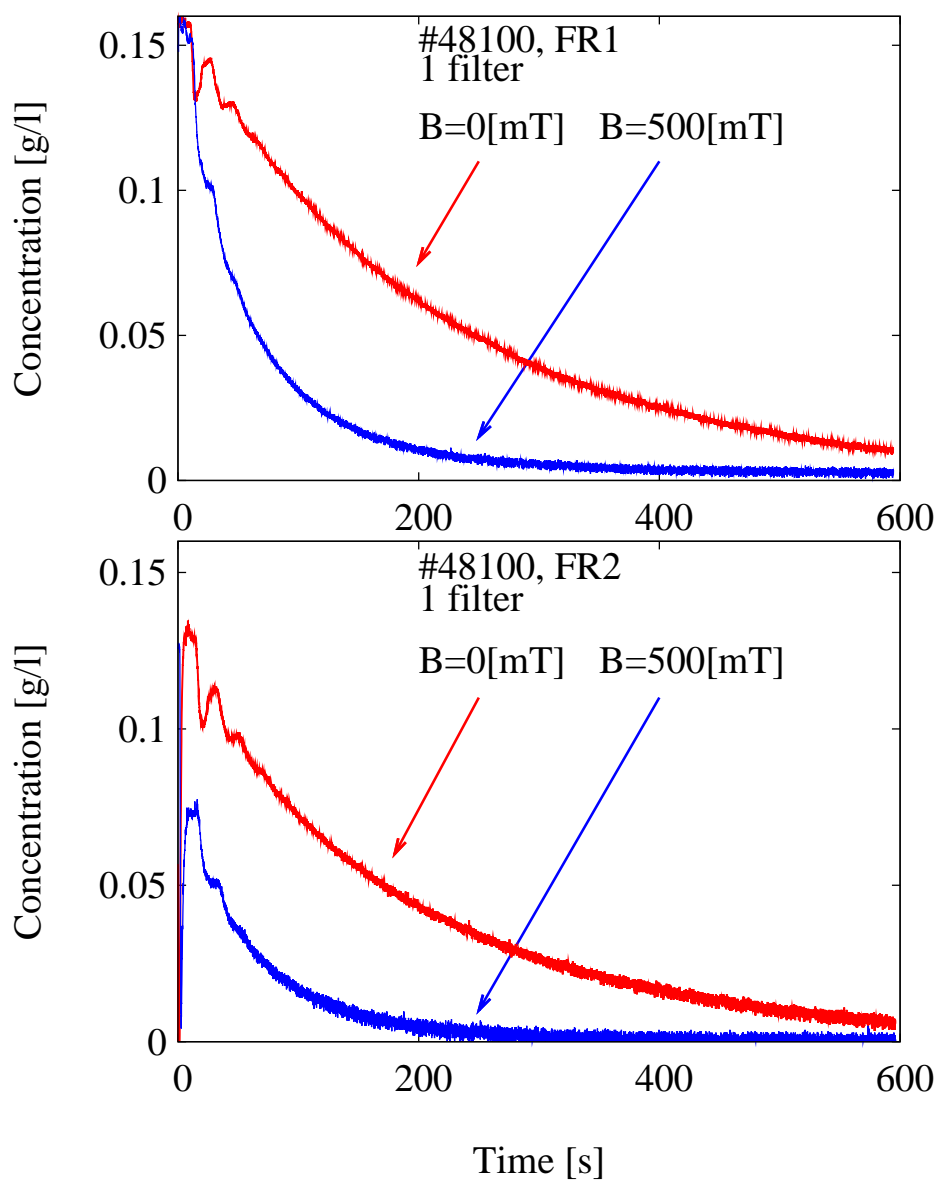
Figure 4.4: Particle concentration with (blue line) and without (red line) the external magnetic field applied on the FR1 (up) and FR2 (down) for #48100, in both cases with one filtering element.
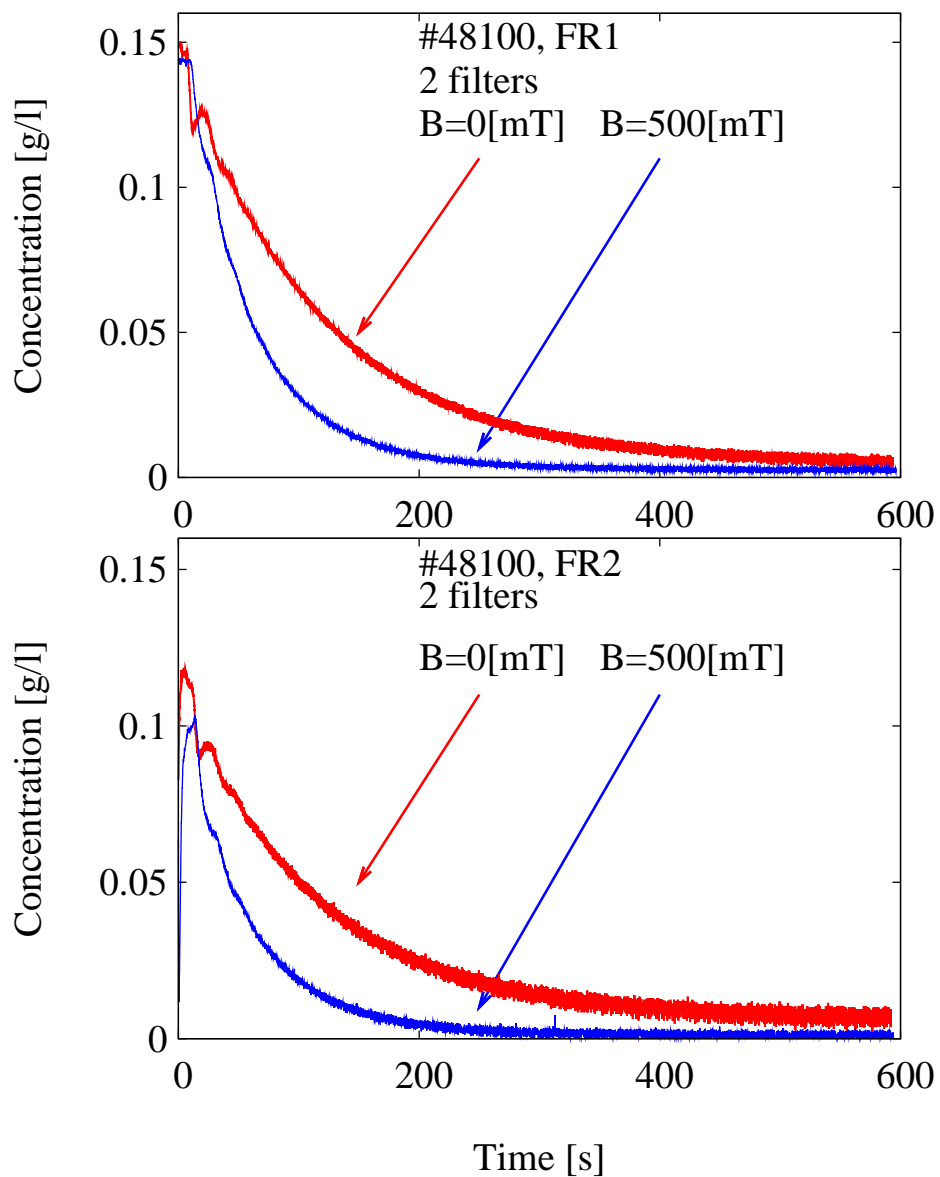
Figure 4.5: Particle concentration with (blue line) and without (red line) the external magnetic field applied on the FR1 (up) and FR2 (down) for #48100, in both cases with two filtering elements.
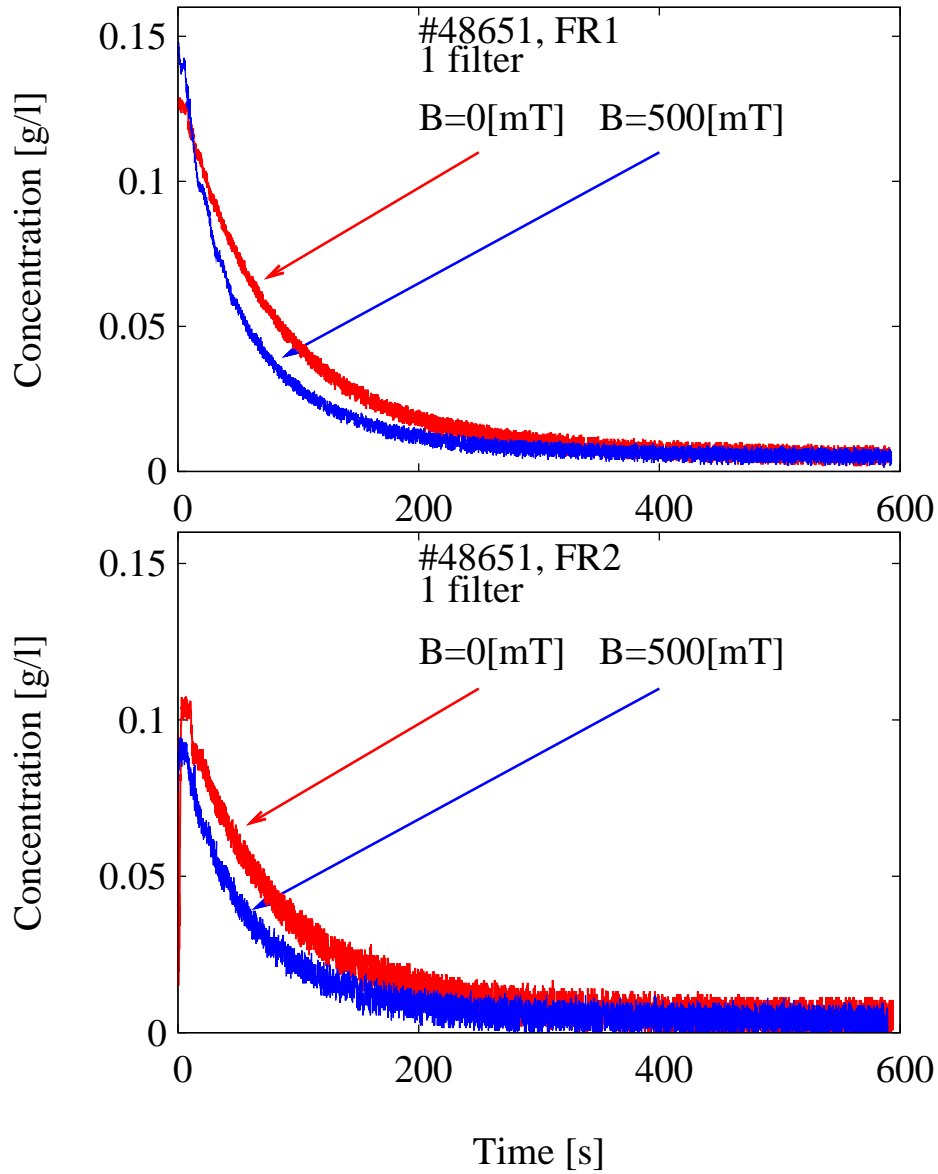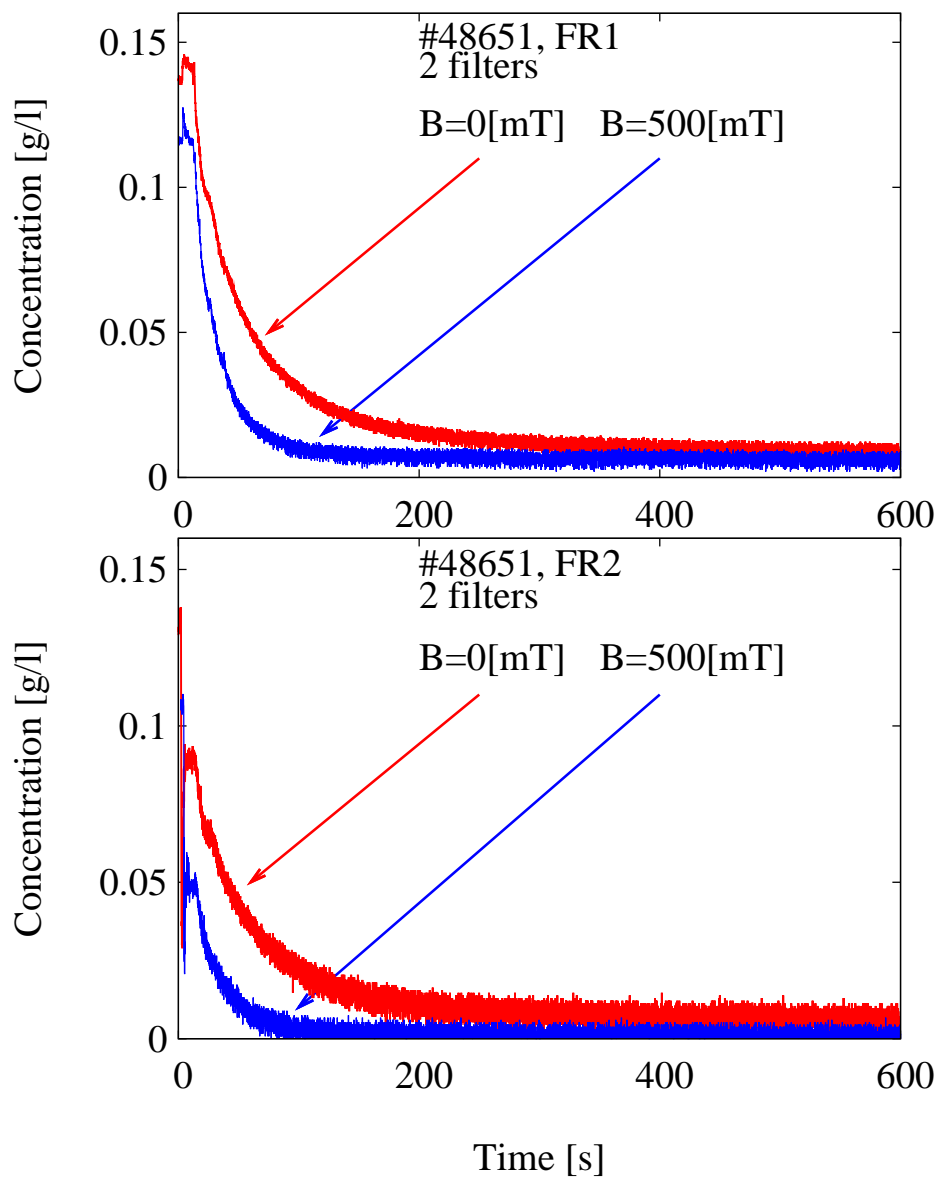
Figure 4.6: Particle concentration with (blue line) and without (red line) the external magnetic field applied on the FR1 (up) and FR2 (down) for #48651, in both cases with one filtering element.

Figure 4.7: Particle concentration with (blue line) and without (red line) the external magnetic field applied on the FR1 (up) and FR2 (down) for #48651, in both cases with two filtering elements.

Figure 4.4-4.7 shows the result of such fitting to the values measured during the filtering phase for the two different powders (for one and two filtering elements)[7]. For both powders a neat improvement in the retention efficiency is visible when the magnetic field is applied. That improvement is more visible with #48100, because the smaller particles are harder to capture with sieving only. An improvement is also visible, for each powder, when two filtering elements are inserted instead of one.

4.2 Numerical values

In order to deduce numerical values from the former qualitative analysis the mass balance model is applied (see Section 2.2). The fitting, performed for each experiment separately, followed this algorithm:

1. the flow rate was determined in order to fit the frequency of the oscillations in the first phase of the calibration[8];

2. the initial concentration was adjusted in order to reach the initial amplitude;

3. the decay rates for population I and for population III were fitted in order to follow the calibration phase slope[9];

4. the decay rate for population II was fitted in order to follow the filtration phase slope.

The results of such process is shown for some cases in Fig. 4.8 and in Fig. 4.9 for #48100 and #48651 respectively[10]. It's worth to note the different behaviour of the two turbidity meters: in FR2 data a neat peak is visible in the filtering phase due to the clean water initially filling the filter. This particular behaviour is well reproduced by the model too. The work performed on each set of measures led to the average values listed in Table 4.1 for one filtering element and in Table 4.2 for two filtering elements. The results show that, as expected, the capture is better with the magnetic field applied and with two filtering elements. Table 4.3 shows the capture efficiencies of the filter in the various experimental conditions calculated from the results

---

[7]The time, equal for each figure and ranging from $0sec$ to $600sec$, is calculated from the second starting of the pump.

[8]This is well visible in the left frame of Fig. 4.8 and 4.9.

[9]This is visible in the right frame of Fig. 4.8 and 4.9 in which the initial values are comparable to the experimental ones.

[10]The time is rescaled starting from the first starting of the pump.
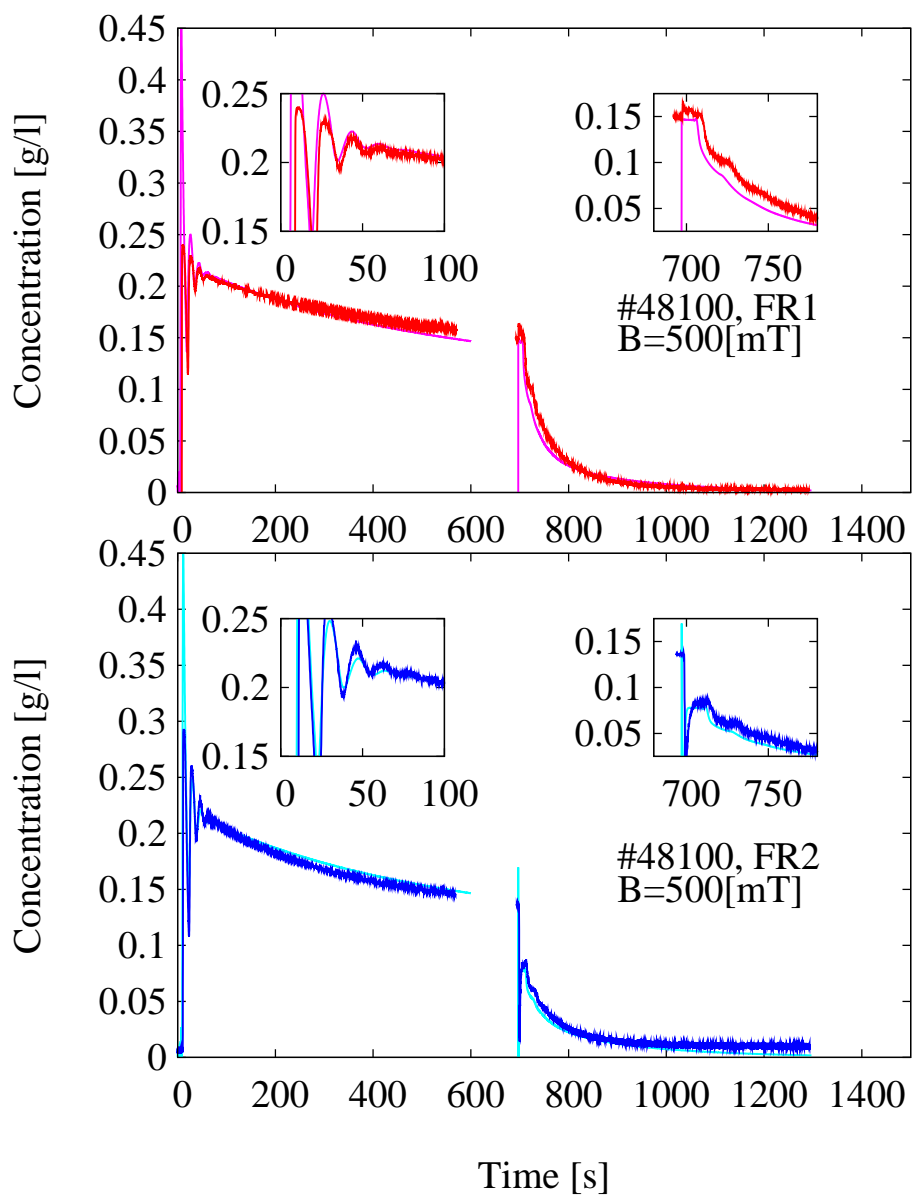
Figure 4.8: Experimental (thick lines) and simulated (thin lines) particle concentration with the external magnetic field applied on the FR1 (red) and FR2 (blue) for #48100.
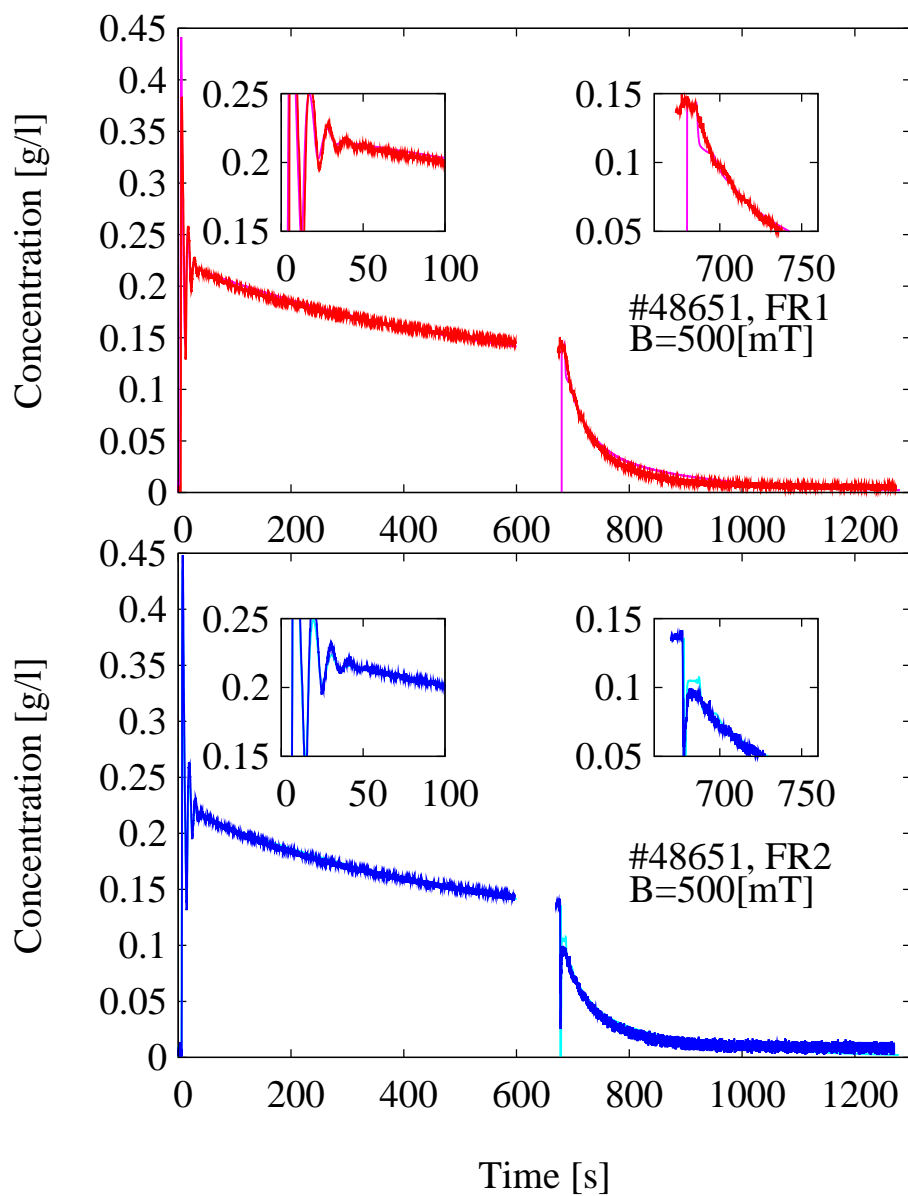
Figure 4.9: Experimental (thick lines) and simulated (thin lines) particle concentration with the external magnetic field applied on the FR1 (red) and FR2 (blue) for #48651.

Table 4.1: Range of values used for the simulations with one filtering element, relative error of 10%.

	#48100 1 filter	#48651 1 filter
$Q\left[m^3/s\right]$	0.11×10^{-3}	0.17×10^{-3}
$\lambda_{1,I}\left[s^{-1}\right]$	0.22×10^{-3}	0.28×10^{-3}
$\lambda_{2,I}\left[s^{-1}\right]$ (B = 0T)	0.20	0.30
$\lambda_{2,I}\left[s^{-1}\right]$ (B = 500mT)	0.34	0.50
$\lambda_{3,I}\left[s^{-1}\right]$	0.22×10^{-3}	0.28×10^{-3}
$\lambda_{1,II}\left[s^{-1}\right]$	0.10×10^{-3}	0.40×10^{-3}
$\lambda_{2,II}\left[s^{-1}\right]$ (B = 0T)	0.01	0.02
$\lambda_{2,II}\left[s^{-1}\right]$ (B = 500mT)	0.02	0.03
$\lambda_{3,II}\left[s^{-1}\right]$	0.10×10^{-3}	0.40×10^{-3}
$\lambda_{1,III}\left[s^{-1}\right]$	1.10×10^{-3}	3.40×10^{-3}
$\lambda_{2,III}\left[s^{-1}\right]$ (B = 0T)	0.12	0.08
$\lambda_{2,III}\left[s^{-1}\right]$ (B = 500mT)	0.27	0.03
$\lambda_{3,III}\left[s^{-1}\right]$	1.10×10^{-3}	3.40×10^{-3}
$m_I\left[g\right]$	0.20	0.18
$m_{II}\left[g\right]$	0.04	0.04
$m_{III}\left[g\right]$	0.25	0.19

Data refers to experiments repeated at least two times.

of the system mass balance model using (2.33). The experimental activity with two filtering elements has been carried out also as a further check of the separation results. In fact, the relation between the capture efficiency on one and two filtering elements in known by definition to be:

$$1 - \sigma_{2filters} = (1 - \sigma_{1filter})^2 \tag{4.1}$$

Equation (4.1) is correct if the two filters are identical. In the present experience conditions two different, i.e. hand made, filters have been used and this circumstance led to an unavoidably slightly big experimental error.

To check the deduced decay rates $\lambda_{i,k}$ with the σ deduced from the cell model a number of cells between 6 and 8 for each filtering element has been assumed. This number is due to the knowledge of the dept of the iron steel wool used in the construction of the filtring elements. The same knowledge lead to the value of the packaging factor $\Gamma = 3.5 \times 10^{-3}$. The capture efficiency for the single cell is then estimated from eq.(2.28) as $0.1 \pm 10\%$. This value must be compared with the results shown in Fig. 2.6. Assuming $d_p = 0.8 \pm 20\%$ μm, $\chi_p = 2 \times 10^{-3}$ [Oka+02], $\mu_0 M = 1$ T [BCD03], $B_0 = 0.5$ T, $\eta = 1$ mPa·s, $u_0 = 0.15$ m/s and $r_c = 15$ μm I can deduce the capture parameter $\Omega = 0.008 \pm 50\%$. This huge variation is not an error, but takes into account the different sizes of the two particulate matters used. The

Table 4.2: Range of values used for the simulations with two filtering elements, relative error of 10%.

	#48100 2 filters	#48651 2 filters
$Q\ [m^3/s]$	0.12×10^{-3}	0.17×10^{-3}
$\lambda_{1,I}\ [s^{-1}]$	0.22×10^{-3}	0.35×10^{-3}
$\lambda_{2,I}\ [s^{-1}]$ (B = 0T)	0.19	0.70
$\lambda_{2,I}\ [s^{-1}]$ (B = 500mT)	0.50	1.00
$\lambda_{3,I}\ [s^{-1}]$	0.22×10^{-3}	0.35×10^{-3}
$\lambda_{1,II}\ [s^{-1}]$	0.11×10^{-3}	0.42×10^{-3}
$\lambda_{2,II}\ [s^{-1}]$ (B = 0T)	0.02	0.03
$\lambda_{2,II}\ [s^{-1}]$ (B = 500mT)	0.03	0.03
$\lambda_{3,II}\ [s^{-1}]$	0.11×10^{-3}	0.42×10^{-3}
$\lambda_{1,III}\ [s^{-1}]$	0.12×10^{-3}	0.40×10^{-3}
$\lambda_{2,III}\ [s^{-1}]$ (B = 0T)	0.21	0.32
$\lambda_{2,III}\ [s^{-1}]$ (B = 500mT)	0.42	0.42
$\lambda_{3,III}\ [s^{-1}]$	0.12×10^{-3}	0.40×10^{-3}
$m_I\ [g]$	0.23	0.18
$m_{II}\ [g]$	0.05	0.04
$m_{III}\ [g]$	0.24	0.22

Table 4.3: Capture efficiency in the various experimental conditions.

	#48100 1 filters	#48100 2 filters	#48651 1 filters	#48651 2 filters
σ_{filter}	$0.25 \pm 10\%$	$0.35 \pm 10\%$	$0.4 \pm 10\%$	$0.7 \pm 10\%$
σ^*_{filter}	$0.4 \pm 10\%$	$0.55 \pm 10\%$	$0.45 \pm 10\%$	$0.8 \pm 10\%$

* These values refer to the applied field case.

stronger limiting value of Ω deduced from (2.25) and (2.26) is $0.003 \pm 50\%$. This limit is not that relevant since the capture efficiencies with and without particles inertia, shown in Fig. 2.6, are nearly the same and quite constant in the considered range. Thus I deduce $\sigma_{cell} = 0.09 \pm 10\%$ from Fig. 2.6, that is consistent with the one obtained with the system mass balance model. It can be seen from Table 4.3 and also from Fig. 4.4-4.7 that the improvement of the capture efficiency due to the application of the field is particularly marked for #48100 probably thanks to the lower size of that powder with respect to the #48651. On the other side, it is worth to note that, even without external magnetic field applied, also the quasi-static model predicts a non zero number of stopped particles due to the fact that there are flow lines arbitrarily close to each fiber. Thus, in the limit case of a wool with inter-fibers distance always lower than the particles' diameter each particle is

stopped. This confirms the applicability of the model to both the considered experimental conditions for each powder. For both powders a test without wool, i.e. with applied field only, gives no capture at all, as expected.

Chapter 5

Conclusions

After a short review of the state of the art in the magnetic separation field a numerical model to simulate the capture process in an HGMS filter is presented. The model is aimed to improve the usual approaches to the problem, which neglect the matrix to matrix interaction and oversimplifies the velocity and flux density fields. The proposed approach divides the filter into a large number of elementary volumes (cells) and assume a spatial periodicity condition. For a given cell geometry the velocity and flux density fields resulting from the complete interaction of all the fibers of the wool are evaluated. This leads us to calculate the capture efficiency using a statistical approach both for the geometry of the cell and the trajectories of the particles. An independent model is presented which describes the temporary evolution of the particle concentration in the whole filter on the base of simple assumption on the conservation of the particle number. With this second model the check of the cell model to the experimental data is made possible. An experimental activity on a laboratory device has been carried out in order to perform the test. An experimental facility has been projected and realized in the LIMSA laboratory overcoming the quest of a REAL-time measuring set-up.

The capture efficiencies for the cell obtained from the trajectory model are well comparable and consistent with the experimental data. Moreover, the results show that the filter efficiency is increased when the magnetic field is applied also for relatively small fields. This confirms the feasibility of the HGMS technology when SC magnets are utilized, but also opens the possibility to utilize permanent magnets evaluating the trade off between efficiency and cost. In order to scale the filter for an industrial process there is the need to join the cell model with the system model taking into account the local conditions of the single cells such as relative orientation among wool fibers, external induction field and mean velocity field. It is also necessary to

implement a model for the filter saturation making the capture efficiency a time dependent function. The problem of the dispose of the filtering element has been overcome using non-toxic iron oxide, but remains as an industrial trial would start. The iron steel wool is very cheap so a disposal of the whole filtering element remains possible. Conversely also its cleaning is available. The cleaning is possible with decreasing oscillating field in order to demagnetize the wool followed by a strong stream of air or liquid in order to drain away the clogging.

Appendix A

Magnetization

A.1 Limiting magnetization of a spherical particle

To verify that the maximum magnetization for a spherical particle can not exceed 3 we consider a sphere $\mathcal{S}$ of radius R immersed in an external and uniform magnetic field $\mathbf{H}_e$ directed along the z axis. We call the magnetic permeability of the sphere and of the medium, respectively, μ_p and μ_f. From Maxwell equations we have, everywhere in space, $\nabla \times \mathbf{H} = 0$ and $\nabla \cdot \mathbf{B} = 0$, on the discontinuity surfaces $\mathbf{H}_{t|\delta\mathcal{S}} = continuos$ and $\mathbf{B}_{n|\delta\mathcal{S}} = continuos$ and, at infinity, $\mathbf{H}_{|\infty} = \mathbf{H}_e$. Being the magnetic field conservative we can introduce the scalar potential ψ; distinguishing the region inside the sphere (in) and the outer one (out) we have $\mathbf{H}_{in} = -\nabla \psi_{in}$ and $\mathbf{H}_{out} = -\nabla \psi_{out}$. Moreover, being the two materials homogeneous, the Laplace equation is satisfied in both domains: $\nabla^2 \psi_{in} = 0$ and $\nabla^2 \psi_{out} = 0$. We search the solution in spherical coordinates, with the polar axis along z. Being the inner field uniform while the outer the superposition of the external one and of the dipole one produced by the sphere we have:

$$\psi_{in} = -\alpha H_e r \sin\theta \Rightarrow \mathbf{H}_{in} = \alpha H_e (\sin\theta \mathbf{e}_r + \cos\theta \mathbf{e}_\theta)$$
$$= \alpha H_e \mathbf{e}_z = \alpha \mathbf{H}_e$$
$$\psi_{out} = -H_e r \sin\theta + \beta H_e \frac{R^3}{r^2} \sin\theta \Rightarrow \mathbf{H}_{out} = \mathbf{H}_e + 2\beta H_e \frac{R^3}{r^3} \sin\theta \mathbf{e}_r$$
$$- \beta H_e \frac{R^3}{r^3} \cos\theta \mathbf{e}_\theta$$

Thank to the polar symmetry we can write the interface conditions in the following form:

$$H_{in,\theta}(r = R) = H_{out,\theta}(r = R) \Rightarrow \alpha = 1 - \beta$$
$$\mu_p H_{in,\theta}(r = R) = \mu_f H_{out,\theta}(r = R) \Rightarrow \alpha\mu_p = \mu_f + \mu_f 2\beta$$

Introducing the susceptibility $\mu_k = \mu_0(1 + \chi_k)$ with $k = p, f$ we achieve:

$$\alpha = \frac{3 + 3\chi_f}{3 + \chi_p + 2\chi_f} \quad \beta = \frac{\chi_p - \chi_f}{3 + \chi_p + 2\chi_f} \tag{A.1}$$

As stated the magnetic field inside the sphere is uniform. Moreover the magnetization is correlated to $\mathbf{H}_e$ with an affective susceptibility which is different from the one of the material:

$$\mathbf{M} = \chi_p \mathbf{H}_{in} = \chi_p \alpha \mathbf{H}_e = \chi_{p,eff}\mathbf{H}_e \tag{A.2}$$

in which we defined:

$$\chi_{p,eff} = \chi_p \frac{3 + 3\chi_f}{3 + \chi_p + 2\chi_f} \tag{A.3}$$

We can notice that when $\chi_f = 0$, i.e. the sphere is surrounded by air:

$$\lim_{\chi_p \ll 1} \chi_{p,eff} = \chi_p$$
$$\lim_{\chi_p \gg 1} \chi_{p,eff} = 3$$

q.e.d..

A.2   Measures of magnetic permeability

An experimental facility has been realized in order to measure the magnetic permeability of samples of magnetite powder[1] and of iron steel wool. The relation between the sample magnetization and the material magnetization has been deduced in two different situation: considering a macroscopically isotropic material and considering a macroscopically non isotropic one.

---

[1]The magnetic permeability of the hematite powder, being a paramagnetic substance, resulted beyond the experimental limit of the described instruments.

A.2.1 Macroscopically isotropic material

Considering a mixture of linear phases with different magnetic permeability it's possible to define $\mathbf{B} = \mu\mathbf{H}$ everywhere. Anyway this function is certainly quickly varying. Following Landau [LL87] the volumetric average operator can be introduced as follow:

$$< \psi > = \frac{1}{V} \int_V \psi d\tau$$

so that $< \mathbf{B} > = \mu_{mix} < \mathbf{H} >$. Considering the mixture filling the space everywhere, the average values of the fields result independent of the position and defining the following local relations:

$$\mathbf{H} = < \mathbf{H} > + \delta\mathbf{H}$$
$$\mu = < \mu > + \delta\mu$$

Noting that, by definition:

$$< \delta\mathbf{H} > = 0$$
$$< \delta\mu > = 0$$

it's possible to write:

$$< \mathbf{B} > = < \mu\mathbf{H} > = < \mu > < \mathbf{H} > + < \delta\mu\delta\mathbf{H} > \tag{A.4}$$

On the first order approximation $\mu_{mix} \approx < \mu > + O\left((\delta\mu)^2\right)$. To improve this result I consider now $\nabla \cdot \mathbf{B} = 0$:

$$0 = \nabla \cdot [\mu\mathbf{H}] \approx < \mu > \nabla \cdot \delta\mathbf{H} + < \mathbf{H} > \cdot \nabla\delta\mu \tag{A.5}$$

Being the mixture almost homogeneous:

$$\frac{\partial}{\partial x}\delta H_x \approx \frac{\partial}{\partial y}\delta H_y \approx \frac{\partial}{\partial z}\delta H_z \approx \frac{1}{3}\nabla \cdot \delta\mathbf{H}$$

and choosing the x axis along the $\mathbf{H}$ axis eq. (A.5) transform as

$$3 < \mu > \frac{\partial}{\partial x}\delta H_x + < H_x > \frac{\partial}{\partial x}\delta\mu \approx 0$$

which can be easily integrated independently of the x direction leading to:

$$\delta\mathbf{H} \approx -\frac{< \mathbf{H} >}{3 < \mu >}\delta\mu$$

from which $< \delta\mu\delta\mathbf{H} > \approx -\frac{<\mathbf{H}>}{3<\mu>} < (\delta\mu)^2 >$ and the mixture permeability can be well approximated by:

$$\mu_{mix} \approx <\mu> - \frac{<(\delta\mu)^2>}{3<\mu>} \tag{A.6}$$

For the sake of simplicity it is possible to search a relation of the form $f(\mu_{mix}) = <f(\mu)>$:

$$f(\mu_{mix}) \approx f\left(<\mu> - \frac{<(\delta\mu)^2>}{3<\mu>}\right) \approx f(<\mu>) - \frac{<(\delta\mu)^2>}{3<\mu>}f'(<\mu>)$$

$$<f(\mu)> = \langle f(<\mu>+\delta\mu)\rangle \approx$$

$$\approx \left\langle f(<\mu>) + f'(<\mu>)\delta\mu + \frac{1}{2}f''(<\mu>)(\delta\mu)^2 \right\rangle =$$

$$= f(<\mu>) + \frac{1}{2}f''(<\mu>)\left\langle(\delta\mu)^2\right\rangle$$

from which

$$\frac{1}{2}f''(<\mu>) = -\frac{f'(<\mu>)}{3<\mu>}$$

that can be easily integrated leading to, apart an addictive constant, $f(<\mu>) \propto <\mu>^{\frac{1}{3}}$ so that it's possible to write:

$$\mu_{mix}^{\frac{1}{3}} \approx \left\langle \mu^{\frac{1}{3}} \right\rangle \tag{A.7}$$

For example, for a mixture of spheres of susceptibility μ_s, in air and with a volume ratio of $\zeta = V_{spheres}/V_{mix}$, it can be written:

$$\mu_{mix} = \left[\zeta\mu_s^{\frac{1}{3}} + (1-\zeta)\mu_0^{\frac{1}{3}}\right]^3$$

that satisfy the following properties:

1. $\zeta = 0 \Rightarrow \mu_{mix} = \mu_0$

2. $\zeta = 1 \Rightarrow \mu_{mix} = \mu_s$

3. $\mu_s = \mu_0 \Rightarrow \mu_{mix} = \mu_0, \forall\zeta$

4. $\mu_0 \leq \mu_{mix} \leq \mu_s, \forall\zeta, \forall\mu_s \geq \mu_0$

A.2.2 Macroscopically non isotropic material

If the considered mixture has a preferred orientation and the magnetization is isotropic orthogonally to that preferred orientation (such as if ferromagnetic wool packet with the fibers mainly disposed along one direction is considered) some of the previous results can be still applied. Pointing the preferred axis with the subscript $\parallel$ and the orthogonal direction (just one symbol thanks to isotropy) with the subscript $\perp$ it is possible to write $\mathbf{H} = \mathbf{H}_\parallel + \mathbf{H}_\perp$ so that $< \mathbf{B} >= \mu_{mix,\parallel} < \mathbf{H}_\parallel > + \mu_{mix,\perp} < \mathbf{H}_\perp >$. It follows that, by definition:

$$< \mathbf{B} > =< \mu(\mathbf{H}_\parallel + \mathbf{H}_\perp) >=$$
$$=< \mu\mathbf{H}_\parallel > + < \mu\mathbf{H}_\perp > + < \delta\mu\delta\mathbf{H}_\parallel > + < \delta\mu\delta\mathbf{H}_\perp >$$

Following the procedure of the previous section, from $\nabla \cdot \mathbf{B} = 0$ eq. (A.5) is obtained. Let follow previous section again : considering $H\hat{k} \equiv \mathbf{H} \equiv \mathbf{H}_\perp$ (being $\hat{k}$ the versor along the z axis) implies

$$\frac{\partial}{\partial x}\delta H_x \approx \frac{\partial}{\partial y}\delta H_y \approx \frac{1}{2}\nabla \cdot \delta\mathbf{H}, \ \frac{\partial}{\partial z}\delta H_z \approx 0$$

so that:

$$\delta\mathbf{H}_\perp \approx -\frac{< \mathbf{H}_\perp >}{2 < \mu >}\delta\mu$$

while considering $\mathbf{H} \equiv \mathbf{H}_\parallel$ implies:

$$\frac{\partial}{\partial x}\delta H_x \approx \frac{\partial}{\partial y}\delta H_y \approx 0, \ \frac{\partial}{\partial z}\delta H_z \approx \nabla \cdot \delta\mathbf{H}$$

so that:

$$\delta\mathbf{H}_\parallel \approx -\frac{< \mathbf{H}_\parallel >}{< \mu >}\delta\mu$$

From these results, substituting:

$$\mu_{mix,\parallel} \approx< \mu > -\frac{< (\delta\mu)^2 >}{< \mu >}, \quad \mu_{mix,\perp} \approx< \mu > -\frac{< (\delta\mu)^2 >}{2 < \mu >} \quad \text{(A.8)}$$

Moreover, searching for a relation of the form $f(\mu_{mix}) =< f(\mu) >$ leads to:

$$f_\perp''(< \mu >) = -\frac{f_\perp'(< \mu >)}{< \mu >}, \quad f_\parallel''(< \mu >) = -2\frac{f_\parallel'(< \mu >)}{< \mu >}$$

which have the following solutions:

$$f_\perp(< \mu >) \propto \ln < \mu >, \quad f_\parallel(< \mu >) \propto 1/< \mu >$$

that is to say:

$$\ln \frac{\mu_{mix,\perp}}{\mu_0} \approx \left\langle \ln \frac{\mu}{\mu_0} \right\rangle, \qquad \frac{1}{\mu_{mix,\|}} \approx \left\langle \frac{1}{\mu} \right\rangle$$

Considering iron steel wool, in air and with a ratio $\zeta = V_{Fe}/V_{wool}$, it easily follows:

$$\frac{\mu_{wool,\perp}}{\mu_0} \approx \left(\frac{\mu_{Fe}}{\mu_0} \right)^\zeta, \qquad \frac{1}{\mu_{mix,\|}} \approx \frac{\zeta}{\mu_{Fe}} + \frac{1-\zeta}{\mu_0}$$

A.2.3 Measure of permeability

The facility aimed to the measures of susceptibility is visible in Fig. A.1. It mainly consists of a thin solenoid and a dynamometer: the field inside the solenoid[2], measured with the Gauss probe described in Section 3.1 and fitted with gnuplot via eq. (A.9) as visible in Fig. A.2, exerts a force[3] on a specimen. That force, measured with the dynamometer, is visible in Fig. A.3a and Fig. A.3b for the magnetite and for the wool respectively. Using gnuplot it is also possible to fit eq. (A.10), the analytical expression of the force, with the experimental measures, as visible, again, in Fig. A.3a and Fig. A.3b. The effective susceptibility of the specimen, as described in Appendix A.1, is related to the *traditional* susceptibility which turns out to be related to the permeability of the mixture by:

$$\mu = \mu_0(1 + \chi) = \mu_0 \mu_r$$

For the magnetite, with $\zeta \approx 0.76$, a value $\chi_{magnetite,eff} = 1.45 \pm 0.05$ was measured which led to $\mu_{magtetite,eff} \approx 3.8 \times 10^{-6} H/m$, that is $\mu_{magnetite,eff,r} \approx 3$. The calculation with the wool data, with $\zeta \approx 0.08$, led to $\chi_{wool,eff} = 0.61 \pm 0.02$ which led to $\mu_{wool,eff} \approx 2 \times 10^{-6} H/m$, that is $\mu_{AISI434L} \approx 500 H/m$

---

[2]The field inside a solenoid is expressed by eq. (A.9) as a known function of some geometrical parameters and of the current in the wire [Sol]:

$$B_e(z) = \frac{\mu_0 n I}{2} \left[\frac{d + 2z}{\sqrt{(d+2z)^2 + 4r^2}} + \frac{d - 2z}{\sqrt{(d-2z)^2 + 4r^2}} \right] \tag{A.9}$$

n is the number of coils per meters, I is the current intensity, r is the inner radius of the solenoid and d its thickness.

[3]The magnetic force acting on a spherical mixture of volume V_p with magnetic susceptibility $\chi_{mix,eff}$ in the main symmetry axis z of a solenoid due to the field B_e expressed by eq. (A.9) is:

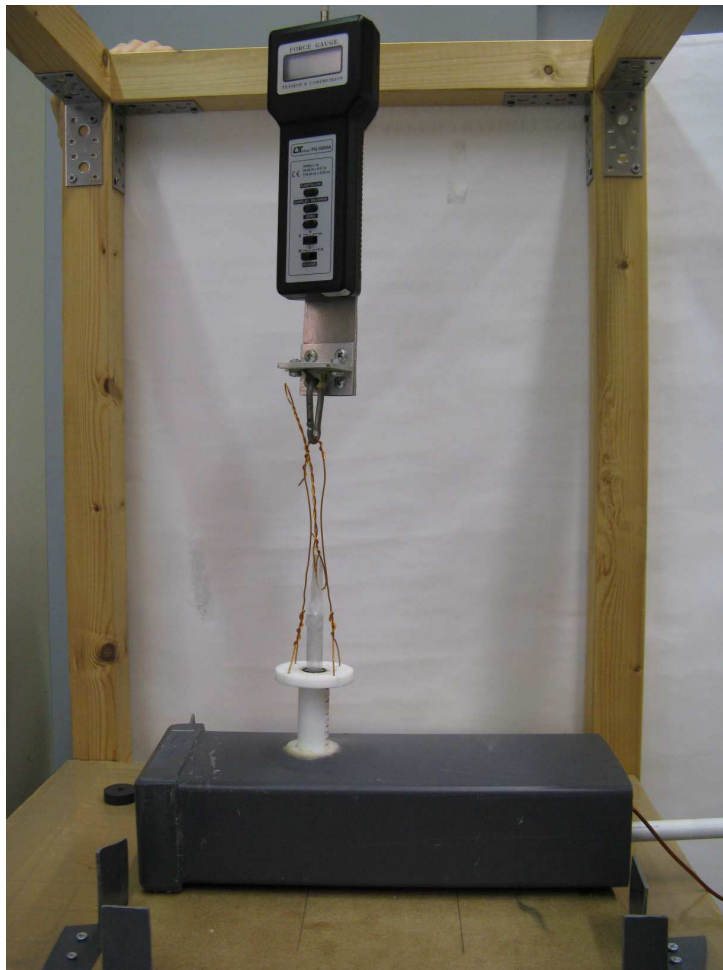$$F_z = \frac{V_p \chi_{mix,eff}}{2\mu_0} \frac{\partial}{\partial z} B_{e,z}^2 \tag{A.10}$$

Figure A.1: Experimental set-up able to measure the magnetic force exerted on a sample.

[4]. The value of magnetic permeability for the AISI 434 steel of the wool has been compared, with a good agreement, with the value in [BCD03]. A comparison for the magnetite powder resulted beyond the experimental and, moreover, the available data limits.

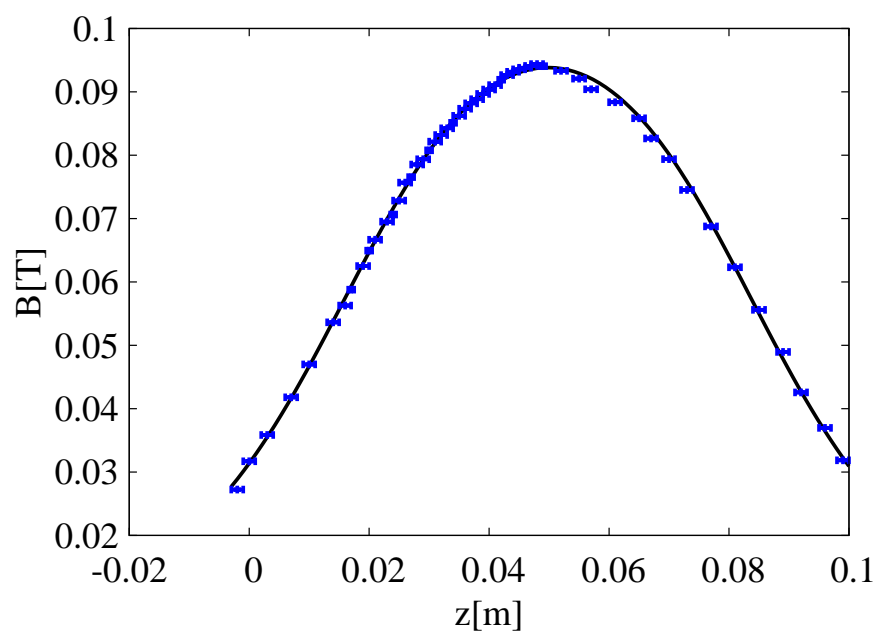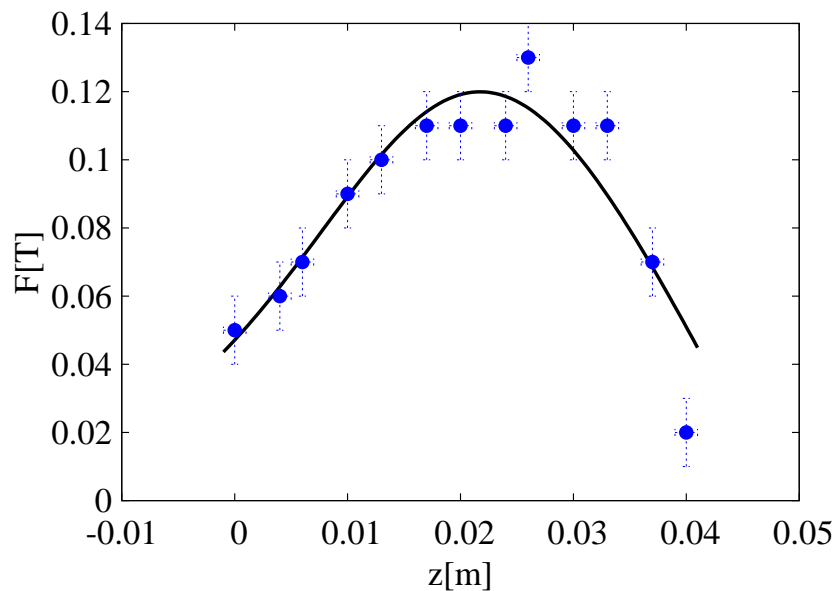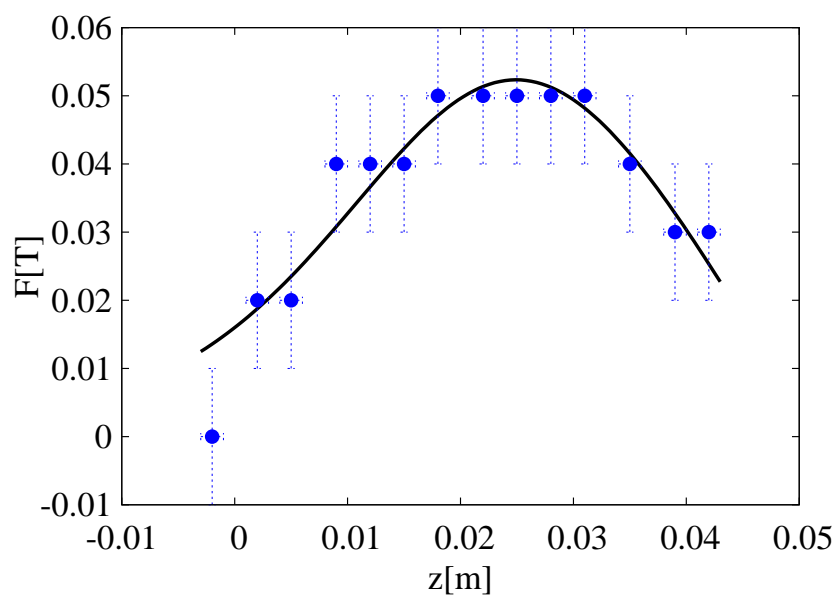[4]The values of ζ for both samples were deduced form their volume and weight.

Figure A.2: Experimental field (dots) and its analytical expression fitted with gnuplot (continuous curve).

(a) Experimental force on the magnetite sample (dots) and its analytical expression fitted with gnuplot (continuous curve).

(b) Experimental force on the wool sample (dots) and its analytical expression fitted with gnuplot (continuous curve).

Figure A.3: Experimental and analytical forces for the two samples.

Appendix B

Adsorption

B.1 Chemical reactions involved in the adsorption process

This work is addressed to the remotion of pollutants from wastewaters through their bound in iron oxide. This adsorption process is a well established one both for magnetite and for hematite. When magnetite acquires a metal it takes the name of *spinel* $\mathbf{M}Fe_2O_4$ where $\mathbf{M} = Ni(II)$, $Co(II)$, $Zn(II)$, $Mg(II)$; when hematite acquires a rare hearth it takes the name of *orthoferrites* $\mathbf{M}FeO_3$ where $\mathbf{M} = Gd(III)$, $Sm(III)$. A typical way to express this relation for the magnetite is the following:

$$Fe^{2+} + Fe^{3+} + Fe^{3+} + 8OH^- \rightarrow FeOFeFeO_3(solid) + 4H_20$$
$$Fe^{2+} + \mathbf{M}^{3+} + Fe^{3+} + 8OH^- \rightarrow FeO\mathbf{M}FeO_3(solid) + 4H_20$$
$$\mathbf{M}^{2+} + Fe^{3+} + Fe^{3+} + 8OH^- \rightarrow \mathbf{M}FeOFeO_3(solid) + 4H_20$$
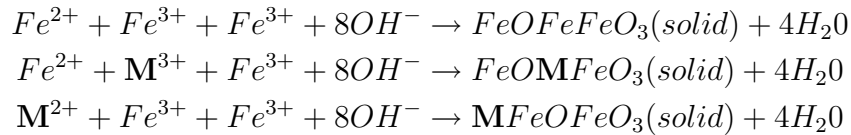
where $FeOFe_2O_3 = Fe_3O_4$ is the chemical formula of the magnetite. Fast and efficient adsorption of the divalent metals Zn, Co, Ni, and Cd to hematite is reported in literature [Jeo+04; Mam+09; Jeo+03]. The sorption experiments for this iron oxide show that it is effective also for $As(V)$, $Se(IV)$, and $Se(VI)$ at room temperature, and is rather independent from the concentration [Mam+09; Gim+07; Rov+08]. Moreover, as expected, the ability to adsorb heavy metals is determined by the specific surface areas [BGE00]. This kind of reaction is well known and often used in various fields (not only in the inorganic separation one, but also, for example, in drugs delivering and biochemical separation) [Gu+95; Gos+02; PDS09; HW82; Han07; Amb+03]. The reactions transform a solution with heavy metals and iron into a solution of heavy metals bounded in iron oxides without the need

of any external energy, provided that the environmental conditions (PH and temperature of the working fluid) are suitable [SMK02].

Appendix C

Concentration

C.1 Particle distribution

As stated in Chapter 2 the particle size distribution is well described by the superposition of three log-normal distribution [Logb]. A log-normal distribution (normalized to K) is written as:

$$\Psi(\zeta, \mu, \sigma) = \frac{K}{\zeta \sigma \sqrt{2\pi}} e^{-\frac{(\ln \zeta - \mu)^2}{2\sigma^2}} \tag{C.1}$$

A fitting of the parameters of a first distribution Ψ_I for the magnetite distribution shown in Fig. C.1, made using gnuplot [Gnub], leads to the following
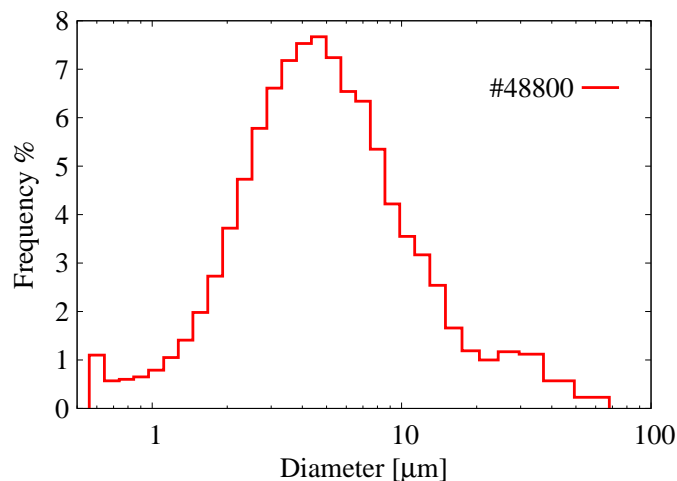
Figure C.1: Experimental size distributions for the magnetite powder (#48800).
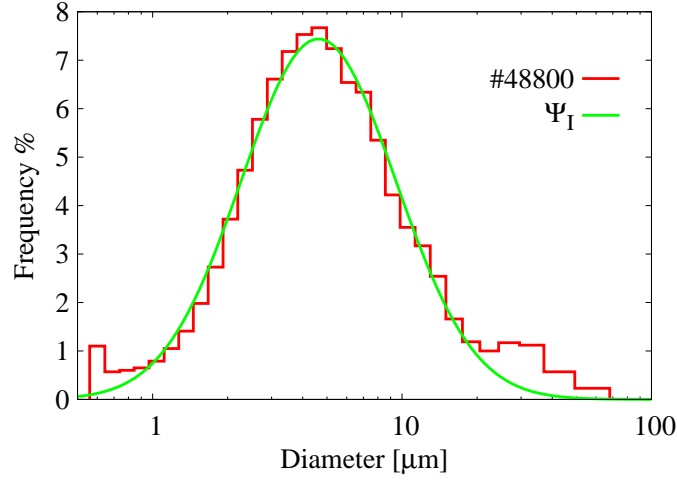
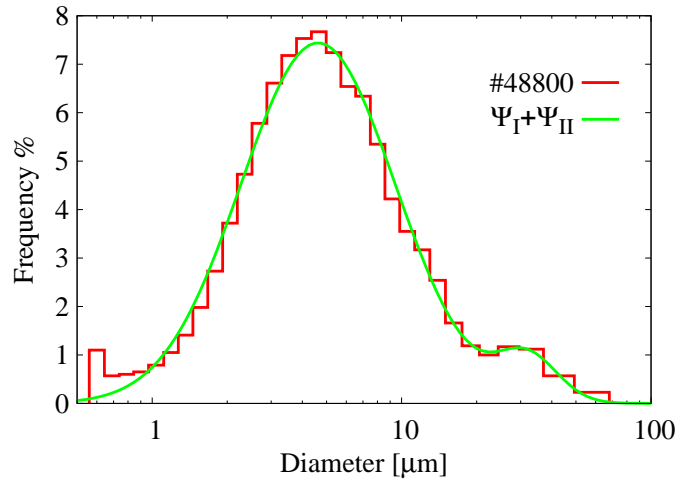**Figure C.2:** Experimental size distributions for the magnetite powder confronted with the primary distribution.

parameters:

$$K_I = 77.648743$$
$$\mu_I = 2.041052$$
$$\sigma_I = 0.713806$$

As visible in Fig. C.2 two queues are visible. The fitting of the difference between the data and the first distribution with a second distribution Ψ_{II} leads to:

$$K_{II} = 20.941135$$
$$\mu_{II} = 3.538794$$
$$\sigma_{II} = 0.277457$$

which corresponds to Fig. C.3. To consider the third queue too (the one concerning the smallest particles) another distribution Ψ_{III} is fitted in the same way obtaining:

$$K_{III} = 1.410121$$
$$\mu_{III} = -1.015040$$
$$\sigma_{III} = 0.346363$$

which correctly describe the real particle distribution in the range of interest, as visible in Fig. C.4. The former procedure may be applied for the

Figure C.3: Experimental size distributions for the magnetite powder confronted with the primary and a secondary distributions.
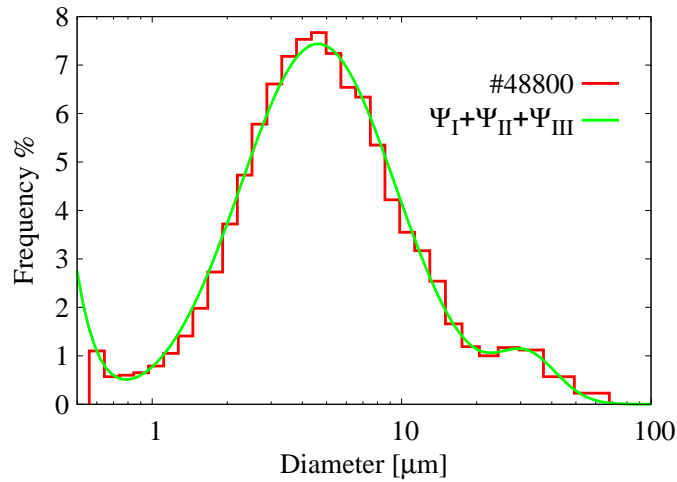
Figure C.4: Experimental size distributions for the magnetite powder confronted with three log-normal distribution..

other particles (#48100 and #48651) with similar results. In Table C.1 the geometric mean $\bar{\zeta}$ and the geometric standard deviation of the mean $\nabla\bar{\zeta}$ for the obtained distributions average size are highlighted [Loga]:

$$\bar{\zeta} = e^{\mu}$$
$$\nabla\bar{\zeta} = e^{\sigma}$$

Table C.1: Mean and standard deviation for the three populations (average size).

Population	$\bar{\zeta}[\mu m]$	$\nabla\bar{\zeta}[\mu m]$
I	7.7	2.0
II	34.5	1.3
III	0.35	1.4

C.2   Model of the concentration vs resistance relation.

Having a reliable description of the distribution of the size of the particles leads to the relation that bounds the measured resistance on the photo-resistor to the particle concentration in the fluid (Chapter 3). As stated by the maker of the photo-resistor [Nor] the following relation subsists between resistance R and incident light intensity I:

$$\log\left(\frac{R}{R_{\#}}\right) = -\beta\log\left(\frac{I}{I_{\#}}\right) \tag{C.2}$$

where the subscript # stands for "normalization constant". Supposing the attenuation of the light intensity through a length ds proportional to the particle concentration ($c(d_p)$, where d_p stands for the particle diameter) through a constant η plus a constant η_0, the variation in the intensity of light can be written as:

$$dI = -\left[\int_0^\infty d(d_p)\eta\frac{\pi d_p^2}{4}c(d_p) + \eta_0\right]I\cdot ds$$

This equation can be integrated from 0 to S leading to:

$$\log\left(\frac{I}{I_0}\right) = -S\frac{\pi\eta}{4}\int_0^\infty d(d_p)d_p^2c(d_p) - S\eta_0$$

where S is the length of the path travelled by the light (in the specific situation the diameter of the pipe). Considering now, for the sake of simplicity, only particles with the same diameter:

$$c(d_p) = C\cdot\delta(d_p - d_p^*)$$

where δ stands for the Dirac's distribution, the previous equation can be written as:

$$\log\left(\frac{I}{I_0}\right) = -S\frac{\pi\eta}{4}d_p^{*2}C - S\eta_0$$

Substituting this equation in eq. C.2 the following one is obtained:

$$\log\left(\frac{R}{R_\#}\right) = -\beta\left\{-S\frac{\pi\eta}{4}d_p^{*2}C - S\eta_0 + \log\left(\frac{I_0}{I_\#}\right)\right\}$$

from which it can be easily extracted the desired relation between resistance and concentration:

$$C = a + b\log R \tag{C.3}$$

where

$$a = \frac{4}{\pi\beta\eta Sd_p^{*2}}\left\{\beta S\eta_0 - \beta\log\left(\frac{I_0}{I_\#}\right) - \log R_\#\right\}$$

$$b = \frac{4}{\pi\beta\eta Sd_p^{*2}}$$

q.e.d..

C.3 Measure of concentration for samples of working fluid

A concentration meter (Fig. C.5) has been realized for the measure of samples of the working water with the same components of the ones described in Section 3.3. These samples were collected into test-tubes and the measured values compared with a scale of resistances as functions of time for known concentrations, as the one in Fig. C.6, for the desired powder and range of concentration. Every scale (for each powder and range of concentrations) has been realized with ten tubes uniformly distributed in the range of interest. The initial concentrations in the tubes were made uniform with the homemade mixer visible in Fig. C.7. A numerical model for deposition of the mixture of particles and bubbles in the tube arising from the mixing has been developed in order to check the behaviour of Fig. C.6 and justify the assumption of the existence of such a scale. I start from the equation for a spherical particle[1] with given diameter d_p, density ρ_p in a fluid with dynamic viscosity μ and density ρ_f subjected to the gravity acceleration g, in a mono-dimensional reference system along the x-axis:

$$\frac{4\pi}{3}\left(\frac{d_p}{2}\right)^2\rho_p\frac{dv}{dt} = \frac{4\pi}{3}\left(\frac{d_p}{2}\right)^2(\rho_p - \rho_f)g - 3\pi d_p\mu v \tag{C.4}$$

---

[1]The equation for the bubbles are formally identical, but their density is negligible.
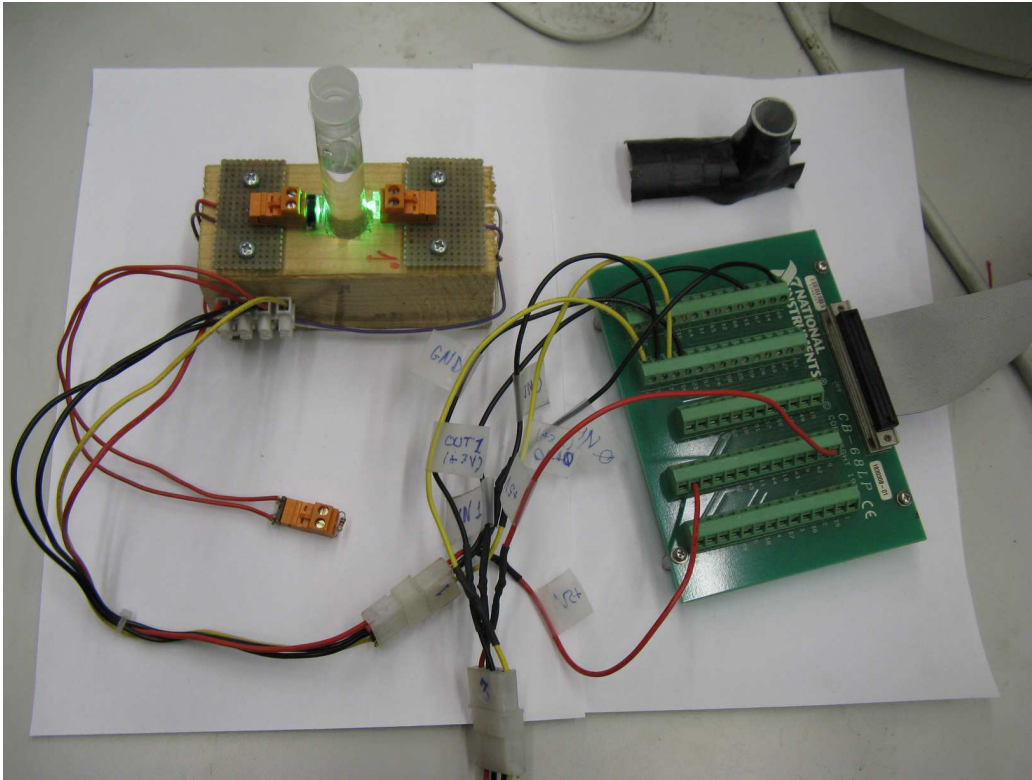
Figure C.5: Picture of the test-tube concentration-meter. The led lamp (powered) is on the right side of the tube while the photo-resistor is on the left side. In the upper right corner a hat used to avoid the environmental light modifying the measured value is visible. In the center-left is visible R_0 and in the right the contact board from National Instrument.

Introducing the time constant

$$\tau = \frac{\rho_p d_p^2}{18\mu}$$

eq. (C.4) becomes:

$$\frac{dv}{dt} = \frac{\rho_p - \rho_f}{\rho_p} g - \frac{v}{\tau}$$

which can be easily integrated obtaining

$$v(t) = \frac{\rho_p - \rho_f}{\rho_p} g\tau \left(1 - e^{-t/\tau}\right)$$
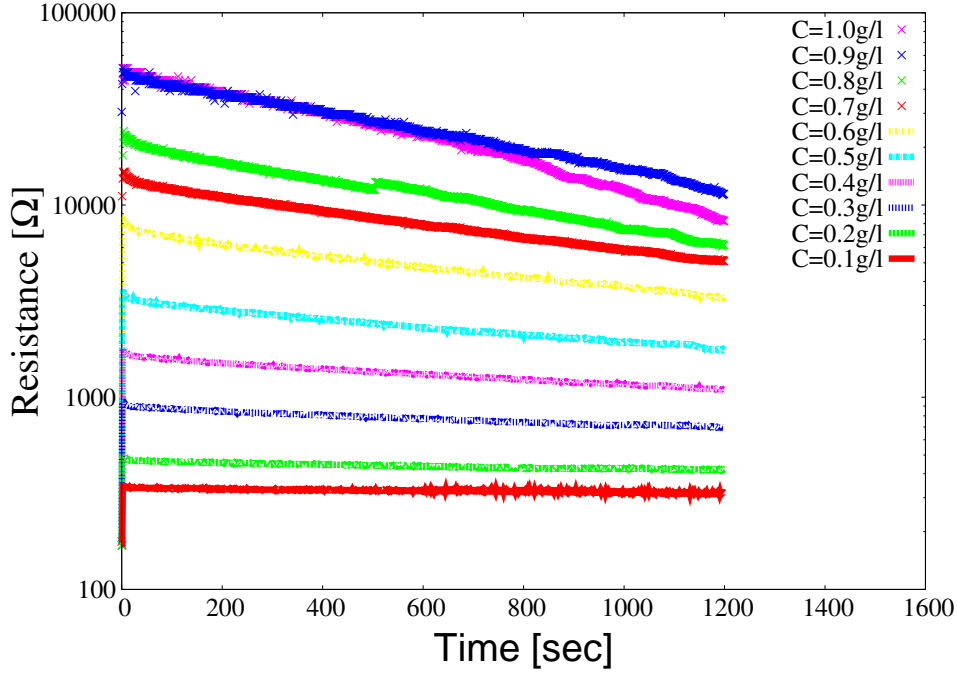
Figure C.6: Resistances as function of time for a set of tubes with given concentration of #48100 powder in water.

Neglecting the 5τ transient (which, in the considered experimental conditions, results of about $50\mu s$) a further integration gives:

$$x = \hat{x}(t; x_0, d_p) = x_0 - \frac{\rho_p - \rho_f}{\rho_p}g\tau t = x_0 - g\tau_p t \qquad \text{(C.5)}$$

where

$$\tau_p = \frac{(\rho_p - \rho_f)d_p^2}{18\mu}$$

Now assume that the particles are falling in a tube of length L and cross section A. The concentration $c(x, t; d_p)$ of identical particles of a given diameter d_p, defined as number of particles of a given diameter d_p per unit volume, in the interval $0 < x < L$, is given by:

$$c(x, t; d_p) = \int_0^L dx_0 c_0(d_p)\delta(x - \hat{x}(t; x_0, d_p)) \qquad \text{(C.6)}$$

where δ is the Dirac distribution and the initial concentration is assumed to be uniform, i.e. independent from x_0. Note the sedimentation in $x = 0$ is

Figure C.7: Homemade mixer used to guarantee initial uniform concentration in the test-tubes.

not taken into account. Substitution and integration leads to:

$$c(x,t;d_p) = \int_0^L dx_0 c_0(d_p)\delta(x - x_0 + g\tau_p t) =$$

$$= c_0(d_p)\int_0^\infty dx_0\delta(x - x_0 + g\tau_p t) - c_0(d_p)\int_L^\infty dx_0\delta(x - x_0 + g\tau_p t) =$$

$$= c_0(d_p)[U(x + g\tau_p t) - U(x - L + g\tau_p t)]$$

where U is the Heaviside step function. Note that, in the interval $0 < x < L$, this equals

$$c(x,t;d_p) = c_0(d_p)[1 - U(x - L + g\tau_p t)]$$

The same is true for the bubbles. Neglecting their emersion, in the interval $0 < x < L$, we get:

$$c_b(x,t;d_b) = c_{b,0}(d_b)U(x - g\tau_b t)$$

Now I define the distribution function $f(d_p)$ defining $f(d_p)d(d_p)$ as number of particles of diameter between d_p and $d_p + d(d_p)$ divided by the total number

of particles. Thus:

$$\int_0^\infty d(d_p) f(d_p) = 1$$

and the cumulative $\Phi(d_p) = \int_0^{d_p} d(d_p) f(d_p)$ is bounded, i.e. $0 < \Phi < 1$. The same is true for the bubbles which have their distribution function $f_b(d_b)$ and their cumulative Φ_b.

Defining the total initial uniform concentration C_0 as the total number of particles and bubbles divided by the tube volume AL, the partial initial uniform concentration of particles is $c_0(d_p) = C_{p,0} f(d_p)$. The same is true for the bubble concentration $c_{b,0}(d_b) = C_{b,0} f_b(d_b)$. The total concentration of particles and bubbles at a given time and quote is given by

$$C(x,t) = \int_0^\infty d(d_p) c(x,t;d_p) + \int_0^\infty d(d_b) c_b(x,t;d_b)$$

Substitution and integration leads to:

$$C(x,t) = \int_0^\infty d(d_p) C_{p,0} f(d_p)[1 - U(x - L + g\tau_p t) + \int_0^\infty d(d_b) C_{b,0} f_b(d_b) U(x - g\tau_b t)$$

$$= C_{p,0} \left[\int_0^\infty d(d_p) f(d_p) - \int_0^\infty d(d_p) f(d_p) U(x - L + g\tau_p t) \right]$$

$$+ C_{b,0} \int_0^\infty d(d_b) f_b(d_b) U(x - g\tau_b t)$$

This function can be integrated and studied, as in Appendix C.2, substituting the log-normal distribution for the particle diameter. This leads to a relation of the form:

$$R = a' + b' log(C) \tag{C.7}$$

which justifies the scaling hypothesis.

C.4   Details of the components of the turbidity meters

This appendix shows some details of the elements constituting the two turbidity meters.

Figures C.8-C.9 show the schematics of the led and of the light-dependent resistor, respectively. All the values are in inches.
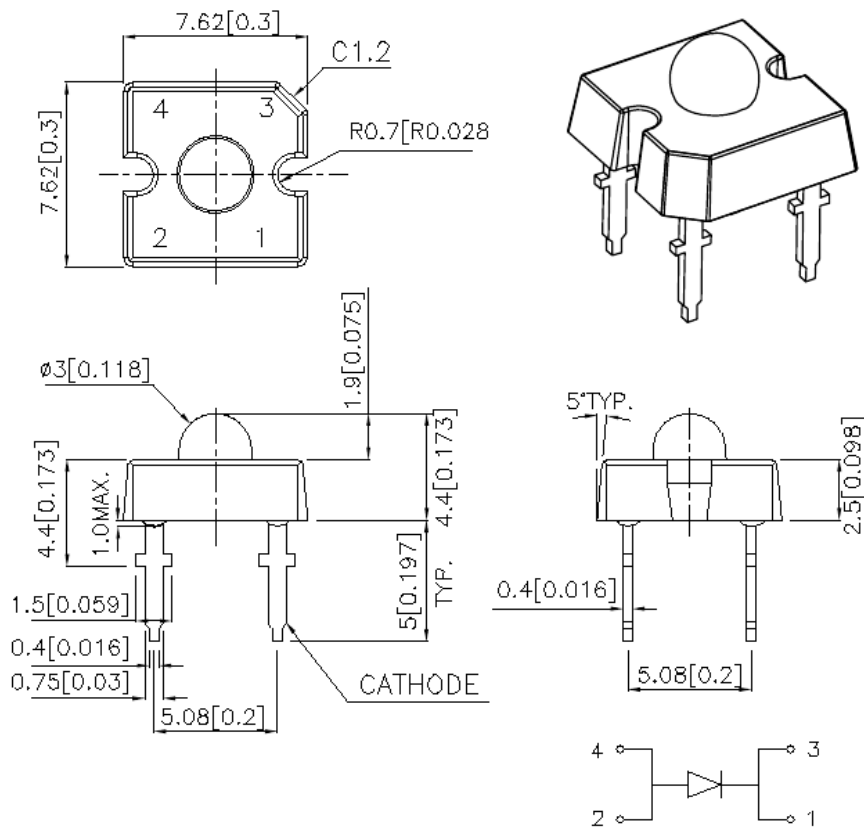

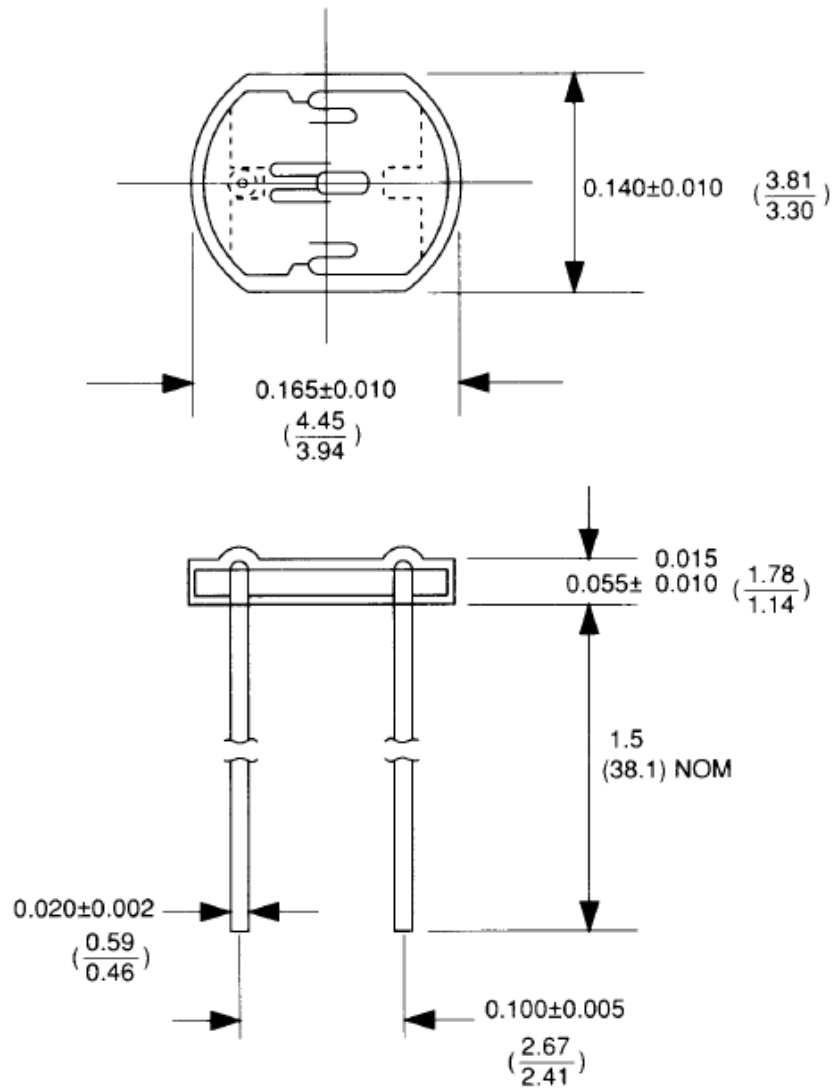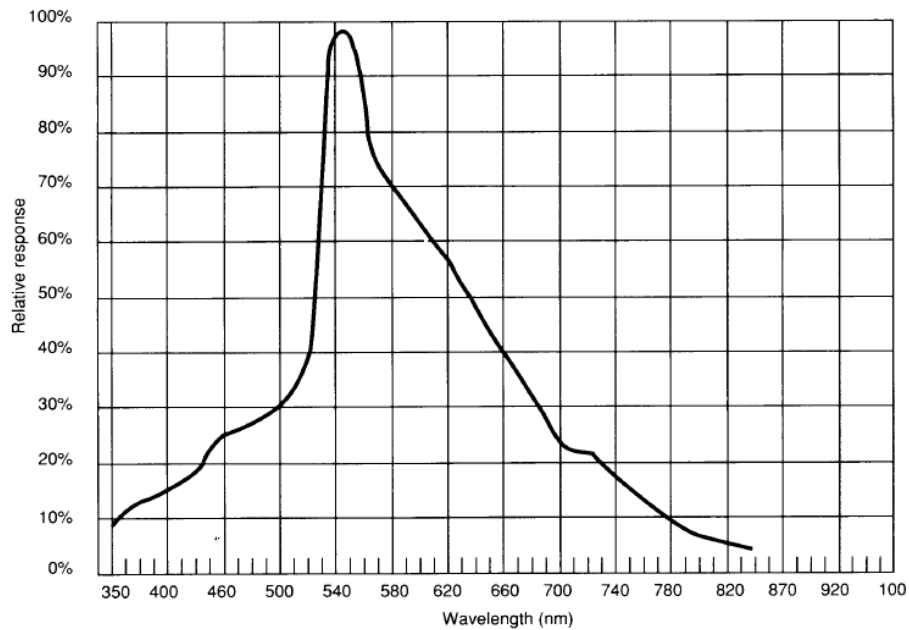**Figure C.8:** Technical scheme of the led (lengths are in inches) [Led].

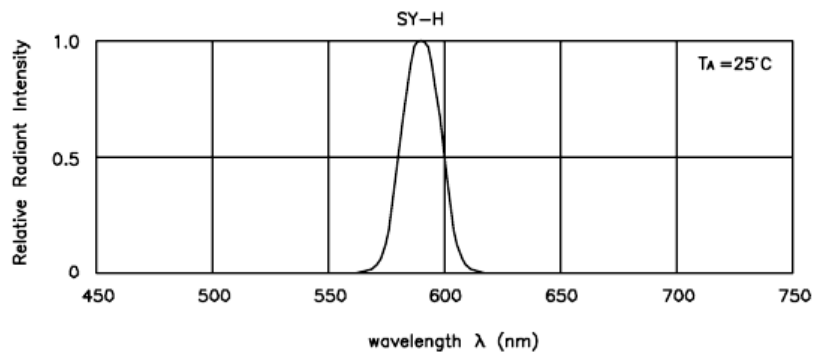**Figure C.9:** Technical scheme of the light dependent resistor (lengths are in inches) [Nor].

Figures C.10a-C.10b show the frequency response of the light-dependent resistor and of the led, respectively. As visible both have a maximum around $6KHz$, i.e. green light, and consequently are well comparable.

(a) Light adsorption as function of its frequency [Nor].

(b) Intensity of the light emission as function of its frequency [Led].

Figure C.10: Frequency compatibility of the two elements.

Bibliography

[AA02]   T. Abbasov and A. S. Altunbas. "Determination of the particle capture radius in magnetic filters with velocity distribution profile in pores". In: *Separation Science and Technology* 37.9 (June 2002), pp. 2037–2053.

[ACA05]   P. A. Augusto, T. Castelo-Grande, and P. Augusto. "Magnetic classification in health sciences and in chemical engineering". In: *Chemical Engineering Journal* 111.2-3 (Aug. 2005), pp. 85–90. ISSN: 1385-8947. DOI: 10.1016/j.cej.2005.02.013.

[Adl+67]   A. D. Adler et al. "A simplified synthesis for meso-tetraphenylporphine". In: *The Journal of Organic Chemistry* 32.2 (Feb. 1967), p. 476. DOI: 10.1021/jo01288a053.

[AKH99]   T. Abbasov, M. Koksal, and S. Herdem. "Theory of high-gradient magnetic filter performance". In: *Magnetics, IEEE Transactions on* 35.4 (1999), pp. 2128–2132. ISSN: 0018-9464.

[ALM03]   M. Ahoranta, J. Lehtonen, and R. Mikkonen. "Magnet design for superconducting open gradient magnetic separator". In: *Physica C* 386 (2003), pp. 398–402.

[Amb+03]   R. D. Ambashta et al. "Nano-aggregates of hexacyanoferrate (II)-loaded magnetite for removal of cesium from radioactive wastes". In: *Journal of Magnetism and Magnetic Materials* 267.3 (Dec. 2003), pp. 335–340. ISSN: 0304-8853. DOI: 10.1016/S0304-8853(03)00401-3.

[Ana02]   G. N. Anastassakis. "Separation of Fine Mineral Particles by Selective Magnetic Coating". In: *Journal of Colloid and Interface Science* 256 (2002), pp. 114–120.

[AP98]   U. M. Ascher and L. R. Petzold. *Computer Methods for Ordinary Differential Equations and Differential-Algebraic Equations.* 1st ed. University City Science Center, Philadelphia: Society for the Industrial and Applied Mathematics, 1998.

[Bar]   *Barometer*. 2010. URL: http://www.wika.de/.

[BB05]   R. Bucher and S. Balemi. "Scilab/Scicos and Linux RTAI - a unified approach". In: *Control Applications, 2005. CCA 2005. Proceedings of 2005 IEEE Conference on.* 2005, pp. 1121–1126. ISBN: 1085-1992. DOI: 10.1109/CCA.2005.1507281.

[BCD03]   J. Bas, J. Calero, and M. Dougan. "Sintered soft magnetic materials. Properties and applications". In: *Journal of Magnetism and Magnetic Materials* 254-255 (2003), pp. 391–398.

[BCZ07]   L. W. Bruch, M. W. Cole, and E. Zaremba. *Physical Adsorption: Forces and Phenomena.* Dover Publications, 2007. ISBN: 0486457672.

[BGE00]   J. P. Beukes, E. W. Giesekke, and W. Elliott. "Nickel retention by goethite and hematite". In: *Minerals Engineering* 13.14-15 (Dec. 2000), pp. 1573–1579. ISSN: 0892-6875. DOI: 10.1016/S0892-6875(00)00140-0.

[Bir+78a]   R. Birss et al. "Laminar flow model of particle capture of axial magnetic filters". In: *Magnetics, IEEE Transactions on* 14.6 (1978), pp. 1165–1169. ISSN: 0018-9464.

[Bir+78b]   R. Birss et al. "Theory and performance of axial magnetic filters in laminar flow conditions". In: *Magnetics, IEEE Transactions on* 14.5 (1978), pp. 389–391. ISSN: 0018-9464.

[BMD06]   S. Babel and D. del Mundo Dacera. "Heavy metal removal from contaminated sludge for land application: A review". In: *Waste Managment* 26 (2006), pp. 988–1004.

[BMN06]   R. Bucher, S. Mannori, and T. Netter. *RTAI-Lab tutorial: Scilab, Comedi, and real-time control.* 2006. URL: www.rtai.org/RTAILAB.

[BPS80]   R. Birss, M. Parker, and T. Sheerer. "Statistics of particle capture in HGMS". In: *Magnetics, IEEE Transactions on* 16.5 (1980), pp. 830–832. ISSN: 0018-9464.

[Bre97]   M. Breschi. "Processi di cattura nei separatori magnetici superconduttivi". Thesys. University of Bologna, 1997.

[Bru+05]   W. Bruckard et al. "Water leaching and magnetic separation for decreasing the chloride level and upgradin the zinc content of EAF steelmaking baghouse dust". In: *Int. J. Miner. Process.* 75 (2005), pp. 1–20.

[CBN98]   A. Cristofolini, M. Breschi, and F. Negrini. "Capture processes in superconducting HGMS". In: *Proceedings of the 1998 International Symposium on Advanced Energy Technology* (Feb. 1998).

[Che98]   N. P. Cheremisinoff. *Liquid Filtration, Second Edition.* 2nd ed. Butterworth-Heinemann, 1998. ISBN: 0750670479.

[CKK76]   C. Clarkson, D. Kelland, and T. King. "Model for calculation of capture radii of a high gradient magnetic separator at moderate Reynolds numbers". In: *Magnetics, IEEE Transactions on* 12.6 (1976), pp. 901–903. ISSN: 0018-9464.

[CKT82]   H. Collan, M. Kokkala, and O. Toikka. "Application of the theory of magnetic filtration in determining the optimum filter configuration". In: *Magnetics, IEEE Transactions on* 18.3 (1982), pp. 827–832. ISSN: 0018-9464.

[Coe02]   J. M. D. Coey. "Permanent magnet applications". In: *Journal of Magnetism and Magnetic Materials* 248.3 (Aug. 2002), pp. 441–456.

[EIA09]   A. Eskandarpour, K. Iway, and S. Asai. "Superconducting magnetic filter: performance, recovery and design". In: *IEEE Trans. on Appl. Supercond.* 19.2 (2009), pp. 84–95.

[ERP97]   A. D. Ebner, J. A. Ritter, and H. J. Ploehn. "Feasibility and Limitations of Nanolevel High Gradient Magnetic Separation". In: *Separation and Purification Technology* 11 (1997), pp. 199–210.

[Esk+07]   A. Eskandarpour et al. "Semi-continuous Magnetic Removal of Phosphate Using an Iron Oxide Hydroxide Adsorbent and Regeneration of Its Adsorbent". In: *ISIJ International* 47.4 (2007), pp. 563–567.

[Fab+03a] M. Fabbri et al. "Infuence of the electro-magnetic stirring on the boundary layer of a molten steel pool". In: *COMPEL* 22.1 (2003).

[Fab+03b] M. Fabbri et al. "Removal of SiC inclusions in molten aluminium using a 12 T static magnetic feld". In: *COMPEL* 22.1 (2003).

[Fab08]   M. Fabbri. "Magnetic flux density and vector potential of uniform polyhedral sources". In: *IEEE Trans. Magn.* 44.1 (Jan. 2008), pp. 32–36.

[Fab+08]   M. Fabbri et al. "High gradient magnetic separation of micro-pollutant from waste waters". In: *Proc. 1st European Conference on Microfluidics (MicroFlu'08)*. Bologna 2008, pp. 270.1–270.13. ISBN: 2-906831-76-X.

[Fab09]   M. Fabbri. "Magnetic flux density and vector potential of linear polyhedral sources". In: *COMPEL* 28.6 (2009), pp. 1688–1700.

[Fle91]   D. Fletcher. "Fine particle high gradient magnetic entrapment". In: *Magnetics, IEEE Transactions on* 27.4 (1991), pp. 3655–3677. ISSN: 0018-9464.

[FS08]   G. Fuchs and L. Schultz. "Encyclopedia of Materials: Science and Technology". In: ed. by K. H. J. Buschow et al. Elsevier Ltd., 2008. Chap. Superconducting Permanent Magnets: Principles and Results, pp. 8947–8955. ISBN: 978-0-08-043152-9.

[FY05]   G. Friedman and B. Yellen. "Magnetic separation, manipulation and assembly of solid phase in fluids". In: *Current Opinion in Colloid Interface Science* 10 (2005), pp. 158–166.

[Gar08]   M. H. Garcia. *Sedimentation Engineering: Theories, Measurements, Modeling and Practice: Processes, Management, Modeling, and Practice*. 1st ed. American Society of Civil Engineers, 2008. ISBN: 0784408149.

[GB83]   R. Gerber and R. Birss. *High Gradient Magnetic Separation*. Research Studies Press, 1983.

[Gim+07]   J. Gimenez et al. "Arsenic sorption onto natural hematite, magnetite, and goethite". In: *Journal of Hazardous Materials* 141.3 (Mar. 2007), pp. 575–580. ISSN: 0304-3894. DOI: `10.1016/j.jhazmat.2006.07.020`.

[GL89]   R. Gerber and P. Lawson. "The HGMS filter performance exponential law". In: *Magnetics Conference, 1989. Digests of INTERMAG '89., International*. 1989, GD4.

[GMS88]   R. Gregory, R. J. Maloney, and M. Stockley. "Water Treatment Using Magnetite: A Study of a Sirofloc Pilot Plant". In: *Water and Environment Journal* 2.5 (1988), pp. 532–544. DOI: `10.1111/j.1747-6593.1988.tb01335.x`.

[Gmt]   *Iron steel wool*. 2007. URL: `www.gmt-inc.com`.

[Gnua]   *Copyright of gnuplot*. 2010. URL: `http://gnuplot.cvs.sourceforge.net/gnuplot/gnuplot/Copyright`.

[Gnub]   *gnuplot*. 2010. URL: `http://www.gnuplot.info/`.

[Gol04]   R. Goleman. "Macroscopic model of particles' capture by the elliptic cross-section collector in magnetic separator". In: *Journal of Magnetism and Magnetic Materials* 272-276.Part 3 (May 2004), pp. 2348–2349. ISSN: 0304-8853. DOI: `10.1016/j.jmmm.2003.12.963`.

[Gos+02]   Y. Gossuin et al. "Cesium Adsorption in Hydrated Iron Oxide Particles Suspensions: An NMR Study". In: *Journal of Magnetic Resonance* 157.1 (July 2002), pp. 132–136. ISSN: 1090-7807. DOI: `10.1006/jmre.2002.2581`.

[Gra01]   J. Graham. *Biological Centrifugation*. 1st. Garland Science, 2001. ISBN: 1859960375.

[Gu+95]   B. Gu et al. "Adsorption and desorption of different organic matter fractions on iron oxide". In: *Geochimica et Cosmochimica Acta* 59.2 (1995), pp. 219–229. ISSN: 0016-7037. DOI: `10.1016/0016-7037(94)00282-Q`.

[Ha+]   D. Ha et al. "Treatment of Wastewater of Iron Manifacturing by Superconducting High Gradient Magnetic Separation". In: ().

[Han07]   K. Hanna. "Sorption of two aromatic acids onto iron oxides: Experimental study and modeling". In: *Journal of Colloid and Interface Science* 309.2 (May 2007), pp. 419–428. ISSN: 0021-9797. DOI: `10.1016/j.jcis.2007.01.004`.

[HBW82]   B. L. Hirschbein, D. W. Brown, and G. M. Whitesides. "Magnetic separations in chemistry and biochemistry". In: *CHEMTECH* 12.3 (1982), pp. 172–179.

[HKA00]   S. Herdem, M. Koksal, and T. Abbasov. "Model for Predicting Filtration Efficiency and Pressure Drop in Axial Magnetic Filters". In: *Separation Science and Technology* 35.7 (2000), p. 941. ISSN: 0149-6395. DOI: `10.1081/SS-100100203`.

[HLG70]   J. P. Herzig, D. M. Leclerc, and P. L. Goff. "Flow of Suspensions through Porous Media Application to Deep Filtration". In: *Industrial & Engineering Chemistry* 62.5 (May 1970), pp. 8–35. DOI: `10.1021/ie50725a003`.

[HNW76]   J. Harland, L. Nilsson, and M. Wallin. "Pilot scale high gradient magnetic filtration of steel mill wastewater". In: *Magnetics, IEEE Transactions on* 12.6 (1976), pp. 904–906. ISSN: 0018-9464.

[Hos+05]   M. A. Hossain et al. "Ineffectiveness and Poor Reliability of Arsenic Removal Plants in West Bengal, India". In: *Environmental Science & Technology* 39.11 (June 2005), pp. 4300–4306. DOI: `10.1021/es048703u`.

[HU80]   K. Hayashi and S. Uchiyama. "On particle trajectory and capture efficiency around many wires". In: *Magnetics, IEEE Transactions on* 16.5 (Sept. 1980), pp. 827–829. ISSN: 0018-9464.

[Hub+01]   J. J. Hubbuch et al. "High gradient magnetic separation versus expanded bed adsorption: a first principle comparison". In: *Bioseparation* 10.1 (2001), pp. 99–112. DOI: `10.1023/A: 1012034923621`.

[HW82]   B. L. Hirschbein and G. M. Whitesides. "Affinity separation of enzymes from mixtures containing suspended solids". In: *Applied Biochemistry and Biotechnology* 7.3 (May 1982), pp. 157–176. DOI: `10.1007/BF02798294`.

[Jeo+03]   B. Jeon et al. "Sorption kinetics of Fe(II), Zn(II), Co(II), Ni(II), Cd(II), and Fe(II)/Me(II) onto hematite". In: *Water Research* 37.17 (Oct. 2003), pp. 4135–4142. ISSN: 0043-1354. DOI: `10. 1016/S0043-1354(03)00342-7`.

[Jeo+04]   B. Jeon et al. "Modeling the sorption kinetics of divalent metal ions to hematite". In: *Water Research* 38.10 (May 2004), pp. 2499–2504. ISSN: 0043-1354. DOI: `10.1016/j.watres.2004. 03.003`.

[JM06]   M. W. Jornitz and T. H. Meltzer. *Pharmaceutical Filtration: The Management of Organism Removal*. PDA/DHI, 2006. ISBN: 193011477X.

[KAH03]   M. Koksal, T. Abbasov, and S. Herdem. "Mathematical modeling of the magnetic filtration processes". In: *IOS Press* 18.4 (2003), pp. 227–234. ISSN: 1383-5416.

[Kak+04]   Y. Kakihara et al. "Superconducting High Gradient Magnetic Separation for Purification of Wastewater From Paper Factory". In: *IEEE Trans. on Appl. Supercond.* 14.2 (2004). Poco interessante.

[Kar03]   N. Karapinar. "Magnetic separation of ferrihydrite from wastewater by magnetic seeding and high-gradient magnetic separation". In: *Int. J. Miner. Process.* 71 (2003), pp. 45–54.

[Kel73]   D. Kelland. "High gradient magnetic separation applied to mineral beneficiation". In: *Magnetics, IEEE Transactions on* 9.3 (1973), pp. 307–310. ISSN: 0018-9464.

[Kir00]   V. A. Kirsh. "The Effect of van der Waals' Forces on Aerosol Filtration with Fibrous Filters". In: *Colloid Journal* 62.6 (Nov. 2000), pp. 714–720. DOI: 10.1023/A:1026678725025.

[Kir04]   V. Kirsh. "Inertial Deposition of Aerosol Particles on Fiberous Filters". In: *Colloid Journal* 66 (5 2004), pp. 613–618.

[KS77]   A. Kirsch and I. Stechkina. "Inertial deposition of aerosol particles in model filters at low reynolds numbers". In: *Journal of Aerosol Science* 8.5 (Sept. 1977), pp. 301–307. ISSN: 0021-8502. DOI: 10.1016/0021-8502(77)90016-7.

[Lat73]   C. de Latour. "Magnetic separation in water pollution control". In: *Magnetics, IEEE Transactions on* 9.3 (1973), pp. 314–316. ISSN: 0018-9464.

[LD75]   F. Luborsky and B. Drummond. "High gradient magnetic separation: Theory versus experiment". In: *Magnetics, IEEE Transactions on* 11.6 (1975), pp. 1696–1700. ISSN: 0018-9464.

[Led]   *High emission led*. 2005. URL: http://www.datasheetarchive.com/pdf/Datasheet-018/DSA00321875.pdf.

[Leu98]   W. Leung. *Industrial Centrifugation Technology*. 1st ed. McGraw-Hill Professional, 1998. ISBN: 0070371911.

[LK75]   C. de Latour and H. Kolm. "Magnetic separation in water pollution control - II". In: *Magnetics, IEEE Transactions on* 11.5 (1975), pp. 1570–1572. ISSN: 0018-9464.

[LL06]   L. Landau and E. Lifshitz. *Fluid Mechanics*. 2nd ed. Vol. 6. Course of Theoretical Physics. Elsevier, 2006.

[LL87]   E. Lifshitz and L. Landau. *Electrodynamics of continuous media*. 2nd ed. Vol. 8. Course of Theoretical Physics. Pergamon Press, 1987.

[Loga]   *Log-normal distribution - Wikipedia*. 2010. URL: http://en.wikipedia.org/wiki/Log-normal_distribution.

[Logb]   *Lognormal Distribution*. 2010. URL: http://www.itl.nist.gov/div898/handbook/eda/section3/eda3669.htm.

[Mam+09]   Y. Mamindy-Pajany et al. "Arsenic adsorption onto hematite and goethite". In: *Comptes Rendus Chimie* 12.8 (Aug. 2009), pp. 876–881. ISSN: 1631-0748. DOI: `10.1016/j.crci.2008.10.012`.

[Mar+09a] G. Mariani et al. "High gradient magnetic separation of micropollutant from waste waters". In: *La Houille Blanche - International Water Journal* 6 (Dec. 2009). DOI: 10.1051/lhb/2009087, pp. 109–117.

[Mar+09b] G. Mariani et al. "High gradient magnetic separation of pollutant from wastewaters". In: *8th International Symposium on Electric and Magnetic Fields (EMF 2009) Book of Summaries.* Mondovi (Italy) 2009, pp. 79–80.

[Mar+10]   G. Mariani et al. "High gradient magnetic separation of micropollutant from wastewaters using permanent magnets". In: *Separation and Purification Technology* (2010). In press.

[Mas+06]   J. Masse et al. "Influence of relative density on the architecture and mechanical behaviour of a steel metallic wool". In: *Scripta Materialia* 54.7 (Apr. 2006), pp. 1379–1383. ISSN: 1359-6462. DOI: `10.1016/j.scriptamat.2005.11.075`.

[May+07]   J. Mayo et al. "The effect of nanocrystalline magnetite size on arsenic removal". In: *Science and Technology of Advanced Materials* 8.1-2 (2007), p. 71. URL: `http://iopscience.iop.org/1468-6996/8/1-2/A13`.

[MBQ07]   W. P. Martignoni, S. Bernardo, and C. L. Quintani. "Evaluation of cyclone geometry and its influence on performance parameters by computational fluid dynamics (CFD)". en. In: *Brazilian Journal of Chemical Engineering* 24 (Mar. 2007), pp. 83 –94. ISSN: 0104-6632. URL: `http://www.scielo.br/scielo.php?script=sci_arttext&pid=S0104-66322007000100008&nrm=iso`.

[McM02]   J. E. McMurry. *Fundamentals of Organic Chemistry.* 5th ed. Brooks Cole, 2002. ISBN: 0534395732.

[MHB05]   C. Mikkelsen, M. F. Hansen, and H. Bruus. "Theoretical comparison of magnetic and hydrodynamic interactions between magnetically tagged particles in microfluidic systems". In: *Journal of Magnetism and Magnetic Materials* 293.1 (May 2005), pp. 578–583. ISSN: 0304-8853. DOI: `10.1016/j.jmmm.2005.01.076`.

[Mit+03]   K. Mitsuhashi et al. "Purification of endocrine disrupter-polluted water using high temperature superconducting HGMS". In: *Physical Separation in Science and Engineering* 12.4 (2003), pp. 205–213.

[MK78]   E. Maxwell and D. Kelland. "High gradient magnetic separation in coal desulfurization". In: *Magnetics, IEEE Transactions on* 14.5 (1978), pp. 482–487. ISSN: 0018-9464.

[Moe+04]   G. D. Moeser et al. "High-gradient magnetic separation of coated magnetic nanoparticles". In: *AIChE Journal* 50.11 (2004), pp. 2835–2848. DOI: `10.1002/aic.10270`.

[MSG99]   L. Morino, F. Salvatore, and M. Gennaretti. "A new velocity decomposition for viscous flows: Lighthill's equivalent source method revisited". In: *Comput. Methods Appi. Mech. Engrg.* 173 (1999), pp. 317–336.

[MW]   A. D. McNaught and A. Wilkinson. *Compendium of Chemical Terminology*. 1997th ed. Oxford: Blackwell Scientific Publications. ISBN: 0-9678550-9-8.

[Nak+03]   H. Nakajima et al. "Separation characteristics of open gradient magnetic separation using high-temperature superconducting magnet". In: *Physica C: Superconductivity* 392-396.Part 2 (Oct. 2003), pp. 1214–1218. ISSN: 0921-4534. DOI: `10.1016/S0921-4534(03)01128-6`.

[Nat]   *Safe Drinking Water Is Essential*. 2007. URL: `http://drinking-water.org/html/en/Treatment/Coagulation-Flocculation-technologies.html`.

[Neg+99]   F. Negrini et al. "A Multi wire Model for Superconducting HGMS Filter". In: *Proc. Int. Conf. on MHD Power Generation and High Temperature Technologies*. Ed. by P. J. Zixiang. Vol. 2. Institute of Electrical Engineering of the Chinese Acadeny of Sciences. Beijing, PRC Oct 1999 1999, pp. 715–720.

[Nor]   *Photo-resistor*. 2007. URL: `http://www.alldatasheet.com/datasheet-pdf/pdf/124422/ETC/NORP12.html`.

[NS03]   J. D. Navratil and M. T. Shing-Tsair. "Magnetic separation of iron and heavy metals from water". In: *Water Science and Technology: A Journal of the International Association on Water Pollution Research* 47.1 (2003). PMID: 12578170, pp. 29–32. ISSN: 0273-1223.

[NT06]   S. Nishijima and S. ichi Takeda. "Superconducting High Gradient Magnetic Separation for Purification of Wastewater from Paper Factory". In: *IEEE Trans. on Appl. Supercond.* 16.2 (2006), pp. 1142–1145.

[Obe+75]   J. A. Oberteuffer et al. "High gradient magnetic filtration of steel mill process and waste waters". In: *Magnetics, IEEE Transactions on* 11.5 (1975), pp. 1591–1593. ISSN: 0018-9464.

[Obe76]   J. A. Oberteuffer. "Engineering development of High Gradient Magnetic Separators". In: *IEEE Trans. Magn.* MAG-12.5 (1976), pp. 444–449.

[Ode76]   R. Oder. "High gradient magnetic separation theory and applications". In: *Magnetics, IEEE Transactions on* 12.5 (1976), pp. 428–435. ISSN: 0018-9464.

[Oka+02]   H. Okada et al. "High gradient magnetic separation for weakly magnetized fine particles". In: *IEEE Trans. on Appl. Supercond.* 12.1 (Mar. 2002), pp. 967–970.

[Oli+02]   L. C. A. Oliveira et al. "Activated carbon/iron oxide magnetic composites for the adsorption of contaminants in water". In: *Carbon* 40.12 (2002), pp. 2177–2183. ISSN: 0008-6223. DOI: `10.1016/S0008-6223(02)00076-3`.

[OM05]   H. Okada and K. Mitsuhashi. "Computational Fluid Dynamics Simulation of High Gradient Magnetic Separation". In: *Separation science and technology* 7 (2005), pp. 1567–1584. ISSN: 0149-6395.

[PDS09]   A. Pathak, M. G. Dastidar, and T. R. Sreekrishnan. "Bioleaching of heavy metals from sewage sludge: A review". In: *Journal of Environmental Managment* 90 (2009), pp. 2343–2353.

[Rho98]   M. Rhodes. *Introduction to Particle Technology*. Wiley, 1998. ISBN: 0471984833.

[Rov+08]   M. Rovira et al. "Sorption of selenium(IV) and selenium(VI) onto natural iron oxides: Goethite and hematite". In: *Journal of Hazardous Materials* 150.2 (2008), pp. 279–284. ISSN: 0304-3894. DOI: `10.1016/j.jhazmat.2007.04.098`.

[RW01]   L. L. Regel and W. R. Wilcox. *Processing by Centrifugation*. 1st ed. Springer, 2001. ISBN: 0306466546.

[Sah+99]   N. Saho et al. "Continuous Superconducting-Magnet Filtration System". In: *IEEE Trans. on Appl. Supercond.* 9.2 (1999).

[San88] A. V. Sandulyak. "Magnetic filtration of liquids and gases". In: *Ximya* (1988). in Russian.

[SF03] H. Shen and E. Forssberg. "An overview of recovery of metals from slags". In: *Waste Management* 23.10 (2003), pp. 933–949. ISSN: 0956-053X. DOI: `10.1016/S0956-053X(02)00164-2`.

[Sha] H. H. Shalaby. "On the potential of large eddy simulation to simulate cyclone separators". In: URL: `http://archiv.tu-chemnitz.de/pub/2007/0013/index.html`.

[SK] J. L. Smith and J. H. Keenan. *Experimental and analytical study of the vortex in the cyclone separator.* http://dspace.mit.edu/handle/1721.1/11792. Thesis (Sc. D.)– Massachusetts Institute of Technology, Dept. of Mechanical Engineering, 1959.

[SMK02] T. K. Sen, S. P. Mahajan, and K. C. Khilar. "Adsorption of Cu2+ and Ni2+ on iron oxide and kaolin and its importance on Ni2+ transport in porous media". In: *Colloids and Surfaces A: Physicochemical and Engineering Aspects* 211.1 (Nov. 2002), pp. 91–102. ISSN: 0927-7757. DOI: `10.1016/S0927-7757(02)00235-2`.

[SML04] R. Scanlan, A. Malozemoff, and D. Larbalestier. "Superconducting materials for large scale applications". In: *Proceedings of the IEEE.* Vol. 92. 10. 2004, pp. 1639–1654.

[Sol] *Finite Solenoid.* 2005. URL: `http://www.netdenizen.com/emagnet/solenoids/solenoidonaxis.htm`.

[Sto06] M. Stolarski. "Magnetic field enhanced press-filtration". In: *Chemical Engineering Science* 61 (2006), pp. 6395–6403.

[Suh00] J. C. Suh. "The evaluation of the Biot-Savart integral". In: *J.Eng.Math.* 37 (2000), pp. 375–395.

[Sut08] K. Sutherland. *Filters and Filtration Handbook, Fifth Edition.* 5th ed. Elsevier Science, 2008. ISBN: 1856174646.

[Svo87] J. Svoboda. *Magnetic Methods for the Threatment of Minerals.* Elsevier, 1987.

[Tar+03] P. Tartaj et al. "The preparation of magnetic nanoparticles for applications in biomedicine". In: *Journal of Physics D: Applied Physics* 36.13 (2003).

[Tar86] V. I Tarushkin. *Electric separator for seed.* Muhammad Ali Society, 1986.

[Tas] "Treatment of Coolant of Hot Rolling Process by High Gradient Magnetic Separation". In: *IEEE Trans. on Appl. Supercond.* 17.2 (2007), pp. 2189–2191.

[Tso+06] C. Tsouris et al. "Surfactant effects on the mechanism of particle capture in high-gradient magnetic filtration". In: *Separation and Purification Technology* 51 (2 2006), pp. 201–209.

[UAA03] T. Uslu, Atalay, and A. Arol. "Effect of microwave heating on magnetic separation of pyrite". In: *Colloids and Surfaces A: Physicochemical and Engineering Aspects* 225.1-3 (2003), pp. 161–167.

[Uch+76] S. Uchiyama et al. "Performance of parallel stream type magnetic filter for HGMS". In: *Magnetics, IEEE Transactions on* 12.6 (Nov. 1976), pp. 895–897. ISSN: 0018-9464.

[Wat73] J. H. P. Watson. "Magnetic filtration". In: *Journal of Applied Physics* 44.9 (1973), pp. 4209–4213. DOI: 10.1063/1.1662920.

[Wat75] J. H. P. Watson. "Theory of capture of particles in magnetic high-intensity filters". In: *Magnetics, IEEE Transactions on* 11.5 (1975), pp. 1597–1599. ISSN: 0018-9464.

[WB86] J. H. P. Watson and C. Boorman. "A Superconducting High-Gradient Magnetic Separator with a Current-carrying Matrix". In: *Internation Juornal of Mineral Processing* 17 (1986), pp. 161–185.

[Wu+04] R. Wu et al. "Removal of azo-dye Acid Red B (ARB) by adsorption and catalytic combustion using magnetic CuFe2O4 powder". In: *Applied Catalysis B: Environmental* 48.1 (Mar. 2004), pp. 49–56. ISSN: 0926-3373. DOI: 10.1016/j.apcatb.2003.09.006.

[Yav+06a] C. T. Yavuz et al. "Low-Field Magnetic Separation of Monodisperse Fe3O4 Nanocrystals". In: *Science* 314.5801 (Nov. 2006), pp. 964–967. DOI: 10.1126/science.1131475.

[Yav+06b] H. Yavuz et al. "Biosorption of mercury on magnetically modified yeast cells". In: *Separation and Purification Technology* 52.2 (2006), pp. 253–260.

[Yav+09] C. T. Yavuz et al. "Magnetic separations: From steel plants to biotechnology". In: *Chemical Engineering Science* 64.10 (May 2009), pp. 2510–2521. ISSN: 0009-2509. DOI: 10.1016/j.ces.2008.11.018.

[Yea+05]   S. Yean et al. "Effect of magnetite particle size on adsorption and desorption of arsenite and arsenate". In: *Journal of Materials Research* 20.12 (2005), pp. 3255–3264.

[You+06]   D. Young et al. "Method of fundamental solutions for multidimensional Stokes equations by the dual-potential formulation". In: *European Journal of Mechanics B/Fluids* 25 (2006), pp. 877–893.

[YYT00]   T. Y. Ying, S. Yiacoumi, and C. Tsouris. "High-gradient magnetically seeded filtration". In: *Chemical Engineering Science* 55 (2000), pp. 1101–1113.

[Zha07]   J. Zhang. "Composite magnetic microspheres: Preparation and characterization". In: *Journal of Magnetism and Magnetic Materials* 309 (2007), pp. 197–201.

Others (Italian)

[Fab+06a]   M. Fabbri et al. "Analisi di sensitivitá sui parametri del processo di magnetizzazione del campo intrappolato da magneti permanenti superconduttivi". In: *Atti della 22ᵃ Riunione annuale dei Ricercatori di Elettrotecnica*. ET2006. Torino 2006, pp. 1–2.

[Fab+06b]   M. Fabbri et al. *Studio sui trasformatori superconduttivi ad alta temperatura critica*. Rapporto Finale Contratto CESI-DIE/2006. Department of Electrical Engeneering, 2006.

[Mar+09c]   G. Mariani et al. "Separazione magnetica dei microinquinanti dalle acque reflue". In: *Atti della 25ᵃ Riunione annuale dei Ricercatori di Elettrotecnica-ET2009*. Lecce 2009, pp. 1–2.

[MFN07]   G. Mariani, M. Fabbri, and F. Negrini. "Studio della separazione magnetica dei microinquinanti prioritari dalle acque reflue". In: *Atti della 23ᵃ Riunione annuale dei Ricercatori di Elettrotecnica*. ET2007. Firenze 2007, pp. 1–2. URL: http://www.cirlab.unifi.it/ET2007/memorie/098.pdf.

[MFN08]   G. Mariani, M. Fabbri, and F. Negrini. "Studio della separazione magnetica dei microinquinanti prioritari dalle acque reflue". In: *Atti della 24ᵃ Riunione annuale dei Ricercatori di Elettrotecnica*. ET2008. Pavia 2008, pp. 1–2.

Index of Cited Authors

115